Tanja Rappitsch, BSc

Optical Ion Sensors - Development of New Indicators for K^+ and Na^+ Sensing

MASTER'S THESIS

to achieve the university degree of

Master of Science

Master's degree programme: Chemistry

submitted to

Graz University of Technology

Supervisor

Assoc.Prof. Priv.-Doz. kand. Sergey Borisov

Institute of Analytical Chemistry and Food Chemistry

Graz, June 2017

Abstract

During this thesis a series of new optical ion sensing materials for potassium and sodium were synthesized and characterized. The fluoroionophores consist of different receptors and bright red-emitting BF_2-chelated dipyrromethene (BODIPY) dyes as fluorophores. Upon binding of the analyte (Na^+, K^+) the fluorescence is enhanced caused by the reduction of the photoinduced electron transfer (PET). For continuous measurement the dyes were physically embedded into water-swellable biocompatible polymer matrices (hydrogels).

For Na^+ sensing, different hydrogels were tested. The most suitable was the Hydrogel D1 which is characterized by the highest water uptake. It showed the best dynamic range between the "on" and "off" states among all tested hydrogels. Moreover, this sensing material showed no leaching, no or only minor cross-sensitivity to other ions (Ca^{2+}, Mg^{2+}, K^+) and to pH within the physiologically relevant range and featured fast and reversible response. The potential applications of these probes were demonstrated by preparation of a fiber optic sensor which is suitable for referenced read out with a commercially available phase fluorimeter. This fiber optic sensor was then used for the determination of sea water salinity in the Baltic Sea.

For K^+ sensing, the aim was to develop a new receptor which shows an increase K^+/Na^+ selectivity. Commonly used receptors for optical K^+ sensing are based on a triazacryptand (TAC) introduced by He et al. [1] or a simplified version with an additional lariat group to an aza-18-crown-6 [2]. Modification of lariat group with an additional CH_2 spacer may improve the binding affinity towards potassium due to higher flexibility of the side-chain. In this work, the synthesis of this new receptor and the comparison with the above mentioned receptors will be presented. The new synthesized dye showed a worse K^+/Na^+selectivity and a worse behaviour in hydrogel D4 compared to the other receptors. These new materials offer numerous possible applications in science and technology, such as the determination of K^+ ions in blood.

Kurzfassung

Im Laufe dieser Arbeit wurde eine Reihe neuer ionensensitiver Farbstoffe, die als Sensoren für Kalium oder Natrium geeignet sind, synthetisiert und charakterisiert. Diese Farbstoffe bestehen aus einem Rezeptorteil und einem Fluorophor, einem rot hell leuchtendem Difluoroboraindacene (4,4-Difluoro-4- borata-3a-azonia-4a-aza-s-indacen) (BODIPY). Nach Bindung des Analyten, kommt es zu einer Hemmung des sogenannten PET (photoinduced electron transfer) Effekts und daraus folgend zu einer Zunahme der Fluoreszenz. Für kontinuierliche Messungen wurden diese Farbstoffe in wasserquellbare, biokompatible Polymere (Hydrogele) physikalisch eingelagert.

Für den Natrium Sensor wurden verschiedene Hydrogele getestet, wobei das geeignetsten Polymer das Hydrogel D1 war, welches eine hohe Wasseraufnahmefähigkeit hat. Es wies den besten dynamischen Bereich zwischen dem "ein-" und dem "ausgeschalteten" Zustand des Fluorophors auf. Dieses Sensormaterial zeigte kein Leaching, kein bzw. nur geringe Querempfindlichkeit gegenüber anderen Ionen (Ca^{2+}, Mg^{2+}, K^{+}) und gegenüber dem pH-Wert (im physiologisch relevanten Bereich) und bot schnelles und reversibles Ansprechverhalten. Durch die Kombination des Sensormaterials mit optischen Fasern und einem kommerziell erhältlichen Phasenfluorometer, als Auslesegerät, konnten Bestimmungen des Salzgehaltes in der Ostsee durchgeführt und somit potentielle Anwendungen gezeigt werden.

Das Ziel für den Kalium Sensor war, einen Rezeptor mit einer besseren K^{+}/Na^{+} Selektivität zu synthetisieren. Für Kaliumbestimmungen mit optischen Sensoren werden normalerweise Rezeptoren, wie der Triazacryptand (TAC), welcher von He et al. [1] entwickelt wurde oder eine einfachere Version, eine aza-18-crown-6 mit einem zusätzlichen Seitenarm (der Lariatgruppe), verwendet [2]. Die Abänderung dieses Seitenarms mit einer weiteren CH_2 Gruppe könnte die Bindungsaffinität zu Kalium durch eine höhere Flexibilität dieses Seitenarms steigern. Entgegen allen Erwartungen, wies der neu synthetisierte Rezeptor ein schlechteres Verhalten im Bezug auf K^{+}/Na^{+} Selektivität, sowie im Polymer auf. In dieser Arbeit wird die Synthese dieses neuen Rezeptors präsentiert und mit den oben erwähnten Rezeptoren verglichen. Die neuen Materialien bieten eine Vielfalt neuer Anwendungsgebiete, wie z.B. die Bestimmung von Kaliumionen im Blut.

AFFIDAVIT

I declare that I have authored this thesis independently, that I have not used other than the declared sources/resources, and that I have explicitly indicated all material which has been quoted either literally or by content from the sources used. The text document uploaded to TUGRAZonline is identical to the present master‘s thesis.

EIDESSTATTLICHE ERKLÄRUNG

Ich erkläre an Eides statt, dass ich die vorliegende Arbeit selbstständig verfasst, andere als die angegebenen Quellen/Hilfsmittel nicht benutzt, und die den benutzten Quellen wörtlich und inhaltlich entnommenen Stellen als solche kenntlich gemacht habe. Das in TUGRAZonline hochgeladene Textdokument ist mit der vorliegenden Masterarbeit identisch.

Datum/Date	Unterschrift/Signature

Danksagung

An erster Stelle möchte ich mich bei Prof. Ingo Klimant bedanken, ohne dich wäre es nicht möglich gewesen in dieser tollen Arbeitsgruppe zu arbeiten.
Weiters möchte ich mich bei dir, Sergey bedanken, dass du für jedes Problem einen Rat hattest, und dass du den gewissen Überblick in dieser Arbeitsgruppe behältst.
Berni, dir möchte ich besonders danken, da du ein wirklich toller Betreuer warst und mir immer weitergeholfen hast sobald ich nicht mehr weiterwusste.
Der wohl tollsten Arbeitsgruppe auf dieser Welt möchte ich danken für die vielen gemeinsamen Aktivitäten und die vielen Stunden, die wir gemeinsam im HS T verbracht haben. Außerdem möchte ich mich bei euch bedanken, dass ihr mir immer weiterhelft sobald ich irgendwo ein Problem habe. Ich habe euch alle sehr ins Herz geschlossen und ich freue mich schon auf weitere Jahre (Danke David dafür), die wir gemeinsam miteinander verbringen werden.
Kathi und Chrisi, euch möchte ich für die gemeinsamen Studienjahre und die vielen Mädlsabenden danken, wo wir den stressigen Unialltag vergessen konnten.
Der "Grazer Gang" (+ Tanja, Tami, Julia) gebührt ebenso ein großer Dank, da ihr meine Studienzeit mit vielen lustigen Partys und Aktivitäten und mit eurer Unterstützung versüßt habt. Hier möchte ich besonders Lisa und Pia hervorheben, da ihr es auch ausgehalten habt all die Jahre mit mir zusammen zu wohnen.
Tina und Elisa, Danke, dass ihr so tolle Schwester seid und mich immer unterstützt. Ein Dank gilt auch dir Harald, dafür, dass ich immer mit dir heimfahren darf. Abschließend möchte ich mich noch bei Papa und Mama bedanken, ohne eure Finanzierung und Unterstützung wäre das Studium nicht möglich gewesen. DANKE nochmal für eure Hilfe!

Tanja Rappitsch, BSc Graz, June, 2017

Contents

1 Introduction

In clinical diagnosis, it is very important to accurately measure the concentration of sodium and potassium in whole blood. A change in concentration in the latter can lead to hyper- or hypokalemia. This in turn could have a negative effect on cardiac rythm and on blood pressure regulations [3]. Traditionally, ion-selective electrodes were used for the determination of these ions in serum or plasma. Nevertheless, the growing importance of near-patient devices increases the interest on small, disposable sensors which are used for the measurement in whole blood. Therefore, fluorescent optical sensors are of major significance and due to their properties (non-invasive, can be miniaturized, disposable, allow multi-analyte measurement) they are suitable for these measurements. Additionally, fluorescent sensors can also be applied in analytical chemistry and environment.

For direct determination of cations, fluorescent PET sensors have been confirmed as suitable sensing materials [4–6]. Such PET sensors consists of two moieties: the recognition moiety (ionophore) and the fluorophore. Typically, in presence of ions the emission is enhanced caused by the reduction of the PET effect thus leading to a switchable intramolecular selfquenching system. As an appropriate fluoroionophore for all synthesized dyes, a red light emitting, rigid tetraaryl-BODIPY chromophore has been chosen, which show good brightness and insensitivity to pH in the relevant physiological range. Furthermore, it has an absorption and emission at higher wavelengths ($> 600\,\mathrm{nm}$) which allows the measurements in autofluorescent media (e.g. biological samples) and also the excitation with inexpensive visible light sources.
For continuous monitoring of the ions the fluoroionophore has to be immobilized into a polymer matrix. This could be a complex task because the material should posses good permeability for the ions whereas the indicator should not leach out of the matrix.

The first part of this thesis includes the synthesis of a Na^+ selective receptor. Sodium is the most abundant ion in the extracellular medium (more than $100\,\mathrm{mM}$) and as mentioned above it is very significant to measure it in a continuous way. Here, this sensor is used for oceanographic application since the Na^+ concentration correlates with the seawater salinity. A crown ether receptor, with appropriate size to selectivity bind Na^+, has been chosen. A red light emitting BODIPY chromophore was linked to the receptor. This fluoroionophore was then immobilized in a hydrogel matrix for enabling continuous measurement.

The aim of the second part of this work was to synthesize a new receptor for the determination of potassium in blood. This can be challenging because a good selectivity against sodium and other extracellular cations, a strong aqueous binding property (with an K_d around 5 mM) and a large fluorescent signal response with an emission above >500 nm (minimize the background fluorescence of biological fluids) are required. Previous work has shown, that the introduction of a 2-methoxyethoxy lariat group at the ortho position give an increase in the stability and a decrease of the K_d value of the receptor whereas retaining the flexibility of the ionophore [7]. Furthermore, more recent work proposed the [2.2.3]-triazacryptand (TAC) as a receptor unit to overcome the poor Na^+/K^+ selectivity [1]. It is thought that an introduction of a CH_2 group at the lariat group would lead to a more flexible arm and therefore to better complexation. In this thesis, the synthesis and characterization of this new receptor and the comparison with other receptors are shown.

2 Theoretical Background

2.1 Luminescence

This section is based on references [8] and [9], other references will be cited independently. Luminescence describes the emission of photons from an electronically excited species due to relaxation. A wide range of compounds exhibit luminescence such as organic compounds (mostly aromatic), inorganic species (ions, crystals, glasses) and organometallic complexes. There are different types of luminescence which can be distinguished according to their mode of excitation and the nature of the excited state. Table 2.1 summarizes the most important types of luminescence. However, for this thesis only absorption as mode of excitation and its relaxation processes (fluorescence, phosphorescence) are of interest and will be described in more detail in the following pages.

Table 2.1: Important luminescence types and excitation pathways

Mode of excitation	Type of luminescence
Absorption of light	Fluorescence, Phosphorescence
Chemical process	Chemoluminescence
Biochemical process	Bioluminescence
Electrical field	Electroluminescence
Thermal energy	Thermoluminescence

2.1.1 Absorption

An electronic transition occurs when a molecule absorbs a photon. After absorption of a photon an electron is promoted from the ground state to an unoccupied energetically higher lying excited state. Mostly, the electron is moved from the HOMO (highest occupied molecular orbital) to the LUMO (lowest unoccupied molecular orbital) although other transitions are also possible. Depending on the kind of molecular orbitals which are involved in this process different transitions can take place. In case of fluorescent dyes the observed transitions are mostly $\pi \rightarrow \pi^\star$ or $n \rightarrow \pi^\star$. The energy for $\pi \rightarrow \pi^\star$ transitions decrease with the increase of the conjugated π system. Other transitions are also possible and they vary in their energy typically in the following order:

$$n \rightarrow \pi^\star < \pi \rightarrow \pi^\star < n \rightarrow \sigma^\star < \sigma \rightarrow \pi^\star < \sigma \rightarrow \sigma^\star$$

However, transition of σ electrons require usually high energy in the far UV and for this reason they are not very important for spectroscopic applications. The absorption efficiency at a certain wavelength is experimentally defined by its absorbance and mostly follows the Beer-Lambert Law. The molar absorption coefficient ε is expressed as the ability of the dye to absorb light.

$$A(\lambda) = log(\frac{I_0}{I}) = c \cdot l \cdot \varepsilon(\lambda) \tag{2.1}$$

A....absorption of the molecule
I_0....light intensity before the sample
I....light intensity after the sample
l....length of the cuvette (1 cm)
c....concentration of the dye solution in $mol \cdot L^{-1}$
ε....molar absorption coefficient in $L \cdot mol^{-1} \cdot cm^{-1}$

2.1.2 Franck-Condon-Principle

This principle is based on the Born-Oppenheimer approximation. According to this approximation the electron movement is much more rapid than those of the nuclei (10^{-15} s for transition compared to 10^{-10} - 10^{-12} s for molecular vibrations). Therefore, the transition time of electrons is too short for significant displacement of the nuclei which means that electronic transition occur most likely without change in the position of the nuclei (they are vertical, see figure 2.1.

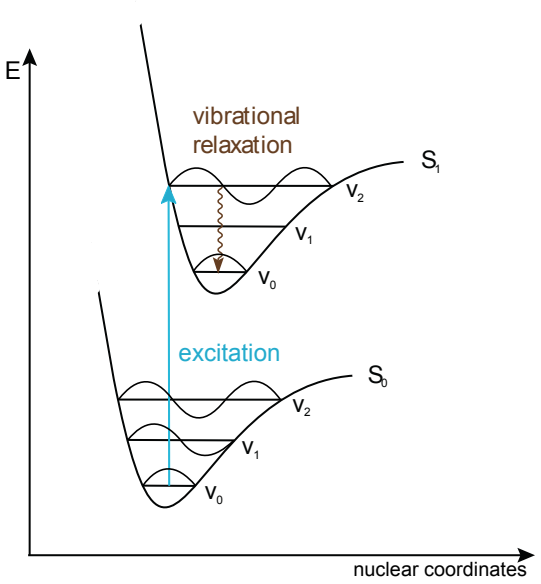

Figure 2.1: Franck-Condon principle

The intensity of several vibronic transitions depends on the relative position and shape of this potential curve whereas the width of the band depends on the fluctuations of the structure of the solvation shell (inhomogeneous broadening) and on the existence of a continuous set of vibrational sublevels (homogeneous broadening).

2.1.3 Transitions between Electronic States

The different energy states of an electron are usually illustrated in a Jablonski diagram.

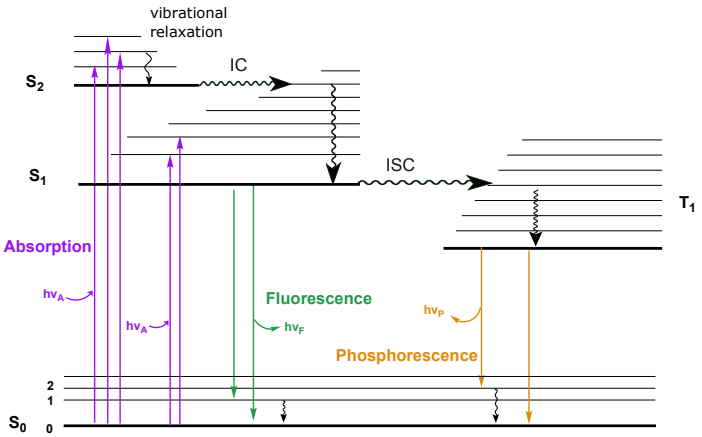

Figure 2.2: The Perrin-Jablonski diagram illustrates the processes that occur in a fluorophore between absorption and emission of light

There are different types of electronic states. The S_0 state is the ground state of the molecule, S_1 and S_2 are the excited singlet states and T_1 is the excited triplet state. Each of these states is associated with vibrational levels. At room temperature the majority of molecules of a fluorophore are in the S_0 ground state and upon excitation molecules can be brought to one of the vibrational levels of S_1 or S_2. Once in the excited state the molecule can return to its ground state in multiple ways, which are displayed in a Jablonski diagram (see figure 2.2) and descriped in the following sections.

Internal Conversion (IC)

A non-radiative transition between a higher and a lower electronic state of the same multiplicity is called IC. It is usually followed by vibrational relaxation from the vibrationally highly excited molecule to its ground state. The efficiency of the IC is increased if the energy gap between the two electronic states gets smaller. Therefore, the IC is most efficient from the S_2 to S_1 transition state and occurs within 10^{-12} s or less. From S_1 to S_0 it is less efficient because of the larger energy gap between them. Here, IC can compete with intersystem crossing to the triplet state (phosphorescence is possible) and with emission of photons from S_1 to S_0 (fluorescence).

Intersystem Crossing (ISC)

Compared to internal conversion, intersystem crossing is a transition of two electronic states with different multiplicities ($S_1 \rightarrow T_1$) to the equal vibrational level. Through vibrational relaxation the molecule is then brought to the lowest vibrational level T_1. Although spin-forbidden, spin-orbit coupling can be large enough to make this transition possible. Through the presence of heavy atoms (e.g Pb, Br) the spin-orbit coupling is increased and therefore ISC is favoured.

Fluorescence

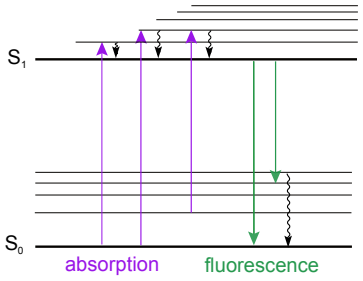

Figure 2.3: Scheme for fluorescence

Fluorescence is the radiative deactivation of an excited state to its ground state, usually from $S_1 \rightarrow S_0$. This emission is as fast as absorption of a photon (10^{-15} s) and before the return to the S_0 state the excited molecule remains in the S_1 state for a certain time (lifetime). The transition is in most cases independent of the wavelength of the excitation. However, the fluorescence spectrum is shifted to longer wavelengths compared to the absorption spectrum due to energy loss through vibrational relaxation in the excited state (Stokes rule). The difference between the maximum of the absorption and emission band is called Stokes shift. For almost all molecules the fluorescence spectrum is a mirror image of the absorption spectrum due to the similarity of the difference of vibrational levels in the ground and excited state (mirror image rule).

Phosphorescence

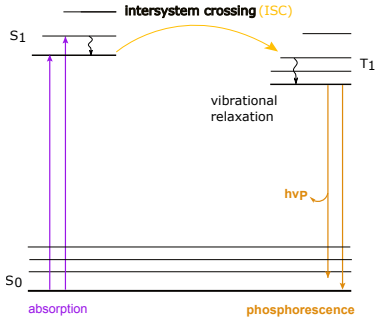

Figure 2.4: Scheme for phosphorescence

Phosphorescence is a radiative de-excitation between the T_1 and the ground state. Due to the same spin orientation of the excited state and the ground state this transition is forbidden. Nevertheless, phosphorescence can be observed because of spin-orbit coupling. The emission rates are slow which leads to long lifetimes (milliseconds to seconds). However, non-radiative transitions are more favourable over phosphorescence, so usually it is not observed in solution at room temperature whereas in rigid medium and at low temperature it can be seen. Also the presence of heavy atoms in a molecule can favour phosphorescence because the efficiency of the spin coupling changes with the fourth of the atomic number. The energy level of T_1 is lower than that of S_1 and therefore the phosphorescence spectrum is located at higher wavelength than the fluorescence spectrum.

Delayed Fluorescence

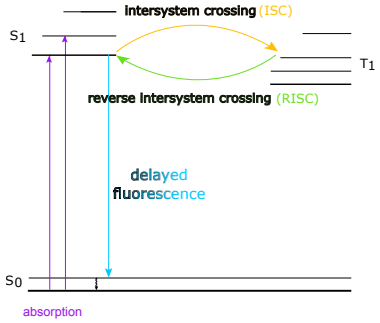

Figure 2.5: Scheme for delayed fluorescence

Delayed fluorescence is the emission of an excited molecule from the S_1 to the ground state after the excited molecule is located in the triplet state ($S_0 \rightarrow S_1 \rightarrow T_1 \rightarrow S_1 \rightarrow S_0$). It shows the same emission spectrum as in fluorescence but has a longer decay time. It can be distinguished between two types of delayed fluorescence: the thermally activated delayed fluorescence (E-type) and the triplet–triplet annihilation (P-type). In thermally activated

delayed fluorescence the emission occurs after reverse intersystem crossing. This is favoured if the difference in energy between the S_1 and the T_1 states is small and the lifetime of T_1 is long enough. In this case the emission is thermally activated. Contrary to that, in the second type of delayed fluorescence the emission occurs after a process which is called triplet-triplet annihilation. During this process a collision between two molecules in concentrated solutions provides enough energy to allow one of them to return to the S_1 state.

2.1.4 Lifetime

As discussed above, after a molecule is promoted to the excited state several nonradiative and radiative de-excitationen processes are possible. This de-excitation processes do not occur immediately. The excited molecule typically remains a certain time in the excited state before returning to the ground state. The lifetime of the excited state S_1 is a measure for this time span and is given by equation 2.3. The kinetics of all described de-excitation processes (except triplet-triplet annihilation) follow all first order kinetics.

$$-\frac{\mathrm{d}\,[A^\star]}{\mathrm{d}t} = k \cdot [A^\star] \tag{2.2}$$

$[A^\star]$....concentration of excited species A
k....sum of all possible de-excitation rates

Integration of this equation leads to following equation, where $[A^\star]$ is the time evolution of the excited state $[A^\star]_0$ is the concentration of excited molecules at time 0 and τ is the lifetime of the excited state.

$$[A^\star]_t = [A^\star]_0 \cdot e^{\frac{-t}{\tau}} \tag{2.3}$$

2.1.5 Quantum Yield

The quantum yield of a substance is defined as the ratio between emitted photons to the number of absorbed photons. Molecules with high quantum yield show also the brightest emission.

$$\phi = \frac{k_r}{k_r + k_{nr}} = k_r \cdot \tau_S \tag{2.4}$$

k_r....rate constant for radiative deactivation of the fluorophore
k_{nr}....rate constant for non-radiative deactivation of the fluorophore
τ_S.... lifetime of the excited state

The quantum yield can be influenced by various parameters, such as temperature, polarity,

pH, solvent viscosity, presence of quencher etc... For instance, with increasing temperature the quantum yield decreases due to favoured non-radiative processes.

2.1.6 Quenching

Quenching is a process where an excited fluorophore F* interacts with another molecule Q which leads to a decrease of the fluorescence intensity. A lot of molecular interactions can result in quenching like collision with heavy atoms, formation of excimer/ exciplex, proton-, electron or energy transfer. In this section two types of quenching will be discussed: dynamic and static quenching. Both require molecular contact between the quencher and the fluorophore. They can be distinguished due to lifetime measurements or by their different dependency on viscosity and temperature. At higher temperature the dynamic quenching is favoured through faster diffusion whereas static quenching is less favourable due to dissociation of weakly bound complexes.

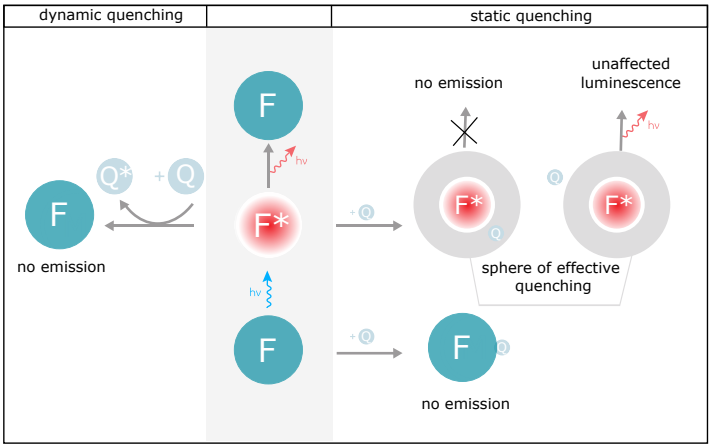

Figure 2.6: Different types of quenching

Dynamic Quenching

Dynamic quenching results from diffusive interaction between the fluorophore (F) and the quencher (Q) during the lifetime of the excited state. Compared to static quenching, the absorption spectra is here not affected because only the excite state of the fluorophore will be influenced. However, it has an impact on luminescence intensity and lifetime.
This time-dependent process can be described by the Stern-Volmer-equation, which is dependent on the quenching rate constant k_q, the unquenched excited state lifetime τ_0 and the quencher concentration $[Q]$. F and F_0 describe the fluorescence intensities in presence and absence of the quencher.

$$\frac{F_0}{F} = 1 + k_q \cdot \tau_0 \, [Q] = 1 + K_D \cdot [Q] \tag{2.5}$$

The quenching is illustrated in the Stern-Volmer plot, where F_0/F is plotted against the quencher concentration $[Q]$. The quenching rate constant k_q represents the slope of this curve.

Static Quenching

Static quenching can be observed if a non-fluorescent complex between the quencher and the fluorophore is formed. This can either occur via a sphere of effective quenching in the excited state of M or in the ground-state. The quenching in the excited state can only occur if the quencher molecule Q is located in the active sphere of the fluorophore. This results in viscous media or rigid matrices when the fluorophore and the quencher cannot change their position in space relative to one another. Outside the active sphere the quencher has no effect on F. Another possibility for static quenching is the formation of the quencher-fluorophore complex in the ground state. This formation leads to a disturbance of the absorption spectrum of the fluorophore. However, the lifetime of the fluorophore remains unchanged because only the fluorescent molecules are observed.

2.2 Chemical Sensors

A chemical sensor transforms chemical information which derived from a physical property of the system investigated or a chemical reaction of the analyte, into an analytically useful signal. In general, a sensor should be selective and able to measure an analyte with a fast response time in a broad dynamic range. It should be cheap, reversible, robust and has to be small [10]. There are two main parts in a chemical sensor: a receptor part and a transducer part. The latter transforms the energy carrying the chemical information about the sample into a useful signal [11]. The recognition unit of a sensor device is one of the key components. It is responsible for the selectivity of a sensor and avoiding interferences with other substances [12]. Chemical sensors can be classified according to the operating principle of the transducer. For example, optical devices transform changes of optical phenomena (e.g. absorbance, fluorescence or refractive index...). Other types of chemical sensors have electrochemical-, electrical-, mass sensitive-, magnetic- and thermometric devices. For the determination of Na^+ and K^+, the most widely used forms of transduction are optical methods like absorbance and fluorescence (e.g. optodes) or potentiometry (e.g ISE). Ionophores, which are able to complex the analytes are the key components of both type of sensors [13].

2.2.1 Ionophores

The ionophore acts as selective recognition unit for the target analyte which is bound via the formation of non-covalent bonds. The ligand should strongly complex the preferred ion (only weakly all the others) in order to facilitate a highly selective sensor and should be conformationally flexible (preorganization) to ensure a rapid exchange [14]. A rapid exchange is necessary in order to get a fast response thus avoiding long response time and deviation in

expected response slope. Another requirement is that the complex formation constant between ion and ionophore should be high enough to bind the ion selectively but not as high that ions are tightly bound so that the binding is virtually irreversible [13]. The ligand toptology, the number and nature of the complexing heteroatoms of the ionophore should also match with the coordination number, the hardness, the ionic diameter and the charge of the cation. It can be either a chelator, a macrocyle (coronand, e.g. crown ether), a macrobicylce (cryptand), or an openchain strucure (podand) [15]. Actually, different antibiotics such as Monesin for sodium sensing and valinomycin for potassium sensing have been used as recognition units (see Figure 2.7).

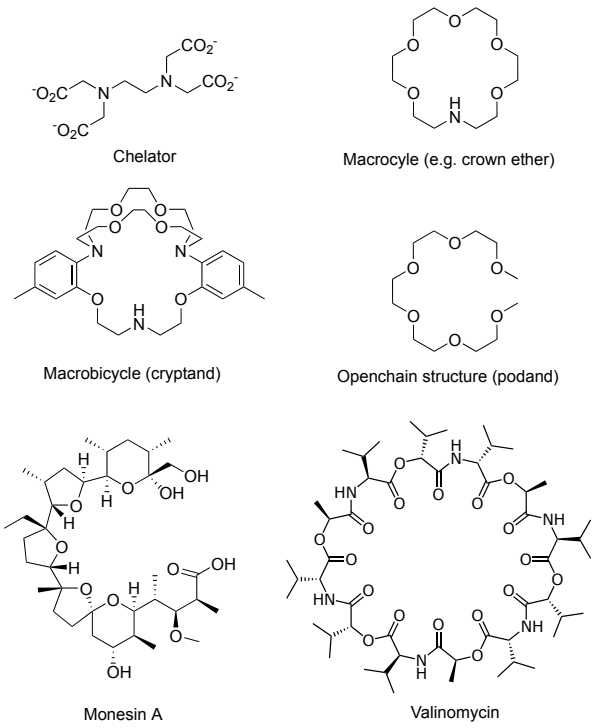

Figure 2.7: Example of a chelator, a coronand, a cryptand, a podand and structures of the antibiotics monesin and valinomycin for cation sensing

Cryptands and Crown Ethers

Crown ethers and cryptands were discovered in the late 1960s and brought new possibilities of cation recognition. Here the cation binding can be described by the best-fit concept due to the direct correlation between the size of the crown ether/cryptand cavity and the metal ion size [16]. If the cation diameter is much larger than the ionophore cavity, the cation cannot fit into it. Conversely, if its too small it cannot use the numerous binding interactions which are available. In other words, ions with an ionic diameter close to that of the ligand cavity of crown ethers or cryptands form the most stable complexes [13]. Crown ethers with oxygen atoms as donors bind the cation (guest) into the cavity of the crown ring (host) through an ion-dipole interaction. Other donor atoms such as sulphur, nitrogen, phosphorus, selenium can also be used and offer the opportunity to use them as heavy metal or transition metal recognition units [17].

The complexation stability of cryptands is usually higher due to their inability to be deformed and also the stability of a cryptand-ion complex (cryptate) is higher because of a three dimensional complexation [15]. The analyte is here totally encapsulated within the cavity of the cryptand [18]. For even better binding polyether side chain arms called "lariat-ether" have been introduced. These sidearms are placed in a position to provide a third dimension and have one or more donor groups (see figure 2.8) [19]. The introduction of such side chain arms can lead to an increase in the stability and a decrease of the the K_d value [20] of the

ionophore.

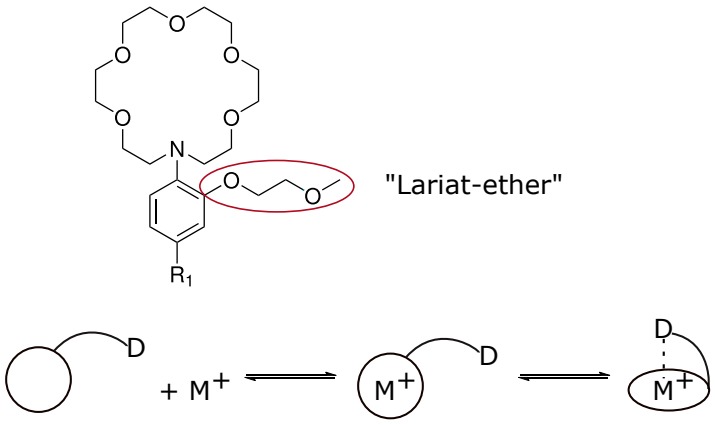

Figure 2.8: Lariat ether complexation process

2.2.2 Ion Selective Electrodes (ISE)

Ion selective electrodes rely on the principle of concentration cells. They have two equivalent half-cells of the same composition linked by a membrane [12]. The sensor reply to the activity of the target ion dissolved in the solution with an electrical potential. It is a direct function of the activities of the analyte and usually exhibits a large sensitivity range (from about 1 to 10^{-6} M). The selectivity of ISE is associated to the equilibrium constant of the exchange reaction of interfering ions and target ions and also to complex formation properties [14].

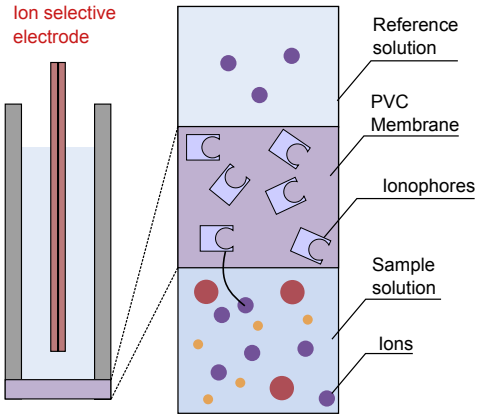

Figure 2.9: Schematic representation of an ion selective electrode

There exists different types of ISE. One type, is the glass membrane electrode, which consists of a thin glass membrane. The universally known example for this type is the pH-electrode. There are also glass membrane electrodes for the measuring of other ions like Na^+, Li^+, K^+ and Ag^+. Nevertheless, for sodium and potassium sensing the liquid ion-exchange membrane type are preferred over glass electrodes. In this type of ISE the membrane consists of a

hydrophobic material such as plasticized poly(vinyl)chloride (PVC). This polymeric membrane is the main part of a ISE and is placed between two aqueous phases (sample and internal electrolyte solution) (see figure 2.9) [14]. A liquid ion exchange material (ionophore) which is able to transfer ions through, is absorbed into this membrane. In this membrane an ion exchange liquid is stored in order to maintain the concentration level in the membrane. Other types of ISE are for example solid state electrodes (selective primarily to anion sensing) or gas electrodes, which are for the determination of ammonia, carbon dioxide and nitrogen oxide [12].

2.2.3 Optical Sensors

Optical chemical sensors are devices which are using optical radiation to yield the analyte information in a transduction element. Optical fibres are used to transmit the electromagnetic radiation from and to the sensing region. They behave as "waveguides" and can be utilized either in the intrinsic mode or in the extrinsic mode. In the latter the waveguide transmit light from the light source to the light collector where Beer´s law can be applied. Here, a signal is produced after the interaction of the analyte with an indicator in a physical or chemical way. Conversely, in the intrinsic mode the signal transduction is based on optical properties of the analyte and the interaction of light with the sample takes place inside the guiding region [12]. However, most optical sensors need an immobilized reagent as the chemical transducer which is usually a dye. It changes optical properties in presence of the analyte and is located in the sensing region of the optical fibre either by immobilizing the dye in a polymeric matrix or by direct decomposition [21]. The polymeric matrix must require that the analyte can pass through it and the dye cannot leach out. The selectivity and the response time of the dye can be influenced by different polymer supports [22]. The number of applications for optical sensors reported is huge. For instance, optical sensors can be used for the detection of oxygen, CO_2, NH_3, pH and ionic species as they respond to optical phenomena like absorption, refractivity or luminescence. Optical chemical sensors offer a lot of advantages compared to their electrochemical counterparts. They are in generally more cost effective to produce, are easy to miniaturize and allow signal readout without physical contact [23]. Furthermore, it allows non-invasive measurements in biological milieus and parallel monitoring of multiple samples [24]. Two main groups of optical sensors have been developed for cation sensing. The first group rely on an indirect sensing principle and the second group consists of fluoroionophores. Both groups are described in more detail in section 2.2.4 and 2.2.5.

2.2.4 Ionophore based Optical Sensors (IBOS)

Ionophore based optical sensors rely on an indirect sensing principle. The sensor film contains molecules (ionophores) which have a high affinity towards the analyte (e.g. cations). This results in extraction of the cations into the sensing film. Therefore, a second optically detectable process is initiated where an equal amount of protons, compared to the extracted cations, is released (see figure 2.10). The protonation degree of the proton carrier is then changed which is available to optical readout methods. A negatively charged ion exchanger is only necessary when the indicator and the ionophore do not possess a net neutral charge. Conversely to surface optodes, the active receptor is not in direct contact with the solution. Here, extraction of the analyte and the activity of this analyte in the sensor phase leads to a sensor signal [23].

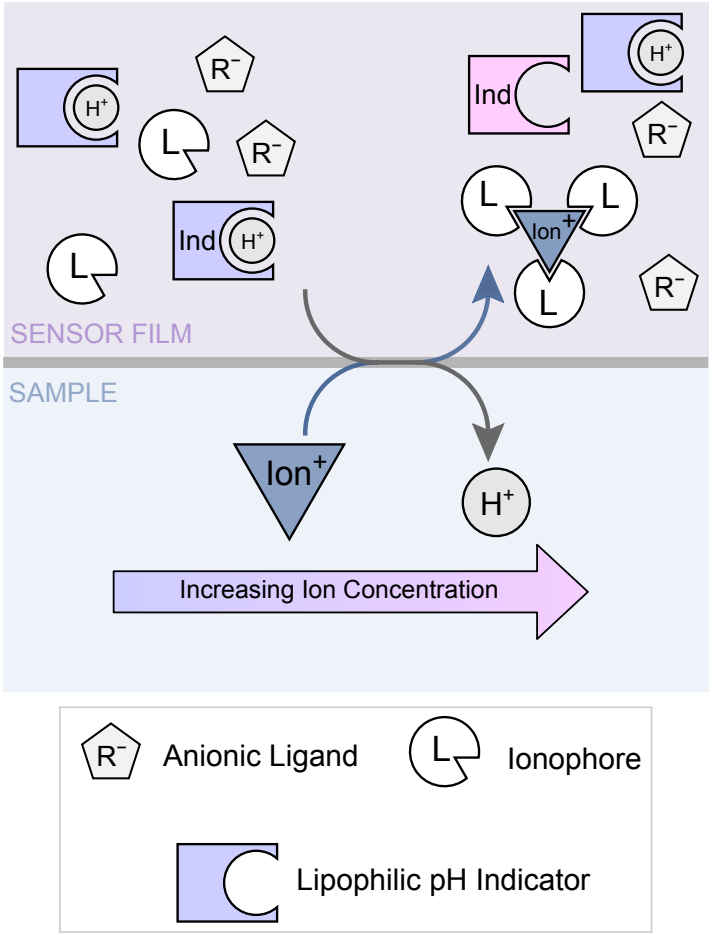

Figure 2.10: Schematic representation of an IBOS

2.2.5 Fluorescent Sensors for Cation Measurement

For an appropriate sensor one has to design a fluoroionophore. They consists of a ionophore which is coupled to a fluorophore and the general structure is shown in figure 2.11. As described in section 2.2.1 ionophores acts as selective recognition unit for the target analyte. For an appropriate sensor this ionophore has to be integrated with a luminophor (see section 2.2.7) to signal the binding with an luminescent response. Upon cation complexation the photopysical properties of the fluorophore are changed. The common mechanism applied in cation sensors are photoinduced electron transfer (PET), internal charge transfer (ICT) and Förster resonance energy transfer (FRET) whereas in this thesis only PET-sensors were synthesized [24].

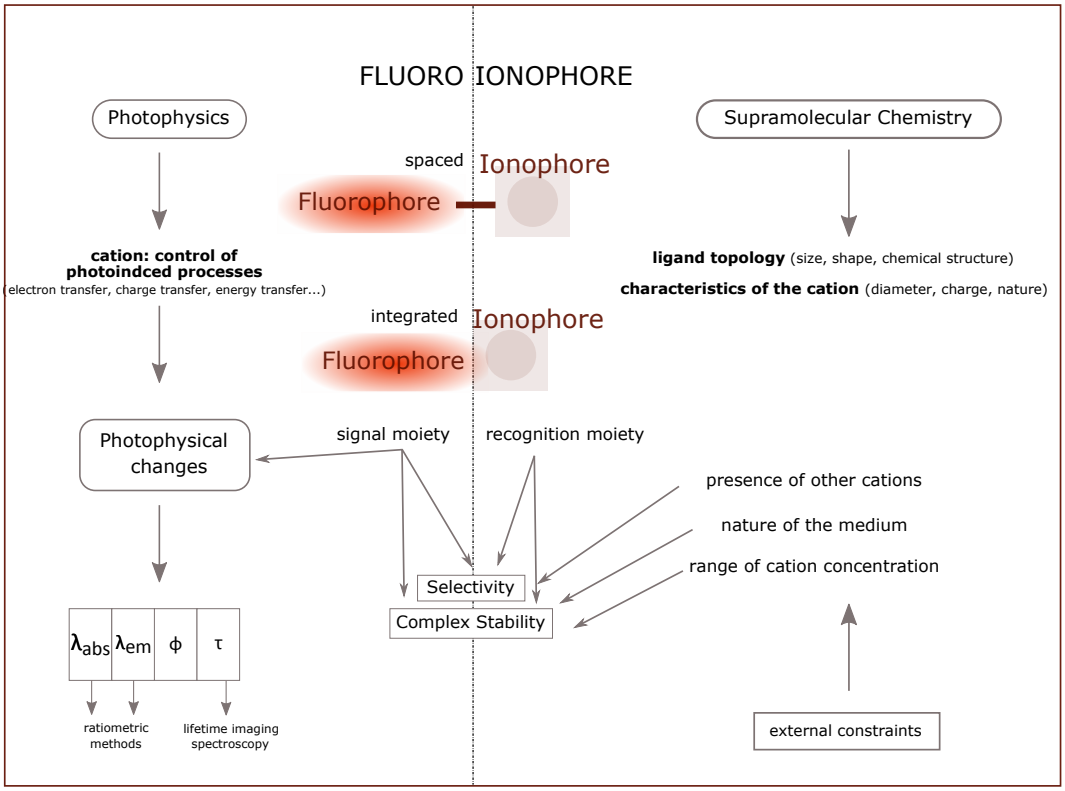

Figure 2.11: Main aspects of fluoroionophores for cation recognition (adapted from [8])

General Principle of ICT-Sensors

Upon excitation of light a fluorophore which contains an electron-withdrawing group attached to an electron-donating group undergoes intramolecular charge transfer form the donor to the acceptor. Interaction of an cation affects the efficiency of intramolecular charge transfer and thus leading to a change in the photophysical properties of the fluoroionophore. It can either be a hypsochromic or bathochromic shift depending on the character of the ionophore. If the ionophore is the donor then the binding of a cation results in a reduction of this electron donating character (conjugation is decreased) and thus leading to a hypsochromic shift (blue shift). In contrast, if the ionophore is a acceptor group then the electron-withdrawing character is enhanced thus leading to a bathochromic shift (red shift). In other words in ICT sensors a change in the absorption spectrum (change in colour, see figure 2.12) will be observed upon complexation of the analyte [15, 25].

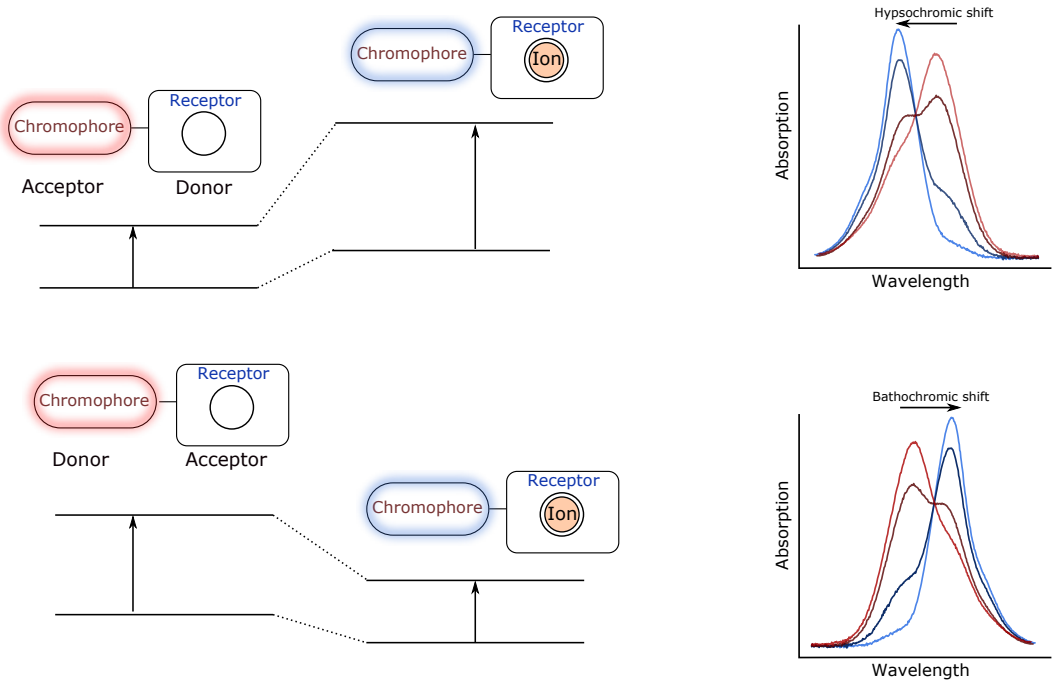

Figure 2.12: Change of the spectral properties of ICT sensors resulting from interaction of a bound cation

General Principle of PET-Sensors

As mentioned above, fluorescent PET sensors consist of two moieties, the first one is the fluorophore which is linked to an amine moiety. The second moiety acts as the recognition unit for cation sensing. Typically, they are linked together via a methylene spacer. In such structures an electron is donated from the amine group to the aromatic hydrocarbon and causes fluorescence quenching [15]. This effect is called photoinduced electron transfer (PET). Upon protonation of the amine group or interaction with a cation the electron transfer is

blocked and therefore the fluorescence is increased [9].

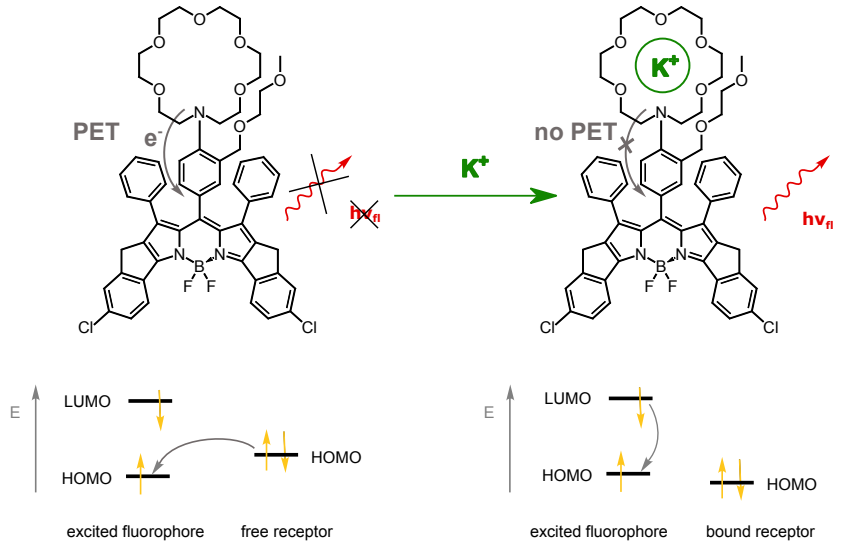

Figure 2.13: Principle of cation sensing by PET sensors

Figure 2.13 explains the mechanism of the PET effect using molecular orbitals. On the left side it can be seen, that after excitation of the dye an electron from the highest occupied molecular orbital (HOMO) from the receptor is promoted to the HOMO of the fluorophore, which leads to fluorescence quenching. Upon binding of a cation with the receptor a decrease of the energy level of the HOMO of the receptor is observed. In this case, PET is not possible because the relevant HOMO is now lower in energy than that of the fluorophore. This results in an increase of the fluorescence [26]. Despite to ICT sensors, the absorption spectrum of PET sensors will not be affected upon complexation of the analyte (figure 2.14).

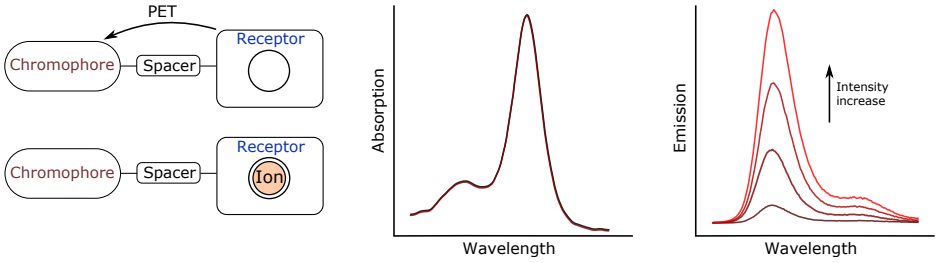

Figure 2.14: Upon inhibition of the PET effect the emission intensity is increased whereas the absorption spectrum do not change

Sodium and Potassium Fluoroionophores

A variety of direct sensing schemes using fluoroionophores are known for sodium sensing. For example, sodium binding benzofuran isophtalate (SBFI) [27] or sodium green (SG) [28] are commercially available and well established sodium fluoroionophores (figure 2.15). They consist of a fluorescein fluorophore and a diaza-15-crown-5 ether as a receptor. However, this indicators require excitation using UV-light ($< 550\,\text{nm}$), thus resulting in high background fluorescence form biological samples, carrier polymers and from optical components. Sodium sensors using the same crown (as in this thesis presented) (N-(o-methoxyphenyl)aza-15-crown-5) were developed from He et al. Here, instead of a BODIPY fluorophore, a 4-amino-1,8-naphthalimide as fluorophore was chosen [29].

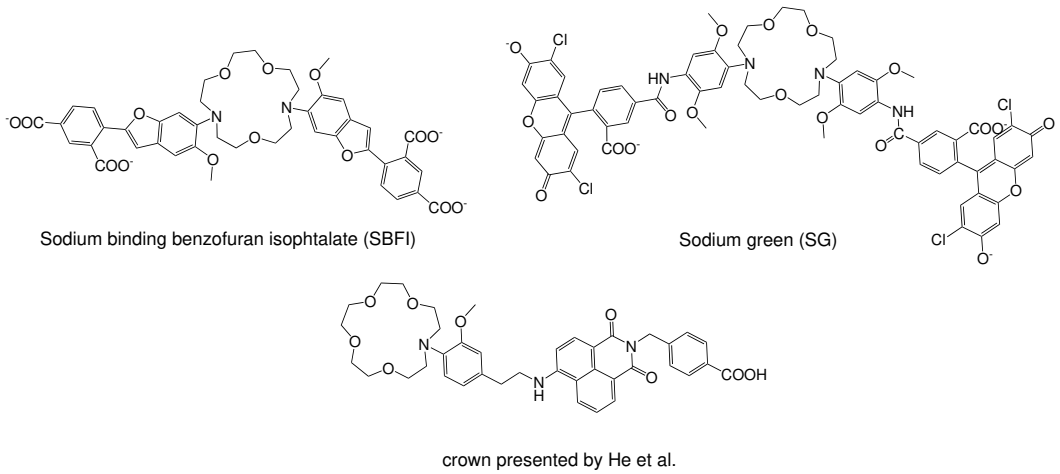

Figure 2.15: Examples of sodium fluoroionophores

One of the most popular indicator dye for potassium sensing is potassium binding benzofuran isophthalate (PBFI). It is commercially available and consists of a diaza-[18]crown-6 ether as the recognition unit and a benzofuran derivative as the fluorophore[30] (see figure 2.16). However, a disadvantage of this fluoroionophore is that it lacks of K^+/Na^+ selectivity. To overcome this, He et. al established a [2.2.3]-triazacryptand(TAC) as receptor unit [1]. Nevertheless, the preparation of this receptor is time consuming due to multistep synthesis. Ast et al. [20] introduced a simple receptor with a good K^+/Na^+ selectivity which consists of a phenylaza-[18]crown-6 receptor with an ortho-substituted 2-methoxyethoxy group (Lariat-group see section 2.2.1). Another highly selective fluoroionophore for potassium sensing is based on a calix[4]bisazacrown as the receptor and a boron-dipyrromethene as the fluorophore. Here, the drawback is that it only worked in a mixture of ethanol and water [31].

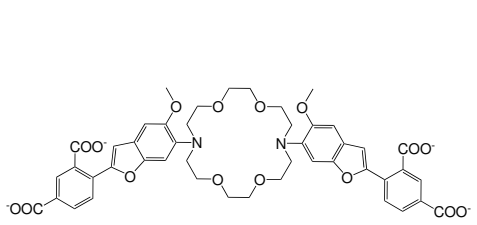

potassium binding benzofuran isophthalate (PBFI)

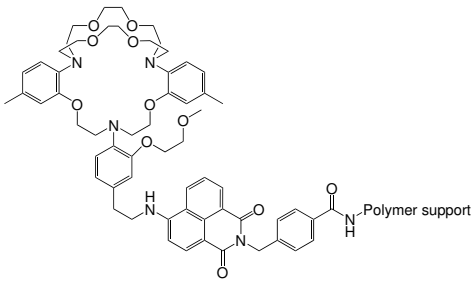

cryptand presented by He et al.

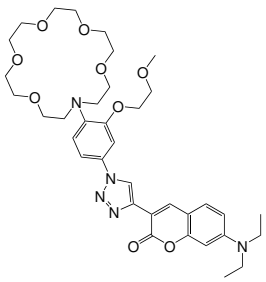

phenylaza-[18]crown-6-lariat-ether based fluoroionophore

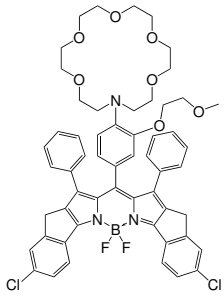

phenylaza-[18]crown-6-lariat-ether-BODIPY fluoroionophore

Figure 2.16: Examples of potassium fluoroionophores

2.2.6 Intensity vs. Lifetime based Sensing

Fluorescence emission contains both, time (typically 10^{-9} s) and spectral information (typically UV/visible). Therefore it is possible to use either time-resolved measurements or steady-state measurements. The latter has traditionally been used for routine analytical applications of fluorescence spectroscopy [32]. Here, the sample is illuminated continuously with light and the emission (intensity) spectrum is observed. A major disadvantage of this technique is the susceptibility to signal change due to photobleaching or leaching of the fluorescent indicator complex or changes in excitation source intensity [22]. On the contrary, lifetime measurement is a more robust technique compared to steady-sate measurement [9]. There are two main methods for time-resolved measurements, namely the time-domain and the frequency domain method. The time-domain method uses a pulse of light for the excitation of the sample to measure directly the lifetime. For this type of measurement, a pulsed laser source and a photon counting photomultiplier tube or intensified CCD camera are necessary, which make such systems quite expensive and complex. For development of low cost, mass-producible systems this measurement is less attractive. The alternative is the frequency domain method where low cost phase detection electronics in conjunction with LED sources and photodiode detetectors can be used. For this technique, the sample is excited with intensity modulated light (typically sine-wave modulation). After the excitation the emission is forced to respond at the same modulation frequency. However, the emission is delayed in time caused by the lifetime of the fluorophore in comparison to the excitation. The difference between excitation and emission is called phase shift ϕ and is related to the decay time according to the following equation:

$$\tan \phi = 2\pi f \tau \tag{2.6}$$

where ϕ is the measured phase angle, f is the modulation frequency and τ is the decay time of the fluorophore. Nevertheless, the system in combination with low-cost electronics can only be used for luminophores with lifetimes in μs-ms time domain. For analytes such as pH, carbon dioxide, or potassium the lifetime is too short and therefore another technique has been investigated: the Dual lifetime referencing (DLR) which is described below [22].

2.2.7 General Principle of DLR Measurement

In DLR measurement two different luminescent indicators are used. They can be excited at the same wavelength because they have overlapping excitation and emission spectra. Therefore, it is also possible to detect the fluorescence with the same photodetector [33]. The luminophores are typically co-immobilized in a solid matrix, where one is sensitive to the analyte (short lived) whereas the other is insensitve and long lived [22]. The latter gives a constant background signal whereas the analyte sensitive dye signal depends on the analyte concentration which

leads to following phase-dependent signals:

$$A_m \cdot cos\phi_m = A_{ref} \cdot cos\phi_{ref} + A_{flu} \cdot cos\phi_{flu} \tag{2.7}$$

$$A_m \cdot sin\phi_m = A_{ref} \cdot sin\phi_{ref} + A_{flu} \cdot sin\phi_{flu} \tag{2.8}$$

A_m....overall signal intensity
ϕ_m....measurable phase shift
A_{flu}....amplitude of the fluorescence indicator
A_{ref}....amplitude of the reference standard
ϕ_{ref}....phase shift of the reference
ϕ_{flu}....phase shift of the fluorescence indicator

If there is a low modulation frequency (e.g.: kHz range) then the phase shift of ϕ_{flu} is zero and the equation can be simplified:

$$A_m \cdot cos\phi_m = A_{ref} \cdot cos\phi_{ref} + A_{flu} \tag{2.9}$$

$$A_m \cdot sin\phi_m = A_{ref} \cdot sin\phi_{ref} \tag{2.10}$$

Equation 2.9 divided by equation 2.10 results in a correlation of the phase signal (ϕ_m) and the intensities of the ratio of indicator and the reference.

$$\frac{A_m \cdot cos\phi_m}{A_m \cdot sin\phi_m} = cot\phi_m = cot\phi_{ref} + \frac{1}{sin\phi_{ref}} \cdot \frac{A_{flu}}{A_{ref}} \tag{2.11}$$

The referenced intensity of the fluorescence indicator is reflected by $cot\phi_m$. If ϕ_{ref} is known and constant then there is a linear relationship between A_{flu}/A_{ref} and $cot\phi_{ref}$ [34]. Changes on the overall phase shift depends on the ratio of these dyes. So if there is a high indicator emission the amplitude is increasing and the phase shift decreases and *vice versa* (see figure 2.17). The modulation frequency is adjusted according to the decay time of the long lived reference dye [33]. Optical system interferences (leaching, bleaching etc.) which leads to drifts are not referenced by this method [35]. Within this thesis, DLR measurement has been used for the referencing of sodium sensors used for detection of the salinity of sea water (see section 4.2.6).

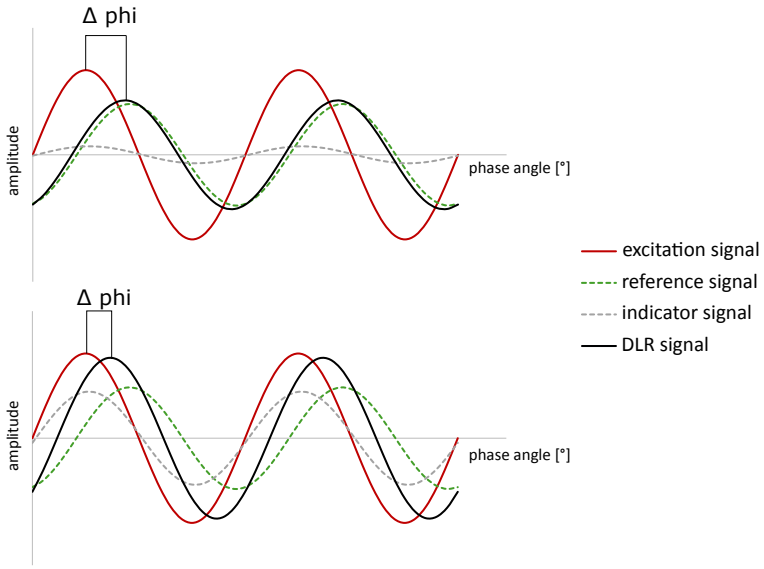

Figure 2.17: Principle of DLR measurement at low and high indicator emission

Bodipy Fluorophores

In the design of a fluoroionophore, much attention is paid to the characteristics of the fluorophore. BODIPY dyes (4,4-difluoro-4-bora-3a,4a-diaza-s-indacene) are suitable candidates for fluorescent sensors for alkali or other metal ions due to their excellent photophysical properties [36]. Moreover, these dyes show outstanding thermal and photochemical stability, negligible triplet-state formation, chemical robustness, fluorescence lifetimes in ns range and high quantum yields [37]. Another feature of this class of dyes are the sharp absorption and emission bands with high peak intensity and excitation/emission wavelengths in the visible spectral region (>500 nm). The molecular backbone can be easily fine tuned which offers further opportunities to change their photophysical and spectroscopic properties [38].

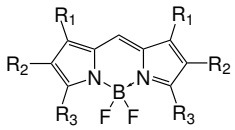

Figure 2.18: Core structure of symmetrical BODIPY dyes

Synthetic Considerations

There are a few different synthetic routes to synthesize BODIPY dyes. The first one includes an acid-catalyzed condensation of the pyrrole and the aromatic aldehyde. This step yields the dipyrromehtane which is air and light sensitive and is used immediately after preparation. Subsequent oxidation using DDQ (2,3-dichloro-5,6-dicyano-p-benzoquinone) or p-chloranil

(2,3,5,6-tetrachloro-p-benzoquinone) and complexation with boron trifluoride etherate yields the new fluorophore.

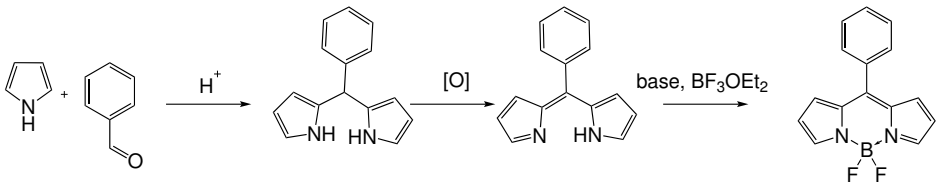

Figure 2.19: General synthesis of a BODIPY dye

The second route consists of the condensation of an acylium equivalent with a pyrrole. This acylium equivalent can either be an orthoester, an acid chloride or an acid anhydride. Here also the formation of asymmetric BODIPYs is possible due to the combination of the isolated acylpyrrole with a second pyrrole moiety in an acidic condensation.

An alternative to this route is to use only one pyrrole and phosphorus oxychloride for the condensation [36].

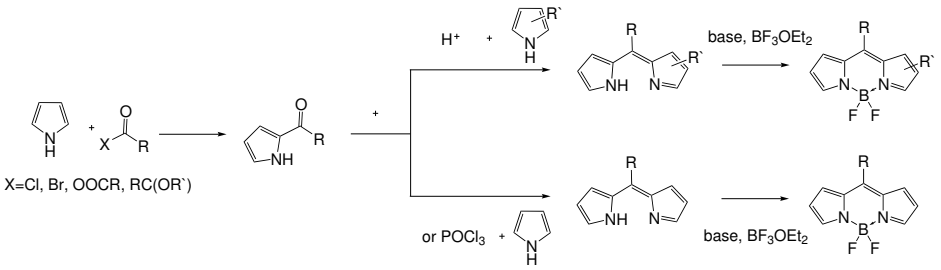

Figure 2.20: BODIPY synthesis via the acylation of pyrrole with subsequent condensation and complexation

3 Experimental

3.1 Materials and Methods

3.1.1 Chromatography

Thin Layer Chromatography

For thin layer chromatography silica gel plates from *Merck* (*silica gel* 60 F_{254} aluminium sheets 20x20) as well as aluminium oxide plates from *Machery-Nagel* (*aluminium oxide* 90 neutral F_{254}) were used. As detection methods UV – detection (at $\lambda = 254$ and 366 nm) as well as ninhydrin, $KMnO_4$ and CAM staining with subsequent developing by hot air stream were used.

Flash Column Chromatography

Silica gel from *Acros Organics* (silica gel, for chromatography 0.035 – 0.070 mm, 60 Å, nitrogen flushed) and aluminium oxide from *Merck* (aluminium oxide, 90 neutral, activity I) were used as stationary phase in preparative flash column chromatography. The amount of stationary phase used was chosen depending on the specific separation problem (100 fold of the amount of crude product).

3.1.2 Chemical Dye Characterization

Nuclear Magnetic Resonance Spectroscopy

^{1}H, COSY and ^{13}C NMR spectra were recorded on a 300 MHz instrument from Bruker (AVANCE III). The analysis of the data was conducted with MNova NMR software. The chemical shifts were reported using the residual signal of the used solvent as an internal standard.

Mass Spectrometry

Mass spectrometry was performed on a *Micromass TofSpec 2E Time-of-Flight Mass Spectrometer* (Bruker Ultraflex Extreme) by Ing. Karin Bartl at the Institute for Chemistry and Technology of Materials at the TU Graz. External calibration was done by using Poly(ethyleneglycol) standards in a suitable mass range. Data analysis was conducted with *MassLynx™V4.1* software from *Waters*.

3.1.3 Optical Dye Characterization

Absorption

Absorption measurements were performed on a *Varian Cary 50* UV-VIS spectrometer in 10 mm precision cuvettes by *Hellma Analytics* (Type 100-OS and 104-OS). The UV-VIS spectrometer was set at a fast scan rate using baseline correction with an adequate blank sample. The molar absorption coefficient were calculated using Lambert-Beers law.

$$A(\lambda) = c \cdot l \cdot \varepsilon(\lambda) \tag{3.1}$$

A is the absorption, l the length of the cuvette (1 cm), c the concentration of the dye solution in $mol \cdot L^{-1}$ and ε the molar absorption coefficient in $L \cdot mol^{-1} cm^{-1}$.

Emission and Excitation Spectra

Emission and excitation spectra were recorded on a *FluoroLog®3* spectrofluorometer by *Horiba Scientific* equipped with a *R2658* photomultiplier by *Hamamazu* or on a *Hitachi-F-700* fluorescence spectrophotometer. For the measurment, 10 mm fluorescence cuvettes from *Hellma Analytics* (Type 100-QS) were used.

Quantum Yield

Quantum yield of the indicator in sensor foils (at 1000 mM NaCl and 0.1 M aqueous HCl) and in solution (THF in presence of 0.3 mM trifluoroacetic acid) were determined with an integrating sphere based set-up from *Horiba Scintific* on a *FluoroLog®3* spectrofluorometer. A neutral density filter (5 % transmission) was placed in front of the detecter.

Lifetime

The single photon counting lifetimes were recorded on a *FluoroLog®3*. For data analysis the *DAS-6 Analysis* software was used. Excitation was performed with a *NanoLED* (λ= 635 nm)controlled by a *Delta Hub* module. Data were fitted using a mono-exponential fit.

3.1.4 Calibration

Calibrations were performed on a *FluoroLog®3* spectrofluorometer by *Horiba Scientific* by fixing a sensor foil diagonally in a quartz cuvette filled with different buffer solutions. Calibrations in solution were also measured on the *Hitachi-F-7000* spectrofluorometer.

3.2 Synthesis

3.2.1 Synthesis of triethylene glycol ditosylate (3)

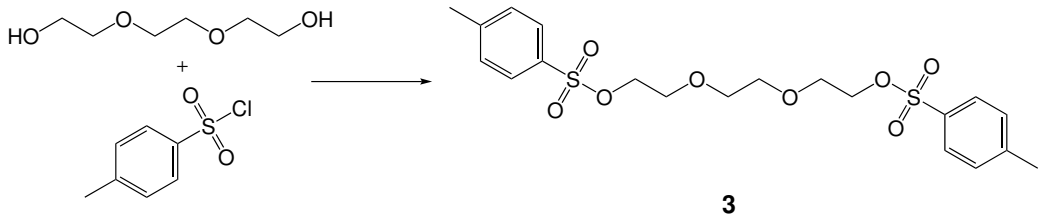

Figure 3.1: Reaction scheme for the synthesis of compound **(3)**

Triethylene glycol (1 eq., 30.0 mmol, 4.50 g) and 4-toluenesulfonyl chloride (2.1 eq., 61.8 mmol, 11.80 g) were dissolved in 100 ml dichloromethane. The solution was cooled down to 0 °C and portions of KOH (8.1 eq., 242.3 mmol, 13.60 g) were added slowly over a period of 15 min and then allowed to warm up to RT for 4 hours. H_2O (60 ml) was added and the reaction mixture was extracted into organic phase (DCM, 2x, 30 ml). The organic phase was dried over Na_2SO_4 and the solvent was removed using a rotary evaporator. The crude product was recrystallized from methyl tert-butyl ether (MTBE) to yield a white crystalline product (10.40 g, 75 %).

^{1}H NMR (300 MHz, $CDCl_3$) δ 7.79 (δ, J = 8.2 Hz, 4H), 7.34 (δ, J = 7.9 Hz, 4H), 4.16 – 4.11 (m, 4H), 3.67 – 3.63 (m, 4H), 3.52 (s, 4H), 2.44 (s, 6H). ^{13}C NMR (76 MHz, $CDCl_3$) δ 145.02, 130.02, 128.13, 70.87, 69.37, 68.93, 21.81.

3.2.2 Synthesis of 5-chloro-3-phenyl-1,4-dihydroindeno[1,2-b]pyrrole (6)

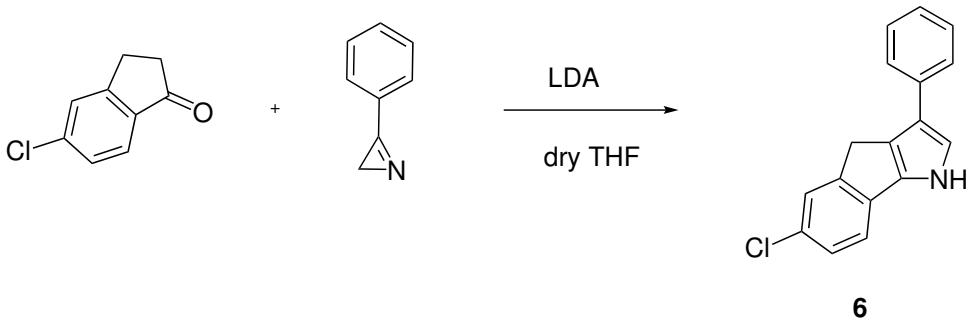

Figure 3.2: Reaction scheme for the synthesis of compound **(6)**

1.01 g of 5-chloro-1-indanone (1 eq., 6.08 mmol) was dissolved in dry THF (12 ml) in a Schlenk tube under inert conditions. Then LDA (1.2 eq., 7.3 mmol, 3.7 ml) and 3-phenyl-2H-azirene (1.2 eq., 7.3 mmol, 0.8 ml) were added dropwise to the reaction solution at -78 °C. The mixture was stirred for 4 hours at -78 °C and afterwards it was quenched with H_2O and neutralized

with HCl (1 M) to a pH of 7. THF was removed using a rotary evaporator and afterwards the product was extracted with DCM (3x). The organic phase was dried over Na_2SO_4 before removing the solvent under vacuum. The crude product was recrystallized from CH to yield the product as white crystals (0.74 g, 46 %).

3.2.3 Synthesis of N,N-bis(2-hydroxyehtyl)-2-methoxyaniline (2)

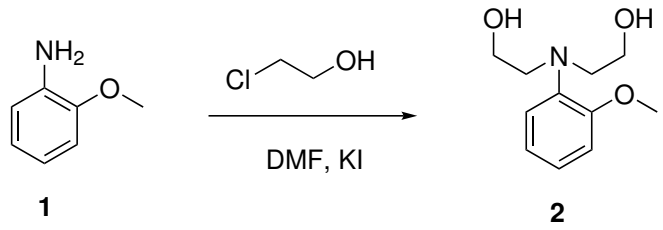

Figure 3.3: Reaction scheme of compound **(2)**

A mixture of 2-anisidine **(1)** (1 eq., 0.177 mol, 21.84 g), 2-chloroethanol (5 eq., 0.655 mol,52.8 g), KI (0.07 eq., 0.013 mol, 2.27 g) and $CaCO_3$ (1 eq., 0.177 mol, 17.75 g) was stirred in 300 ml H_2O at 90 °C until TLC indicated full conversion (eluent: CH/EA, 1/2). The reaction mixture was filtered and the filtrate was then extracted with DCM. The organic phase was dried over Na_2SO_4 before removing the solvent in vacuo. The product was purified using column chromatography on silica gel (eluent DCM to EA, EA/MeOH, 90/10) to yield the product as brown oil (15.36 g, 40.9 %).

^{1}H NMR (300 MHz, CD_2Cl_2 δ 7.25 – 7.08 (m, 2H), 7.02 – 6.90 (m, 2H), 3.85 (s, 3H), 3.50 – 3.44 (m, 4H), 3.20 – 3.15 (m, 4H), 3.10 (bs, 2H). ^{13}C NMR (76 MHz, CD_2Cl_2) δ 155.84, 138.90, 125.99, 125.24, 121.78, 112.08, 60.10, 57.60, 55.87.

3.2.4 Synthesis of 2-methoxyphenylaza-15-crown (4)

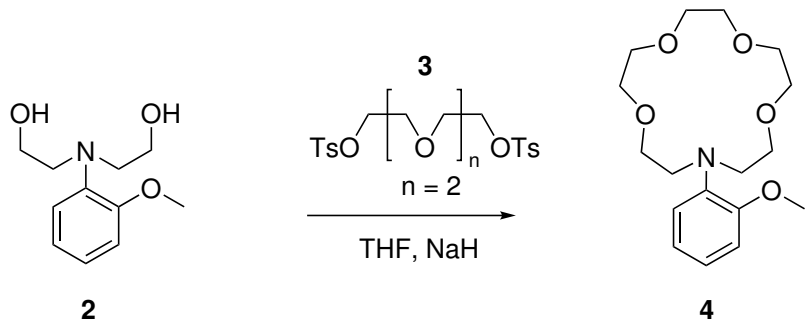

Figure 3.4: Reaction scheme for the synthesis of compound **(4)**

N,*N*-bis(2-hydroxylethyl)-2-methoxyaniline **(2)** (1 eq., 31.8 mmol, 6.719 g) was dissolved in anhydrous THF (150 ml). Then, NaH (2.5 eq., 81.0 mmol, 3.243 g of 60 % NaH suspension in mineral oil) was slowly added to this solution under an argon counterflow. This mixture was heated at reflux and a solution of triethylene glycol ditosylate **(3)** (1 eq., 31.8 mmol, 14.66 g) was added dropwise over a period of 30 min and was heated at reflux for 18 h. After cooling down, the suspension was filtered and the solvent was removed under reduced pressure. The residue was dissolved in MeOH (20 ml) and was again heated to reflux and $NaClO_4 \cdot H_2O$ (1.08 eq., 34.45 mmol, 4.84 g) dissolved in 10 ml MeOH was added. After 30 min, EA (20 ml) was added and the solution was concentrated to a volume of 10 ml on the rotary evaporator. This suspension was refluxed and EA was added until a total volume of 450 ml. The clear solution was then put in the fridge for 18 hours. The obtained white crystals were filtered, dried in an oven and then dissolved in DCM (10 ml) and extracted with H_2O (3x 10 ml) to obtain the free crown (2.80 g, 27 %).

^{1}H NMR (300 MHz, $CDCl_3$) δ 7.12 (dd, J = 7.5, 2.0 Hz, 1H), 6.98 – 6.81 (m, 3H), 3.83 (s, 3H), 3.73 – 3.64 (m, 16H), 3.52 – 3.44 (m, 4H). ^{13}C NMR (76 MHz, $CDCl_3$) δ 152.78, 140.08, 122.12, 120.84, 120.74, 111.77, 70.97, 70.60, 70.37, 70.18, 55.40, 53.00.

MALDI TOF: m/z: $[MH]^+$ calc.: 326.19, found: 326.20.

3.2.5 Synthesis of 4-formyl-2-methoxyphenylaza-15-crown-5 (5)

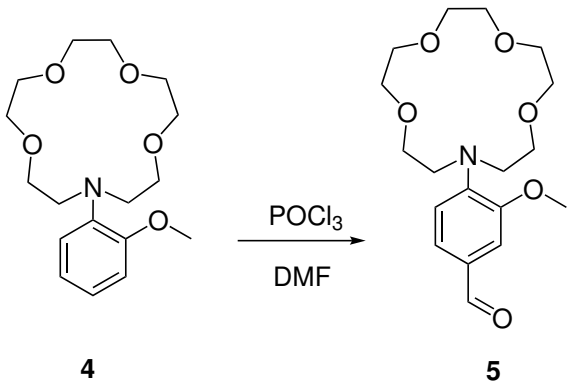

Figure 3.5: Reaction scheme for the synthesis of compound **(5)**

2-Methoxyphenylaza-15-crown-5 **(4)** (1 eq., 7.7 mmol, 2.51 g) was dissolved in DMF (4 ml) in a Schlenk flask. The mixture was cooled down to -8 °C and $POCl_3$ (2.1 eq., 16.1 mmol, 1.68 g) was added slowly so that the temperature did not raise over 0 °C. Afterwards, the reaction mixture was stirred at RT for 20 hours and was then heated to 60 °C for 2 hours. Aldehyde formation could be seen by TLC (DCM/MeOH, 75/5, dinitrophenylhydrazine (DNP)). The solution was cooled down to RT, poured slowly over ice and neutralized with K_2CO_3 to pH 7.

The reaction mixture was extracted with DCM (3x, 30 ml), the solvent was removed and the product purified by column chromatography (gradually from DCM to DCM/MeOH, 100/5) to yield the product as brown oil (1.12 g, 41 %).

^{1}H NMR (300 MHz, CD_2Cl_2) δ 9.73 (s, 1H), 7.38 – 7.28 (m, 2H), 6.98 (d, J = 8.3 Hz, 1H), 3.84 (s, 3H), 3.72 – 3.64 (m, 4H), 3.62 – 3.55 (m, 15H). ^{13}C NMR (76 MHz, CD_2Cl_2) δ 190.49, 151.36, 146.49, 129.04, 126.71, 116.80, 110.42, 71.3, 70.74, 70.56, 70.32, 55.91, 54.05.

MALDI-TOF: m/z $[MH]^+$ 354.18 calc.:, found 354.19.

3.2.6 Synthesis of the BODIPY Fluoroionophore (Na-FI3)

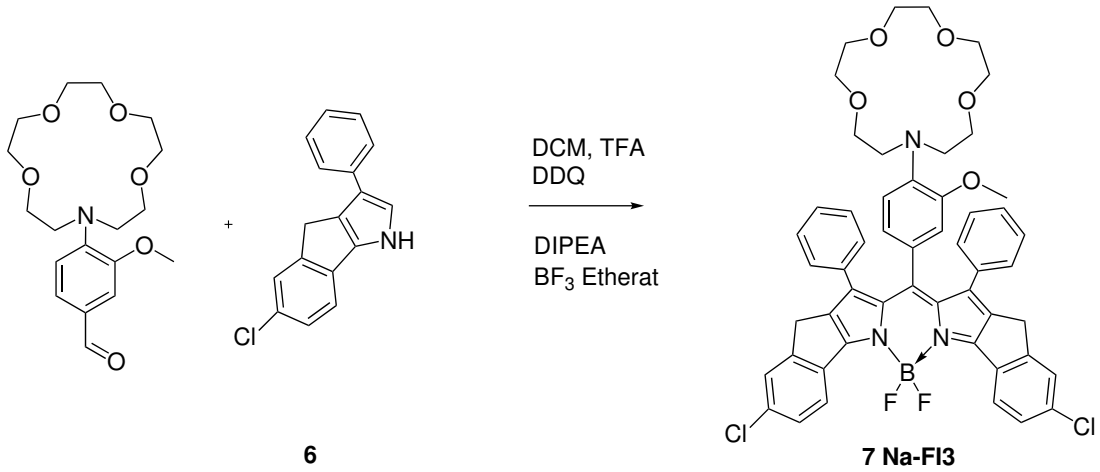

Figure 3.6: Reaction scheme for the synthesis of the BODIPY Fluoroionophore **(Na-FI3)**

4-Formyl-2-methoxyphenylaza-15-crown-5 **(5)** (1 eq., 3.11 mmol, 1.10 g) and 5-chloro-3-phenyl-1,4-dihydroindeno[1,2-b]pyrrole **(6)** (2.05 eq., 6.38 mmol, 1.69 g) were dissolved in anhydrous DCM (5 ml) and 1 drop of trifluoroacetic acid was added. The mixture was stirred at RT for 48 hours under absence of light. Then, DDQ was added (1.04 eq., 3.26 mmol, 0.741 g), changing the colour of the reaction mixture to dark blue. After stirring for another 15 min, DIPEA (10 eq., 31.4 mmol, 4.07 g) and boron trifluoride diethyl etherate (15 eq., 48.6 mmol, 6.9 g) were added under argon counterflow. The reaction mixture was stirred for another 15 minutes and was then extracted with H_2O and DCM, the organic phase was dried over Na_2SO_4 and the solvent was removed. The product was purified by column chromatography on silica gel. (2x, eluent DCM gradually to DCM/ MeOH, 100/5) yielding the product as purple crystals (211 mg, 7.4 %).
UV-VIS (DCM): λ max = 538 nm, ε = 130,000 $M^{-1}cm^{-1}$.

^{1}H NMR (300 MHz, CD_2Cl_2) δ 8.30 (d, J = 8.4 Hz, 2H), 7.54 – 7.45 (m, 4H), 7.05 – 6.83 (m, 10H), 6.66 – 6.58 (m, 2H), 6.39 – 6.31 (m, 1H), 3.82 – 3.45 (m, 27H).

MALDI TOF: m/z: $[MH]^+$ calc.: 912.29, found: 912.30

3.2.7 Synthesis of tetraethylene glycol ditosylate (12)

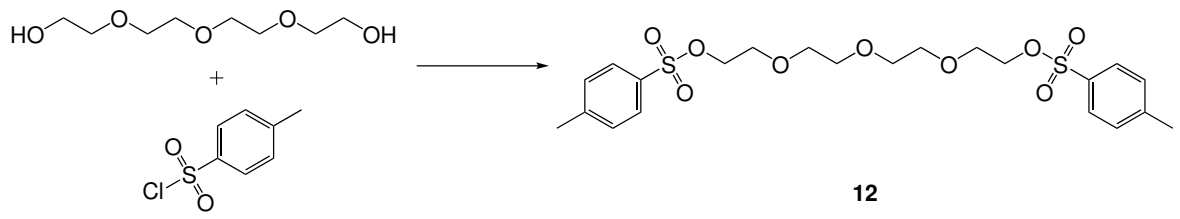

Figure 3.7: Reaction scheme for the synthesis of **(12)**

Tetraethylene glycol (1 eq., 56.64 mmol, 11.0 g) was dissolved in THF (50 ml) and KOH (3.2 eq., 180 mmol, 12.0 g) was added. A solution of 4-toluenesulfonyl chloride (2.1 eq., 61.8 mmol, 11.80 g in 50 ml THF) was added dropwise to the iced cooled reaction over a period of 90 min and it was stirred for another 4 hours at 0 °C and for 18 hours at RT. The resulting suspension was filtered and the product was purified using column chromatography on silica gel (CH/EA, 2/1) to yield the product as a white oil (23.1 g, 81 %).

^{1}H NMR (300 MHz, $CDCl_3$) δ 7.79 (d, J = 8.1 Hz, 1H), 7.33 (d, J = 7.9 Hz, 1H), 4.18 – 4.11 (m, 1H), 3.67 (dd, J = 5.7, 3.8 Hz, 1H), 3.56 (s, 2H), 2.44 (s, 1H). ^{13}C NMR (76 MHz, CD_2Cl_2) δ 145.61 , 133.46 , 130.40 , 128.36 , 71.12 , 70.94 , 70.05 , 69.09 , 21.88 .

3.2.8 Synthesis of 1-((2-methoxyethoxy)methyl)-2-nitrobenzene (9)

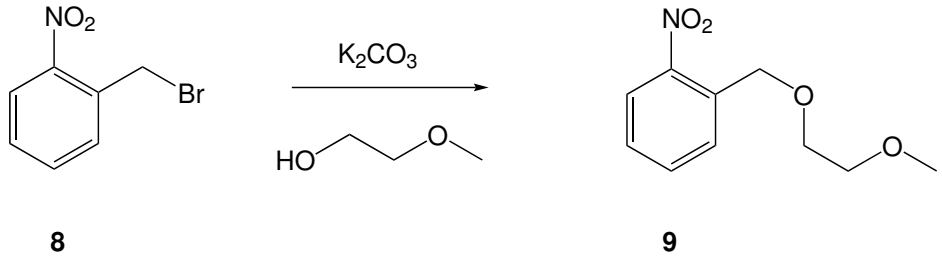

Figure 3.8: Reaction scheme for the synthesis of compound **(9)**

4.15 g of 2-nitrobenzyl bromide **(8)** (1 eq., 19.21 mmol) and 6.64 g of K_2CO_3 (2.5 eq., 48.01 mmol) were dissolved in 24 ml 2-methoxyehanol (16 eq., 307 mmol). The reaction solution was stirred for 3 h at RT and the mixture was then extracted with CH_2Cl_2 (3x). The combined organic phases were dried over Na_2SO_4, concentrated in vacuo, and the residue was purified using column chromatography on silica gel (CH/EA, 8/1, v/v) to yield the product as a brown oil (3.36 g, 82 %).

^{1}H NMR (300 MHz, $CDCl_3$) δ 8.05 (d, J = 7.6 Hz, 1H), 7.83 (d, J = 7.6 Hz, 1H), 7.63 (t, J = 7.3 Hz, 1H), 7.42 (t, J = 7.6 Hz, 1H), 4.94 (s, 2H), 3.73 (d, J = 8.8 Hz, 2H), 3.69 –

3.58 (m, 2H), 3.40 (s, 3H). ^{13}C NMR (76 MHz, $CDCl_3$) δ 135.24 , 133.76 , 128.87 , 128.01 , 124.72 , 71.94 , 70.58 , 69.87 , 59.21 .

3.2.9 Synthesis of 2-((2-methoxyethoxy)methyl)aniline (10)

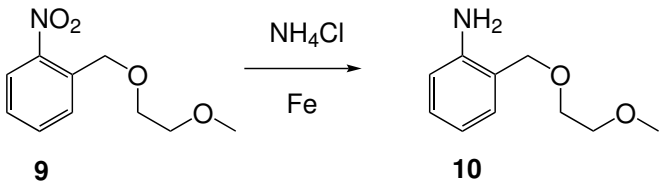

9 **10**

Figure 3.9: Reaction scheme for the synthesis of compound **(10)**

2.64 g iron powder (47.35 mmol) and 0.39 ml of concentrated HCl (4.73 mmol,) were added to EtOH (15 ml) and the suspension was stirred at 65 °C for 2 h. Then 25 % aqueous NH_4Cl solution was added and afterwards 2.0 g of compound **(9)** (9.47 mmol) was added in portions over a period of 30 min. The reaction mixture was stirred for additional 40 min. Ethanol (20 ml) and celite were added and then the reaction mixture was filtered over a pad of celite with suction. The solvent was then removed, saturated $NaHCO_3$ was added and the reaction mixture was extracted with EA (2x). The organic layer was dried over Na_2SO_4, the solvent was removed and the product was purified using column chromatography on silica gel (CH/EA, 6/1, v/v) to yield the product as a brown oil (1.62 g, 94 %)

^{1}H NMR (300 MHz, $CDCl_3$) δ 7.18 – 7.01 (m, 2H), 6.74 – 6.61 (m, 2H), 4.57 (s, 2H), 4.18 (s, 2H), 3.61 – 3.52 (m, 4H), 3.38 (s, 3H). ^{13}C NMR (76 MHz, $CDCl_3$) δ 146.57 , 130.04 , 129.34 , 121.96 , 117.67 , 115.75 , 72.36 , 71.81 , 68.56 , 58.92 .

3.2.10 Synthesis of N,N-bis(2-hydroxyethyl)-2-methoxyethoxymethylaniline (11)

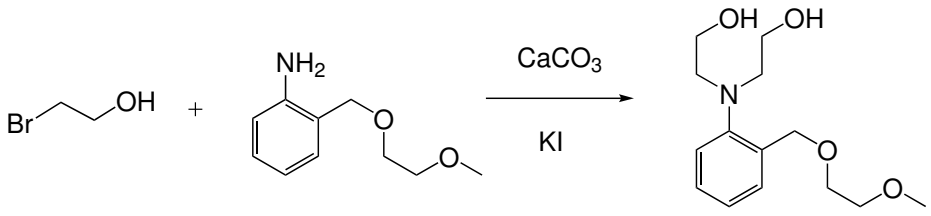

10 **11**

Figure 3.10: Reaction scheme for the synthesis of compound **(11)**

A mixture of compound **(10)** (1 eq., 22.73 mmol, 4.12 g), 2-bromoethanol (3 eq., 68.2 mmol, 4.83 ml), KI (1.5 eq., 34.1 mmol, 6.83 g) and $CaCO_3$ (3 eq., 68.2 mmol, 6.83 g) was stirred in H_2O (60 ml) at 60 °C for 2 days until TLC indicated full conversion (eluent: EE). The reaction mixture was filtered and the filtrate was then extracted with DCM. The organic phase was dried over Na_2SO_4 and the solvent was removed under reduced pressure. The product was purified using column chromatography on silica gel (EA/MeOH, 99/1) to yield the product as a brown oil (4.48 g, 73 %).

^{1}H NMR (300 MHz, CD_2Cl_2) δ 7.31 – 7.19 (m, 3H), 7.10 – 7.01 (m, 1H), 4.54 (s, 2H), 3.65 – 3.57 (m, 2H), 3.57 – 3.50 (m, 2H), 3.47 – 3.37 (m, 6H), 3.23 (s, 3H), 3.00 (t, J = 5.2 Hz, 4H). ^{13}C NMR (76 MHz, CD_2Cl_2) δ 151.65 , 136.12 , 132.00 , 130.00 , 125.66 , 125.30 , 72.19 , 71.17 , 70.07 , 59.98 , 59.15 , 58.01 .

3.2.11 Synthesis of N-(((2-methoxyethoxy)methyl)phenyl)1-aza-[18]crown-6 ether (13)

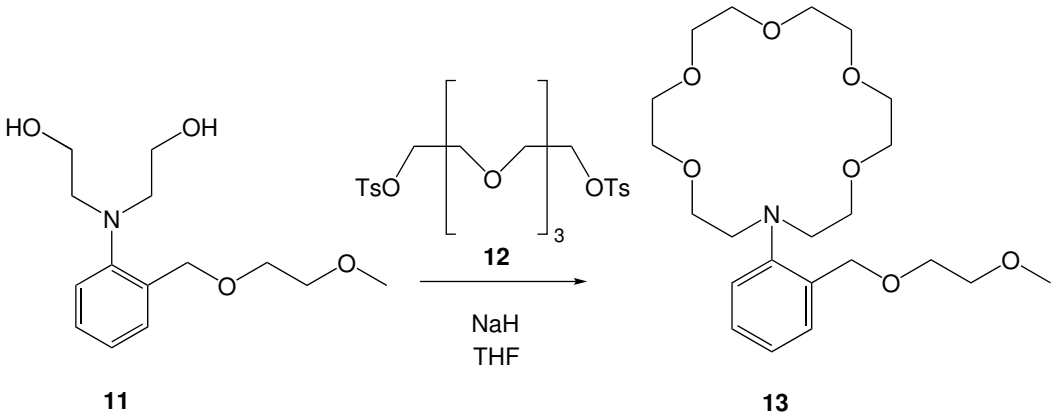

Figure 3.11: Reaction scheme for the synthesis of compound **(13)**

Compound **(11)** (1 eq., 14.07 mmol, 3.79 g) was dissolved in anhydrous THF (100 ml). NaH (2.2 eq., 32.0 mmol, 0.74 g of 60 % NaH suspension in mineral oil) was added slowly to this solution under an argon counterflow. This mixture was heated at reflux and a solution of tetraethylene glycol ditosylate **(12)** (1 eq., 14.07 mmol, 7.07 g) was added dropwise over a period of 30 min and was heated at reflux overnight. After cooling down, the suspension was filtered and the solvent was removed under reduced pressure. The residue was dissolved in MeOH (20 ml) and was again heated to reflux and $NaClO_4 \cdot H_2O$ (1 eq., 14.07 mmol, 1.98 g) dissolved in 10 ml MeOH was added. After 1 hour, EA (20 ml) was added and the solution was concentrated to a volume of 10 ml on the rotary evaporator. This suspension was refluxed and EA (100 ml) was added. The obtained white crystals were filtered and dissolved in DCM (10 ml) and extracted with H_2O (3x 10 ml) to obtain the free crown (0.65 g, 11 %).

^{1}H NMR (300 MHz, $CDCl_3$) δ 7.52 – 7.45 (m, 1H), 7.31 – 7.20 (m, 2H), 7.15 – 7.06 (m, 1H), 4.67 (s, 2H), 3.76 – 3.56 (m, 20H), 3.51 (t, J = 5.9 Hz, 4H), 3.40 (s, 3H), 3.29 (t, J = 5.9 Hz, 4H). ^{13}C NMR (76 MHz, CD_2Cl_2) δ 152.62 , 135.12 , 133.24 , 130.82 , 126.27 , 124.68 , 72.18 , 70.53 , 70.48 , 70.18 , 69.92 , 69.50 , 69.33 , 67.92 , 59.41.

MALDI TOF: m/z: $[MH]^+$ calc.: 428.26, found: 428.24

3.2.12 Synthesis of N-(4-formyl-((2-methoxyethoxy)methyl)phenyl)-1-aza-[18]crown-6 ether (14)

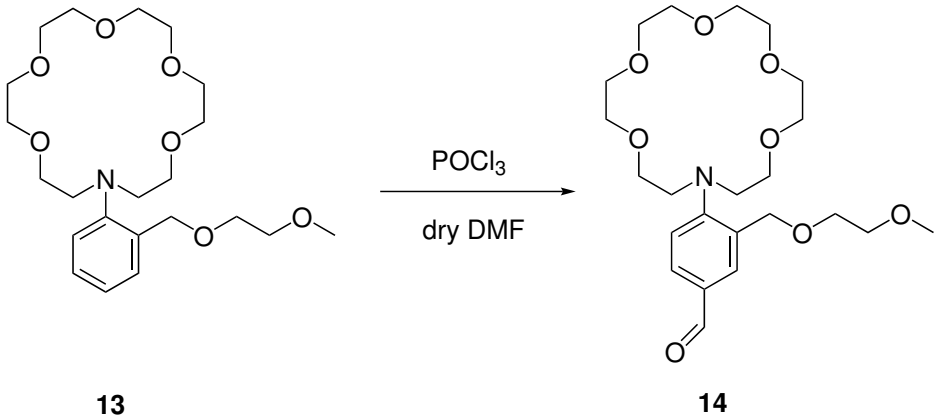

Figure 3.12: reaction scheme for the synthesis of compound **(14)**

Compound **(13)** (1 eq., 1.1 mmol, 0.47 g) was dissolved in DMF (2 ml) in a Schlenk flask. The mixture was cooled down to -8 °C and $POCl_3$ (5 eq., 5.5 mmol, 0.51 ml) was added slowly so that the temperature did not raise over 0 °C. Afterwards, the reaction mixture was stirred at RT for a day and was then heated to 60 °C for 1 hour. The reaction solution was then poured slowly over ice and neutralized with Na_2CO_3 to pH 7. The reaction mixture was extracted with DCM, the solvent was removed and the product purified by column chromatography (gradually from DCM to DCM/MeOH, 100/5) to yield the product as a brown oil (0.18 g, 36 %).

^{1}H NMR (300 MHz, CD_2Cl_2) δ 9.88 (s, 0H), 7.93 (d, J = 2.1 Hz, 0H), 7.72 (dd, J = 8.4, 2.2 Hz, 0H), 7.34 (d, J = 8.4 Hz, 0H), 4.58 (s, 1H), 3.70 – 3.60 (m, 3H), 3.55 (dt, J = 8.9, 3.6 Hz, 5H), 3.43 (d, J = 5.7 Hz, 1H), 3.35 (s, 1H). ^{13}C NMR (76 MHz, CD_2Cl_2) δ 156.31 , 133.75 , 132.40 , 131.45 , 129.51 , 122.38 , 72.48 , 71.21 , 71.10 , 71.07 , 70.85 , 70.47 , 69.96 , 69.71 , 59.24.

MALDI TOF: m/z: $[MH]^+$ calc.: 456.25, found: 456.27.

3.2.13 Synthesis of the BODIPY Fluoroionophore (K^{2nd}-FI3) (15)

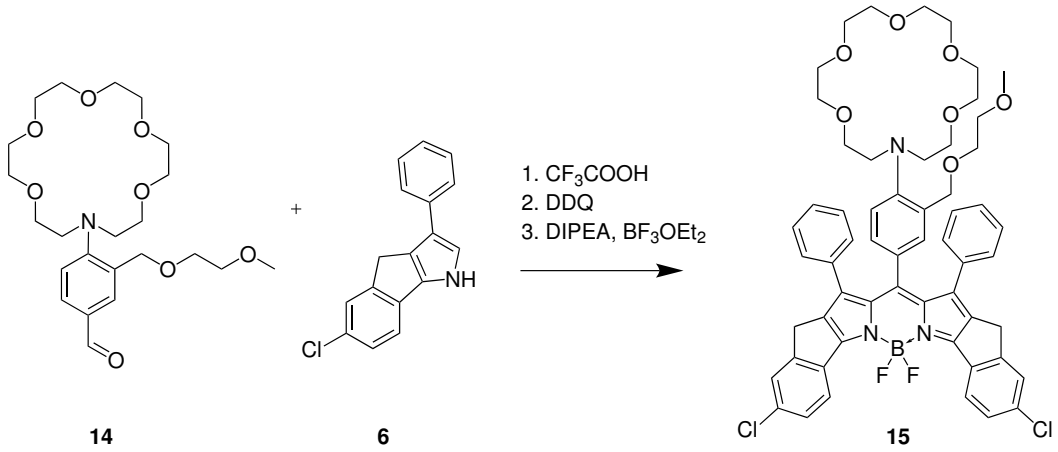

Figure 3.13: Reaction scheme for the synthesis ofcompound **(15)**

Compound **(14)** (1 eq., 0.35 mmol, 0.16 g) and 5-chloro-3-phenyl-1,4-dihydroindeno[1,2-b]pyrrole **(6)** (2.00 eq., 0.70 mmol, 0.19 g) were dissolved in anhydrous DCM (10 ml) and 2 drops of trifluoroacetic acid was added. The mixture was stirred at RT for 48 hours under absence of light. DDQ was added (1.5 eq., 0.35 mmol, 0.80 g), changing the colour of the reaction mixture to dark blue. After stirring for another 15 min, DIPEA (10 eq., 35.0 mmol, 0.60 ml) and boron trifluoride diethyl etherate (10 eq., 35.0 mmol, 0.37 ml) were added under argon counterflow. The reaction mixture was stirred for another 15 minutes and was then extracted with H_2O and DCM, the organic phase was dried over Na_2SO_4 and the solvent was removed. The product was purified by column chromatography on aluminium oxide. (2x, eluent DCM gradually to DCM/ MeOH, 100/4) yielding the product as blue-green powder (24 mg, 6.7 %). For this structure no proper NMR-spectrum could be observed. Substance identification was confirmed by mass spectrometry.

MALDI TOF: m/z: $[MH]^+$ calc.: 1014.36, found: 1014.38.

3.2.14 Synthesis of TAC-CHO (19)

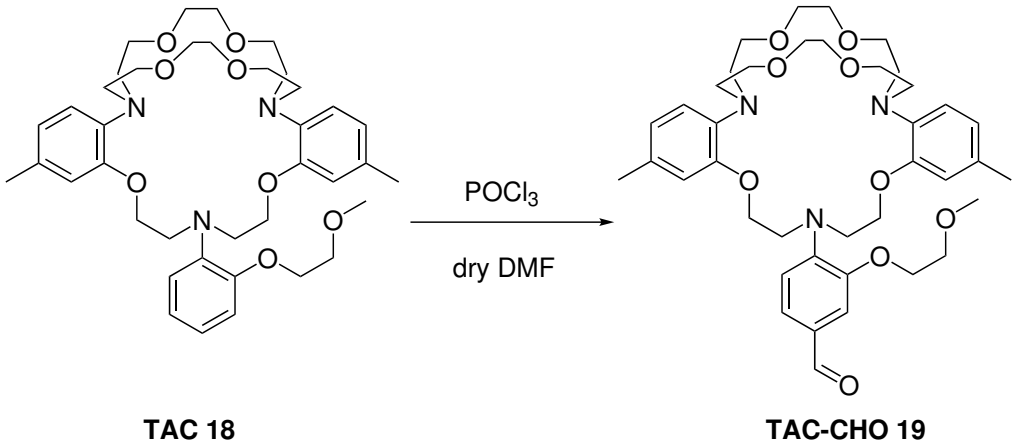

Figure 3.14: reaction scheme for the synthesis of compound **(19)**

1.06 g of the TAC crown (friendly gift from Dr. Huarui He) (1 eq., 1.53 mmol) was dissolved in dry DMF (3 ml) in a Schlenk flask. The mixture was cooled down to -8 °C and $POCl_3$ (5 eq., 7.7 mmol, 0.7 ml) was added slowly so that the temperature did not raise over 0 °C. Afterwards, the reaction mixture was stirred at RT for a day and was then heated to 60 °C for 3 hours. The reaction solution was then poured slowly over ice and neutralized with Na_2CO_3 to pH 7. The reaction mixture was extracted with DCM, the solvent was removed and the product purified by column chromatography (gradually from DCM to DCM/MeOH, 100/5) to yield the product as brown oil (0.73 g, 65 %).

^{1}H NMR (300 MHz, $CDCl_3$) δ 9.76 (s, 1H), 7.40 – 7.32 (m, 2H), 7.13 – 7.04 (m, 1H), 6.87 (d, J = 7.9 Hz, 2H), 6.66 (d, J = 8.4 Hz, 2H), 6.60 (s, 2H), 4.27 – 4.07 (m, 9H), 3.84 – 3.57 (m, 18H), 3.50 – 3.21 (m, 12H), 2.24 (s, 6H), 1.78 (s, 2H).

MALDI TOF: m/z: $[MH]^+$ calc.: 722.39, found: 722.38.

3.2.15 Synthesis of the TAC-BODIPY Fluoroionophore (TAC-FI3) (20)

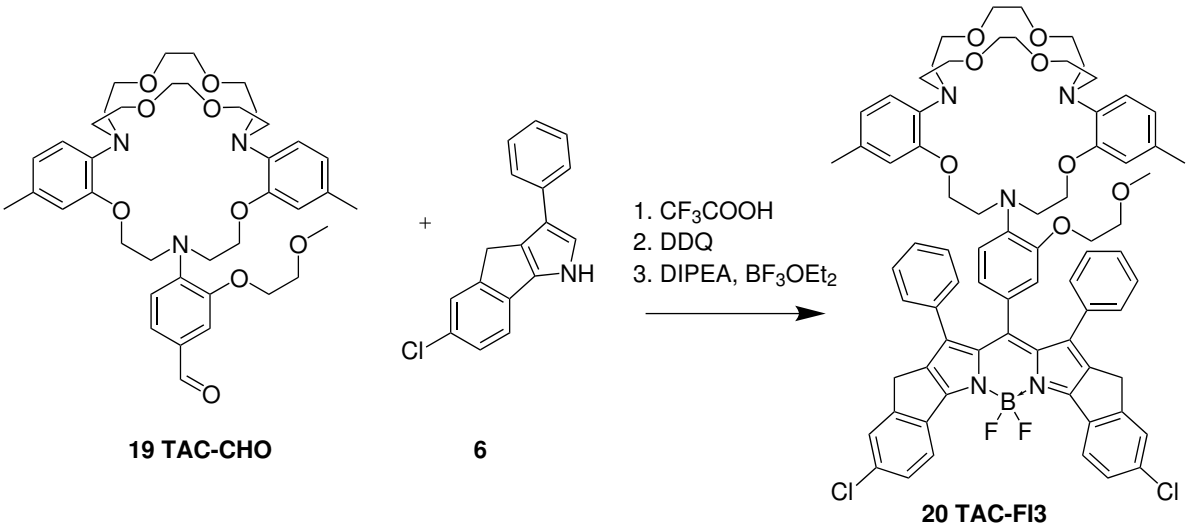

Figure 3.15: Reaction scheme for the synthesis of compound **(20)**

TAC-CHO **(19)** (1 eq., 0.34 mmol, 0.25 g) and 5-chloro-3-phenyl-1,4-dihydroindeno[1,2-b]pyrrole **(6)** (2.00 eq., 0.69 mmol, 0.18 g) were dissolved in anhydrous DCM (10 ml) and 2 drops of trifluoroacetic acid was added. The mixture was stirred at RT for 3 days under exclusion of light. DDQ was added (1 eq., 0.34 mmol, 0.78 g), changing the colour of the reaction mixture to dark blue. After stirring for another 15 min, DIPEA (10 eq., 34.0 mmol, 0.60 ml) and boron trifluoride diethyl etherate (10 eq., 34.0 mmol, 0.42 ml) were added under argon counterflow. The reaction mixture was stirred for another 15 minutes and was then extracted with H_2O and DCM, the organic phase was dried over Na_2SO_4 and the solvent was removed. The product was purified by column chromatography on silica gel. (2x, eluent DCM gradually to DCM/ MeOH, 100/5) as blue-green crystals (28 mg, 6.3 %). For this structure no proper NMR-spectrum could be observed. Substance identification was confirmed by mass spectrometry.

MALDI TOF: m/z: $[MH]^+$ calc.: 1280.50, found: 1280.47.

3.3 Preparation of Sensor Foils

3.3.1 Preparation of Sodium-sensitive Sensor Foils

Stock solutions of Hydrogel polymers (Hydromed D1, D4 and D7) were prepared (10 w%). Therefore the appropriate amount of Hydrogel polymer was dissolved in THF. 0.2 wt. % and 1 wt. % dye "cocktails" related to the amount of polymer were knife coated (25 μm wet film) onto dust-free polyethylene terephthalate foils and were allowed to dry for several hours at RT. For the leaching experiment the dye concentration was 1 wt.% and for calibrations and QY determination the dye concentration were 0.2 wt.%.

Table 3.1: Weighed portions of Na-FI3 for "cocktail" preparation

dye [mg]	dye [w%]	Polymer [w%]	Polymer Stock to add [g]	Used Polymer
0.29	0.2	10	1.445	D1
0.32	0.2	10	1.582	D4
0.34	0.2	10	1.709	D7
0.35	1	10	0.346	D1

3.3.2 Preparation of sensor foil for ratiometric DLR readout

The reference layer was prepared using a dye "cocktail" with 12 mg Egyptian Blue and 100 mg polysulfon in 888 mg $CHCl_3$. This was knife coated (25 μm wet film) on dust-free polyethylene terephthalate support foils and was allowed to dry in the oven at 60 °C for 2 hours. The "cocktail" for the first sensing layer was prepared by dispersing 0.5 mg of Na-FI3, 100 mg diamond powder and 100 mg hydrogel D1 in 566 mg THF. The cover layer was prepared by dispersing 0.5 mg Na-FI3, 100 mg carbon black and 100 mg hydrogel D1 in 566 mg THF. Both "cocktails" were knife coated onto the back-side of the polyethylene terephthalate support foil and were allowed to dry for 2 hours at RT. A sensor spot was then either stamped out (5 mm diameter) and glued on a plastic screw cap or stamped out (2 mm diameter) and fixed with a metal cap on a 1 m PMMA fiber.

3.3.3 Preparation of Potassium Sensor Foils

Sensor foil preparation was performed analogously as described in 3.3.1. Here only 0.2 wt.% dye "cocktails" with Hydromed D4 were prepared. This foils were used for calibration measurements (see section 4.3.4).

Table 3.2: Weighed portions of Na-FI3 for "cocktail" preparation

dye	dye [mg]	dye [w%]	Polymer [w%]	Polymer Stock to add [g]
K^{2nd}-FI3	0.28	0.2	10	1.410
K^{1st}-FI3	0.33	0.3	10	1.660
TAC-FI3	0.25	0.4	10	1.265

4 Results and Discussion

4.1 Synthetic considerations

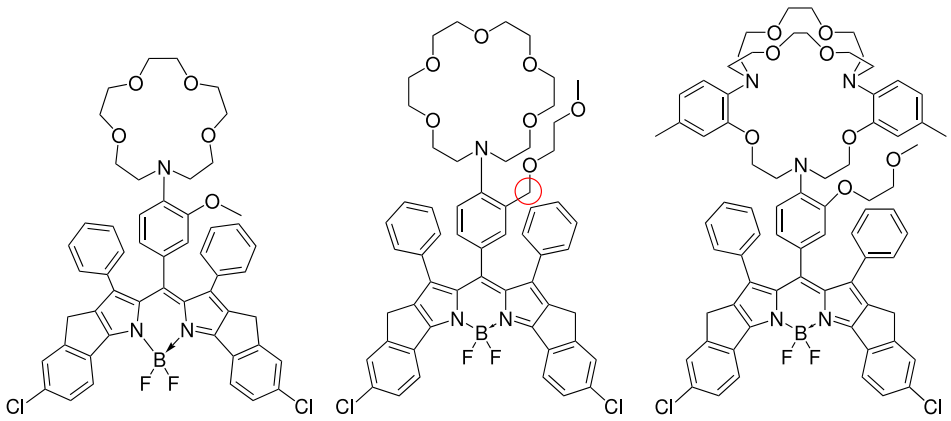

Figure 4.1: overview of the synthesized dyes

The aim of this work was to synthesize new fluoroionophores for potassium and sodium sensing. All of these fluoroionophores consist of two building blocks. The receptor which is the first building block controls the sensitivity of the fluoroionophore. The spectral properties are controlled by the second building block - the chromophore. For all fluoroionophores a rigid BF_2-chelated tetraaryl-BODIPY chromophore was selected since the rigidification and planarization of the chromophore results in a bathochromic shift of absorption and emission and ensures excellent fluorescence brightness compared to other BODIPY chromophores [2]. The absorption and emission bands are very sharp which is typical for BODIPY dyes. The PET efficiency is favourably affected by the introduction of chlorine because the electron withdrawing character enhances the reduction potential of the fluoroionophores in the excited state. Therefore, when no analyte is present the fluorescence is almost completely "switched off". The sodium sensitive dye was synthesized because the determination of sea water salinity can be done by only measuring the sodium content. Despite to a change in seawater salinity, the ratio between the ions remains constant. Thus, enabling the determination of the salinity by simply measuring one ion of the seawater. Typically, it is measured with a conductivity sensor but an optical sensor which detects the Cl^- concentration has already been reported

before [39]. In this thesis it is shown that the determination of seawater can also be done with the detection of sodium. The synthetic route for the sodium receptor was similiar to the literature [29] and is shown in the following chapter.
The task for the potassium sensor was to synthesize different receptors while the chromophore basis remains unchanged. An aza-18-crown-6 with the desired chromophore was already available (K^{1st}-FI3) [2] for the comparison with the new dyes. However, we attempted to improve the complex stability with two new dyes. The first synthesized dye also consisted of an aza-18-crown-6 receptor but compared to the K^{1st} receptor an additional CH_2 group was introduced at the side arm (lariat ether) which might improve the flexibility of this side-chain. Furthermore, the commercially available TAC cryptand was coupled to the same chromophore. The synthetic routes for this dyes are described below.

4.1.1 Synthesis of Na^+ Fluoroionophore (7)

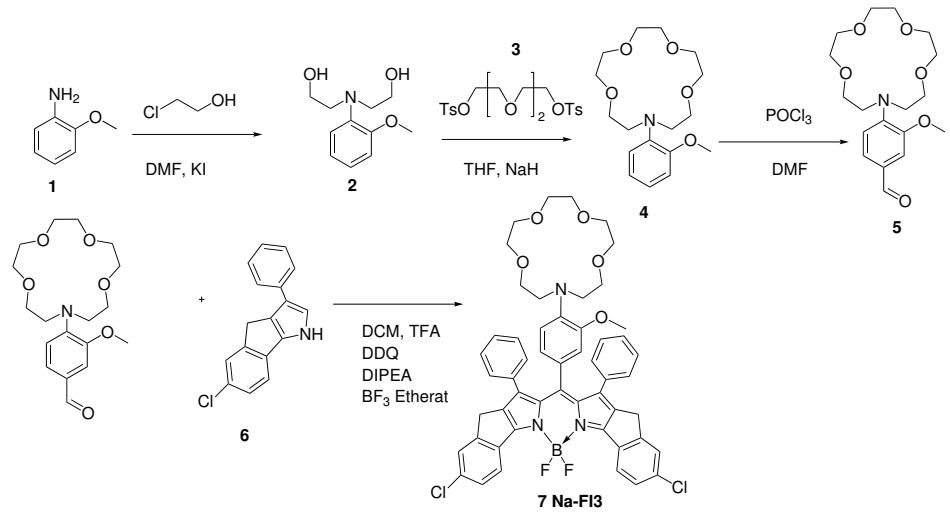

Figure 4.2: synthetic strategy of the formation of Na^+ Fluoroionophore

The synthetic route for the sodium receptor was similiar to the literature [29]. The first step was the alkylation of 2-methoxyaniline **(1)** to N,N-bis(2-hydroxyehtyl)-2-methoxyaniline **(2)**. **(2)** reacts then with triethylene glycol ditosylate **(3)** to yield the crown **(4)**. Compound **(4)** was used as an educt in a Vilsmeier-Haack-Reaction to yield the formylated crown **(5)**. In a simple one-pot reaction the new fluoroionophore **(Na-FI3)** was formed through condensation of the pyrrole **(6)** and the aromatic aldehyde **(5)** with subsequent oxidation using DDQ and complexation with BF_3-etherate.

4.1.2 Synthesis of K^{2nd}-FI3 (15)

For the synthesis of this receptor two different approaches have been tried. In the first approach the crown ether was synthesized in several steps, whereas in the second approach

the commercially available 1-aza-18-crown-6 was attempted to be coupled directly to the phenylring via a Buchwald-Hartwig amination.

4.1.3 Synthesis of K^{2nd}-FI3 (15): First Approach

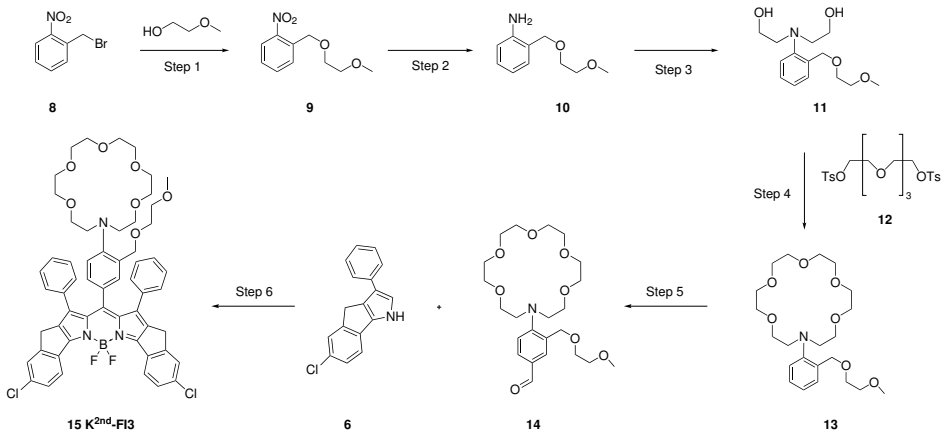

Figure 4.3: synthetic strategy of the formation of **K^{2nd}-FI3 (15)** Fluoroionophore

The synthesis of the new potassium receptor **(13)** started from commercially available nitrobenzylalcohol **(8)** which was alkylated with 2-methoxyethanol to yield the desired product **(9)**. Reduction of this compound and subsequent ring closure step yielded to the new receptor **(13)**. The formylation of compound (13) was performed as described by Ast et al. Condensation of the pyrrole and the aromatic aldehyde, subsequent oxidation using DDQ and complexation with BF_3-etherate yields the fluoroionophore **(K^{2nd}-FI3)** with the new receptor. The successful and unsuccessful attempts are described in the following sections.

Step 1: Synthesis of 1-((2-methoxyethoxy)methyl)-2-nitrobenzene

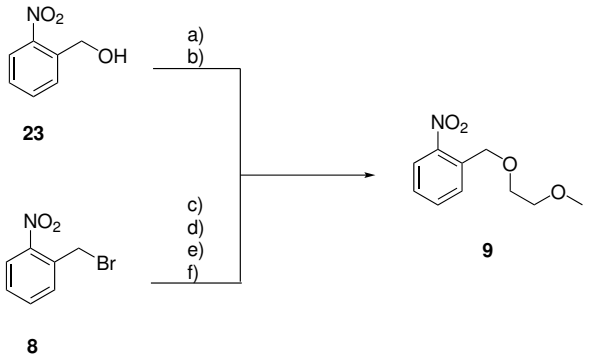

Figure 4.4: Synthesis of compound **(9)**

A few attempts were made to synthesize the side arm with the additional CH_2-bond. At first (2-nitrophenyl)methanol was used as a educt, but reactions with different reagents (see table 4.1) showed no conversion to the desired product. The attempt of using 2-nitrobenzyl bromide with 2-methoxyethanol also failed with sodium, without any base and with K_2CO_3 at higher temperature. Nevertheless, at RT and with K_2CO_3 as a base the reaction worked out in a good yield (82 %).

Table 4.1: Reaction conditions of the alkylation step

#	educt	solvent	T [°C]	reagents	time [h]	yield [%]
a	chloroethylmethylether	DMF	110	K_2CO_3, KI	48	0
b	chloroethylmethylether	DMF	60	NaH	24	0
c	2-methoxyethanol	-	125	Na	3	0
d	2-methoxyethanol	-	125	-	5	0
e	2-methoxyethanol	-	125	-	1	0
f	2-methoxyethanol	-	RT	K_2CO_3	3	82

Step 2: Synthesis of 2-((2-methoxyethoxy)methyl)aniline

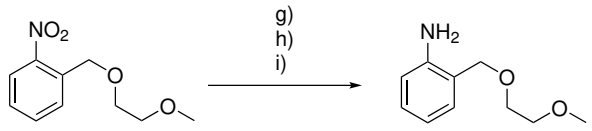

9 **10**

Figure 4.5: Synthesis of compound **(10)**

The reduction of compound **(9)** was done using iron as an reducing agent with different reagents. According to TLC, reduction with iron and AcOH yielded in the formation of many by-products whereas the reduction with Fe and $CaCl_2$ (according to [40]) showed no conversion at all. Only the reduction with Fe, HCl and NH_4Cl which was done according to [41] yielded to the desired product in a good yield (94 %).

Table 4.2: Reaction conditions of the reduction step

#	educt	solvent	T [°C]	reagents	time [h]	yield [%]
g	chloroethylmethylether	AcOH, EtOH	RT	Fe	3	0
h	chloroethylmethylether	H_2O, EtOH	60	Fe, $CaCl_2$	24	0
i	2-methoxyethanol	EtOH	60	Fe, HCl, NH_4Cl	3	94

Step 3: Synthesis of N,N-bis(2-hydroxyethyl)-2-methoxyethoxymethylaniline (11)

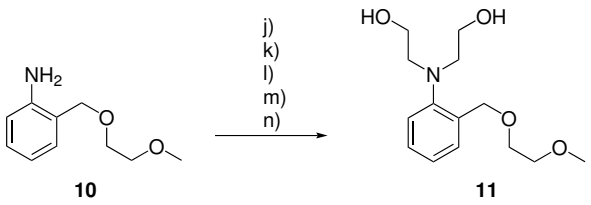

Figure 4.6: Synthesis of compound **(11)**

The synthesis of N,N-bis(2-hydroxyethyl)-2-methoxyethoxymethylaniline occurred via S_N2 reaction. The first attempt (j) of this alkylation was done according to literature [20]. During this reaction and after flash column chromatography only the monosubstituted product could be isolated. Changing the solvent to H_2O led also only to the monosubstituted product. The second attempt via alkylation with 2-(2-bromoethoxy)tetrahydro-2H-pyran and a following deprotection failed already at the first step because too many by-products were formed. In the last attempt, 2-bromoethanol was used instead of 2-chloroethanol as 2-bromoethanol is more reactive because it is a better nucleophile compared to 2-chloroethanol. The reaction solution was stirred at 60 °C in H_2O with $CaCO_3$ as base and after 48 h the desired product was separated via flash column chromatography in a good yield (73 %).

Table 4.3: Reaction conditions for the alkylation of the amin-group

#	educt	solvent	T [°C]	reagents	time [h]	yield [%]
j	2-Chloroethanol	H_2O	80	$CaCO_3$, KI	48	0
k	2-Chloroethanol	DMF	100	$CaCO_3$, KI	48	0
l	2-(2-Bromoethoxy)tetrahydro-2H-pyran	H_2O, EtOH	RT/80	$CaCO_3$, KI	48	0
m	2-(2-Bromoethoxy)tetrahydro-2H-pyran	DMF	60	$CaCO_3$, KI	48	0
n	2-Bromoethanol	H_2O	60	$CaCO_3$, KI	48	73

Step 4+5+6: Synthesis of compound (13), (14) and of K^{2nd}-FI3 (15)

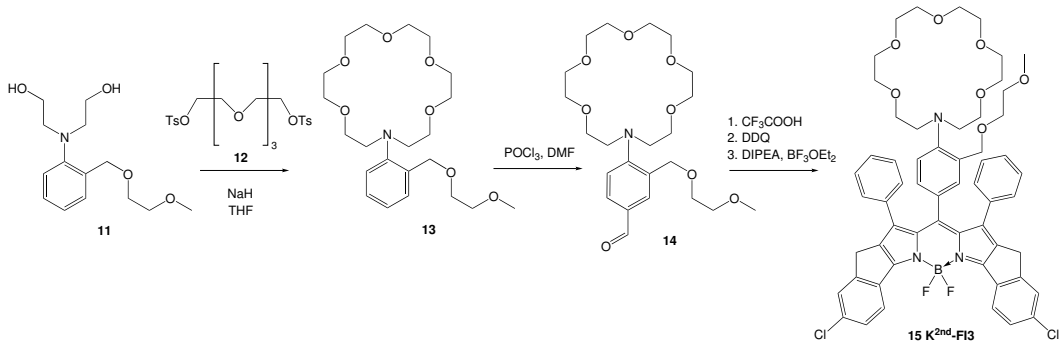

Figure 4.7: Synthesis of compound **(13)**, **(14)** and **(15)**

The ring closure of compound **(11)** and the formylation of compound **(13)** was performed as described by Ast et al. [20]. Both steps worked out well without any further problems. Synthesis of the BODIPY-dye **(15)** was conducted according to Sui et al. [42]. The reaction solution was stirred overnight after the addition of boron trifluoride diethyl etherate. However, in presence of boron trifluoride, ethers can be split up to form esters. This could be seen on the TLC because many spots appeared and neither with flash column chromatography nor with HPLC the product could be separated. For this reason the reaction was done again and after the addition of boron trifluoride diethyl etherate it was only stirred for 15 min. Afterwards the product could be isolated through flash column chromatography ($2x$, aluminium oxide, silicium oxide as stationary phases) (6.7 % yield).

4.1.4 Synthesis of K^{2nd}-FI3 (15): Second Approach

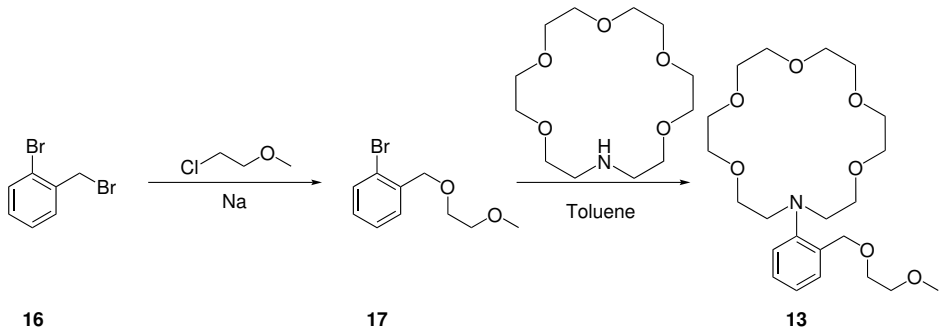

Figure 4.8: second approach for the synthesis compound **(13)**

In figure 4.8 the second approach for the synthesis of compound **(13)** (K^{2nd}-FI3) is shown. The first step was successfully done according to [43] using sodium as a base and 2-methoxyethanol as reagent/solvent. The subsequent step is a Buchwald-Hartwig amination and a few attemps were made with different reaction conditions (table 4.4) to gain the desired product **(13)**. Each of this reaction conditions failed and therefore this step was not further investigated.

Table 4.4: reaction condition for the Buchwald-Hartwig amination

#	T [°C]	reagents	catalyst	ligand	time [h]	yield [%]
o	100	KOtBu	PEPPSI^{TM}-IPr	-	24	0
p	100	NaOtBu	$Pd_2(dba)_3$	SPhos	24	0
q	100	NaOtBu	$Pd_2(dba)_3$	DavePhos	24	0
r	100	KOtBu	$Pd_2(dba)_3$	DavePhos	24	0

4.1.5 Synthesis of TAC-BODIPY Fluoroionophore (TAC-FI3)

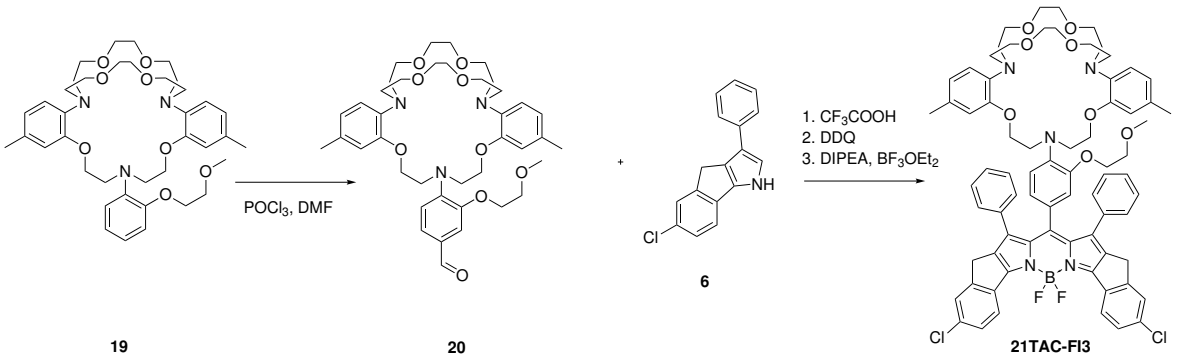

Figure 4.9: Synthesis of the BODIPY-dye **(21)**

The synthesis of the BODIPY-dye **(21)** started from compound **(19)** (friendly gift from Dr. Huarui He) and was done according to [20]. The formation of the BODIPY-dye was conducted according to Sui et al. [42]. The purification of the desired product was challenging due to similar polarity of the educt and the product. The purification was done using flash column chromatography several times.

4.2 Characterization: Sodium Fluoroionophore Na-FI3

4.2.1 Absorption- and Emissionspectra

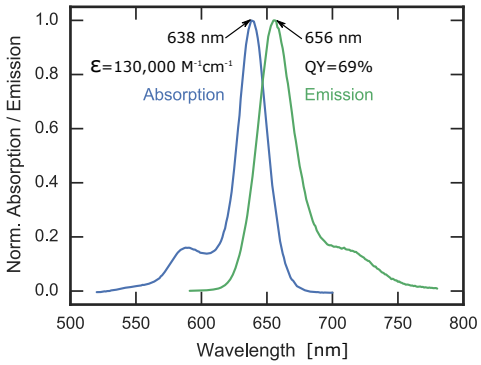

Figure 4.10: Normalized absorption and emission spectra in dichloromethane. Molar absorption coefficient was determined in dichloromethane and the quantum yield in THF with 0.3 mM TFA to ensure full protonation of the crown ether

Absorption and emission spectra are recorded in dichloromethane. As can be seen in figure 4.10 the absorption maximum of Na-FI3 is at 638 nm whereas the emission maxima is at 656 nm. It has an high molar absorption coefficient of about 130,000 M^{-1} cm^{-1} and a quantum yield of 69 % in the "on" state. Typically for BODIPY dyes, the absorption and emission bands are very sharp. Compared to other BODIPY chromophores ([2]) the selected rigid tetraaryl-BODIPY chromophore shifts the emission and absorption spectra bathochromically due to rigidification and planarization. The PET efficiency is favourably affected by the introduction of chlorine because the electron withdrawing character enhances the reduction potential of the fluoroionophores in the excited state. Therefore, when no analyte is present the fluorescence is almost completely “switched off”.

4.2.2 Sensor Material

For the application described in section 4.2.6 it is necessary to immobilize the fluoroionophore into a polymer matrix. A non-covalent coupling was preferred over a covalent coupling since several additional synthetic steps that would be necessary to introduce the required functionalities. The procedure for a non-covalent immobilisation and also the implementation of sensor foils is described in section 3.3.1. As a polymer matrix, commercially available swellable hydrogels (commercialized under the name Hydromed D1, D4 and D7) were chosen. This hydrogels are ether-based polyurethanes with hydrophobic and hydrophilic blocks. Depending on the ratio of the blocks the uptake of water is different. Swollen Hydrogel D1 contains 70 %, D4 contains 50 % and D7 contains 30 % water [44]. The polymer matrix acts as a solvent for the indicator dye. It cannot be too hydrophobic, due to poor PET of the FI in hydrophobic

environment or too hydrophilic, as the FI can either leach out of the matrix or aggregate. Leaching tests were done in the most hydrophilic hydrogel D1 with high dye concentration (1 wt.%). Therefore, the foil was rinsed with a 500 mM NaCl with simultaneously recording the absorption spectra over 24 h to see potential dye loss. In figure 4.11 can be seen that no leaching or aggregation of the immobilized fluoroionophore was observed.

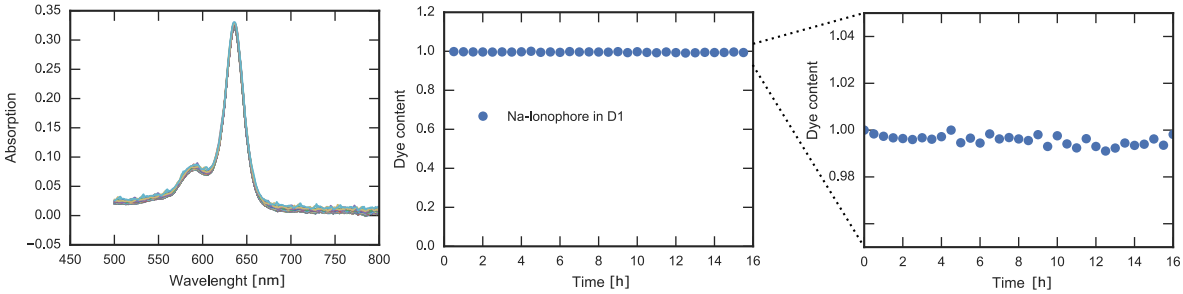

Figure 4.11: Left: Recorded absorption spectra of the indicator immobilized in hydrogel D1 during continuous rinsing the sensor foil with a solution containing 500 mM NaCl. Middle: Normalized absorption maxima of the recorded absorption spectra during the leaching experiment. Absorption maximum of the first measurement point was used for normalization to indicate % dye loss. Right: Zoom in

4.2.3 Influence of the Polymer Matrix

The sensitivity is strongly influenced by the hydrophilicity of the different hydrogels. In more hydrophilic hydrogel D1 the fluorescence enhancement factor is the highest (12-fold at 1000 mM Na^+) compared to the other hydrogels (D4: 9-fold, D7: 4-fold, see figure 4.12) Quantum yields of the different hydrogels are in absence of Na^+ similiar, at high Na^+ concentration (1000 mM) the QYs are different (see table 4.5). For fluorescence enhancement in acidic media it can be seen that only for D1 and D4 the fluoroionophore is completely "switched on" (QY of 86 % and 84 % respectively in 0.1 M HCl). In case of D7, a QY of 50 % was determined in 0.1 M HCl. Even with highly concentrated HCl solution it was not possible to fully protonate the fluoroionophore. It seems that the dye is located in more hydrophobic domains, which are not fully accessible to Na^+-ions or protons. The difference in analyte accessibility is indicated by the decrease of QYs in 1000 mM Na^+ with increase in the hydrogel hydrophobicity and also by the decrease of the apparent pK_a value (table 4.5). Hydrogel D1 has the highest degree of swelling and therefore best accessibility of the fluoroionophore to Na^+-ions. Even though the QY in hydrogel D1 in presence of 1000 mM Na^+ is 23 %, the overall brightness is very good considering high molar absorption coefficients. Beneficial for high brightness is that the thickness of the sensing layer could be reduced which leads to a sensor with fast response time. The dynamic response of about 2.5 μm-thick sensing foil was very fast ($t_{90} < 20$ seconds). Due to the best properties of hydrogel D1, this material was used for further experiments.

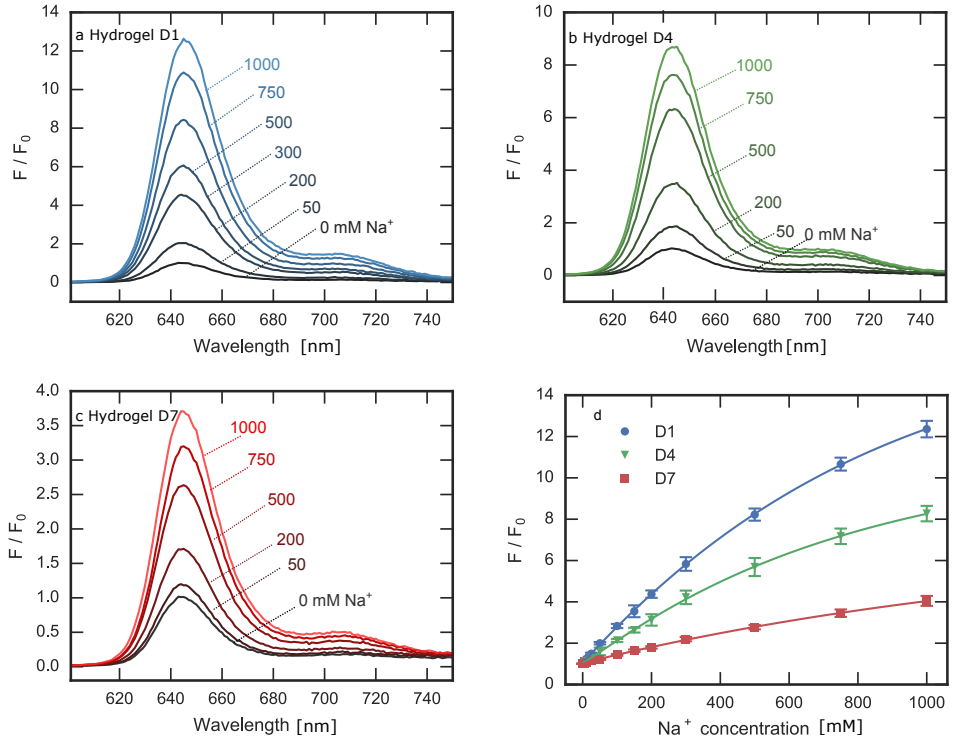

Figure 4.12: a, b, c: Normalized emission spectra of Na-FI3 in hydrogel D1, D4 and D7 at different Na^+ concentrations (20 mM TRIS buffer pH 7.4) d: F\F_0 calibration curves for the indicator immobilized in hydrogel D1, D4 and D7. The values of F and F_0 were taken at $\lambda = 645$ nm

Table 4.5: Fluorescence intensity ratios F/F_0 at 645 nm and fluorescence quantum yields for Na-FI3 in different hydrogel matrices. *pK_a was estimated assuming a QY of 0.85 in the fully protonated state to enable a sigmoidal fit

	F/F0 at 1000 mM NaCl	QY at 1000 mM NaCl	QY at 0.1 M HCl	Apparent pKa value
Hydrogel D1	12.4	0.23	0.86	3.03
Hydrogel D4	8.3	0.16	0.84	2.60
Hydrogel D7	4.0	0.09	0.50	1.46*

4.2.4 Cross-Sensitivity

The selectivity of the fluoroionophore is mostly determined by the size of the recognition unit (crown). Figure 4.13 shows the selectivity of the **Na-FI3** sensor. At very high K^+ concentration some cross-talk is visible. Obviously, even at very high concentration of Ca^{2+} or Mg^{2+} no enhancement of fluorescence is observed. Furthermore no cross-sensitivity to pH in the range 5.5-8.5 is observed (see figure 4.13). The response to Na^+ is fully reversible without hysteresis or drift which can also be seen in this figure.

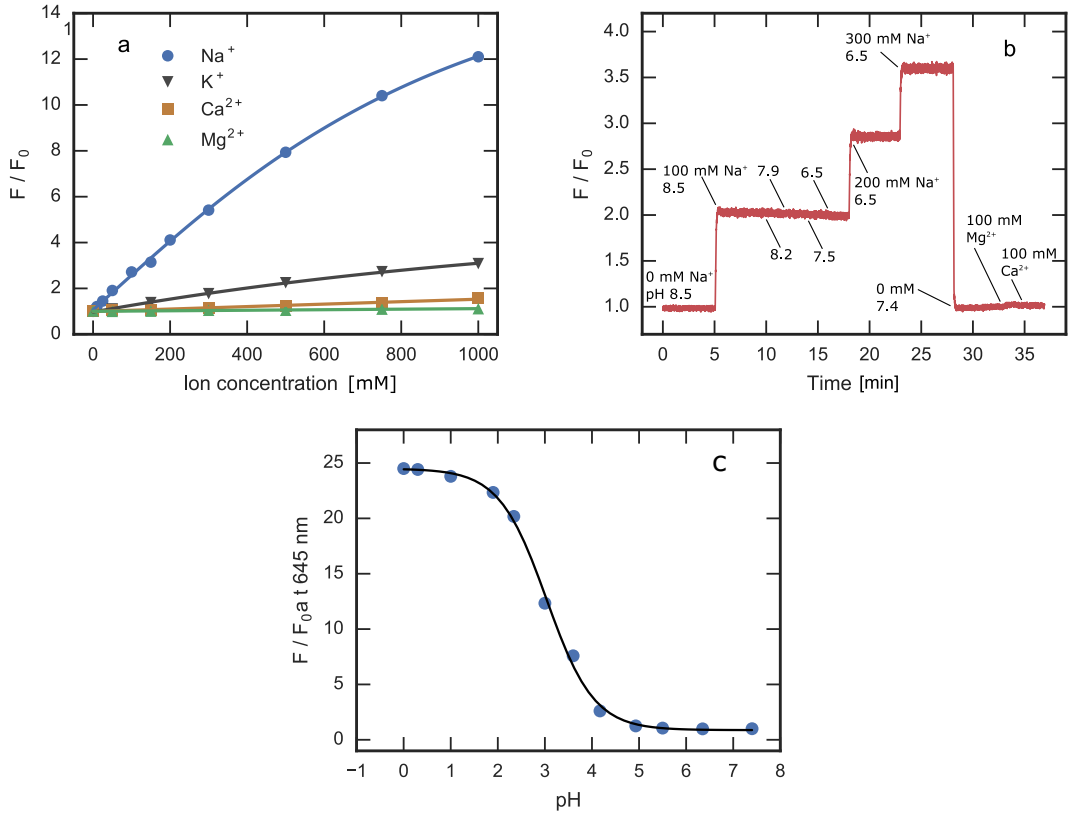

Figure 4.13: a: Cross-sensitivity of Na-FI3 in hydrogel D1 to K^+, Ca^{2+} and Mg^{2+} at pH 7.4 (20 mM TRIS buffer). b: Fuorescence response of Na-FI3 in hydrogel D1 in a flow-cell and solutions with different Na^+, Mg^{2+}, Ca^{2+} concentrations or pH values were pumped through it c: Cross-sensitivity of Na-FI3 in hydrogel D1 in the pH range of 0-5

4.2.5 Miniaturized Referenced Na^+ Optode

For practical application intensity based measurement is unsuitable because the intensity is affected by many parameters. Therefore, dual lifetime referencing (DLR) ratiometic scheme was applied [34]. This method is described in detail in section 2.2.7. As a reference dye a phosphorescent dye (Egyptian Blue) which features a long decay time was chosen. Egyptian blue is an inorganic phosphor which is excitable in the green-red part of the electromagnetic spectrum and emits in the NIR (figure 4.14). It is almost an ideal reference material for DLR, due to a luminescence lifetime of ~ 10^{-7} μ s, its high photostability and its good QY of 10 %.

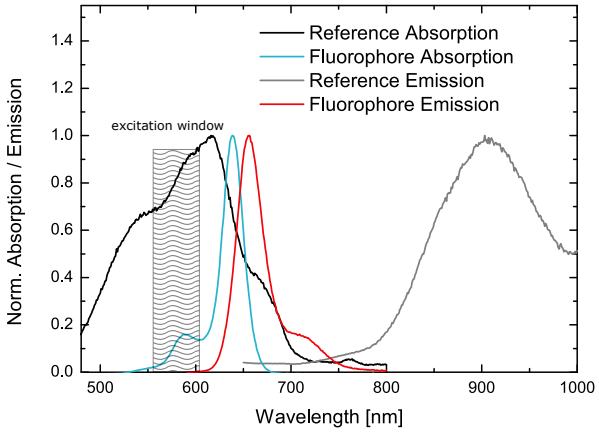

Figure 4.14: Absorption and emission spectra of the reference dye (Egyptian Blue) and of the fluoroionophore (Na-FI3)

The referenced sensor consists of three layers coated onto a transparent polyester support (Figure 4.15). The reference layer (d) was prepared using an dye "cocktail" with Egyptian Blue which was immobilised in polysulfon. This was knife coated on the opposite side of the sensing layer to prevent potential interaction. The sensing layer consisted of two additional layers. The first consisted of the indicator dye Na-FI3 and diamond powder immobilized in hydrogel D1 (b). As the final layer a further hydrogel D1 layer consisting of Na-FI3 and carbon black was used. The diamond powder enhanced the signal by light scattering whereas carbon black acted as optical isolation in order to prevent interference of ambient light. In both layers the dye was added in the same concentration in order to prevent migration which would lead to a change of the signal intensities. A sensor spot was then either stamped out (5 mm diameter) and glued on a plastic screw cap which could be fixed directly on the read-out device or stamped out (2 mm diameter) and fixed with a metal cap on a PMMA fiber. A phase-fluorimeter (FireStingGO_2 from Pyro Science) which is commercially available was used for measurement of the phase shift.

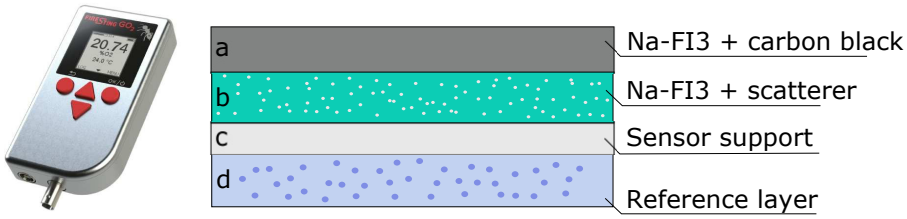

Figure 4.15: Miniaturized phase fluorimeter FireStingGO_2 from Pyro Science. a: Immobilized indicator dye and carbon black for optical isolation in Hydrogel D1. b: Immobilized indicator dye and diamond powder for enhancing signal by light scattering in Hydrogel D1. c: sensor support. d: Egyptian blue microparticles immobilized in polysulfone

4.2.6 Application - Measurement of Seawater Salinity

One of the possible applications of the new sensor is the measurement of sodium for the determination of seawater salinity. It is an important indicator of water quality due to fact that the survival of different species of animal and plant life depends on the salinity range within their habitat. Salinity is expressed as practical salinity unit (PSU) and is defined as the mass fraction of salts in water (grams salt per kilogram solution) [45]. The pracitical salinity in open ocean varies between 33 and 37 PSU, wheras the average is 35. In brackish water the practical salinity is much lower due to dilution by a high quantity of freshwater (0-30)[46]. The ratio of the different ion concentrations remains the same since the only change occurring to seawater is a change in the entire concentration of dissolved ions (e.g. dilution with water). Therefore, the salinity can be determined by simply measuring one component of the seawater. The new sensing material based on Na-FI3 could be used for the measurement of the seawater salinity since the dynamic range of this sensing material matches very well the concentration of Na^+ present in seawater. Furthermore, the the minor cross-sensitivity of the sensor to K^+ is not critical for seawater measurement since the concentration of K^+ is too low to be detected by the sensor (see table 4.6).

Table 4.6: Mean composition of seawater with a PSU of 35 at 25 °C [39]

Cations	g/kg	mM	Anions	g/kg	mM
Na^+	10.77	479	Cl^-	19.37	559
Mg^{2+}	1.30	54.4	$SO_4{}^{2-}$	2.71	28.9
Ca^{2+}	0.409	10.5	$CO_3{}^{2-}$	0.0026	2.33
K^+	0.388	10.4	Br^-	0.065	0.86
Sr^{2+}	0.010	0.09	F^-	0.0013	0.075

A minor disadvantage of this sensor was, that a high dependency towards temperature was observed (see figure 4.16). At lower temperature, the complexation of the analyte is more favourable and therefore more fluorescence is observed in comparison to the complexation at higher temperature. Nevertheless, this dependency can be compensated with the introduction of the temperature coefficient into the calibration equation (equation 4.1).

$$cot(d\phi) = (A + A_T \cdot (T - 20)) \cdot (1 - e^{(-(k+k_T \cdot (T-20) \cdot Na))}) + (B + B_T \cdot (T - 20)) \qquad (4.1)$$

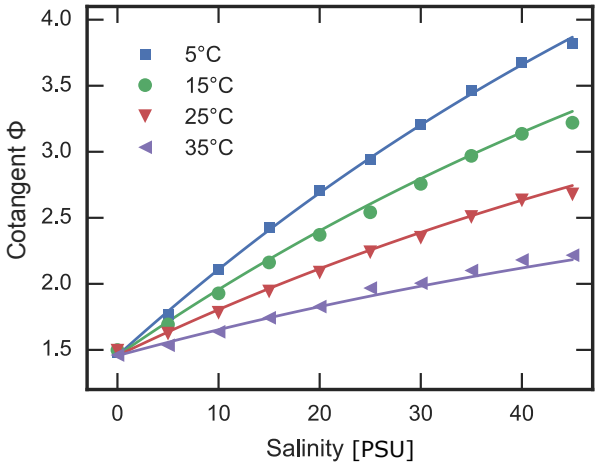

Figure 4.16: Temperature-dependent calibration of the salinity optode

The constructed sensor was then used for the measurement of sea water salinity in the Baltic Sea. Two different read-out devices were used for three different application areas. For quick in situ salinity measurements a commercially available phase fluorimeter (FireStingGO_2, Pyro Science) was used. Furthermore, profiling measurements (up to a depth of 25 m) and surface salinity measurements were performed. Therefore, the phase fluorimeter was embedded into a polyoxymethylene pressure housing. The read-out devices were also equipped with an internal temperature sensor.

The 24 h measurement of salinity in surface water is shown in Figure 4.17.a. The sensor was calibrated at RT using salinity solutions containing Na^+ ranging from 0 to 1000 mM. The data which are shown in this figure are in good agreement with the reference data obtained via conductivity measurements (CTD). Profiling measurements up to 25 m depth are shown in figure 4.17.b. The first measured point of the CTD at the surface was used as a reference calibration point for the optode as it showed a difference of around 4 PSU. The measured salinity values are in good agreement with the reference measurement. The disparity beyond a depth of 5 m could be explained that the response time (speed of profiling: 0.15 m/s) at lower temperature (from 19.4 °C at 5 m to 11.3 °C at 25 m) was reduced. At figure 4.17.c several measurement points along the mouth of river Schwentine are shown. Measurements closer to the harbour showed an increase in the salinity whereas the lowest salinity (2.2 PSU) was measured in the river before a bridge. The highest salinity was measured in a fjord and had a PSU of 20.7. Again this measurement was in good agreement with commonly measured salinity values in the harbour.

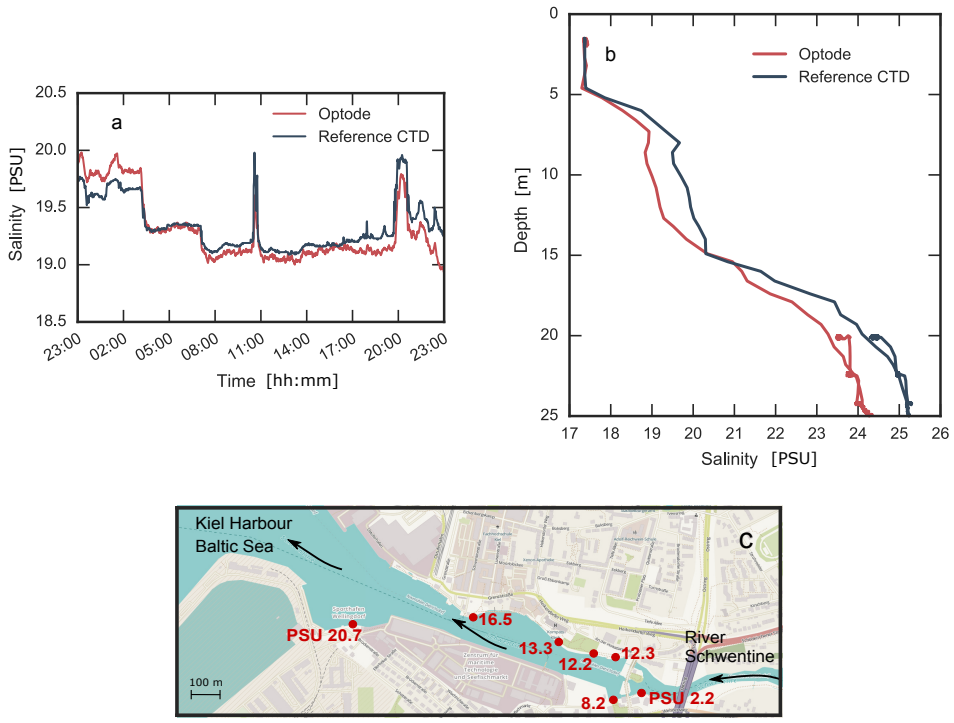

Figure 4.17: Measured salinity in the Baltic Sea compared to reference conductivity measurements from the CTD rosette. a: in surface water for one day. b: Profiling measurement with a speed of 0.15 m/s and stops of 10 min at 24, 22 and 20 m. c: Measurement points and salinity values determined with the sensor material and a handheld phase fluorimeter as the read-out device

4.3 Characterization of the Potassium Fluoroionophores K^{1st}-FI3, K^{2nd}-FI3 and TAC-FI3

In this sections the new synthesized receptor K^{2nd}-FI3 is compared to TAC-FI3 and to K^{1st}-FI3 (figure 4.18). Calibration in solution with increasing potassium concentration as well as calibration with a constant sodium concentration as background have been performed. Furthermore, the cross sensitivity to other ions such as Na^+, $NH_4{}^+$, Ca^{2+} and Mg^{2+} was tested. Upon immobilization of the dyes in hydrogel D4, calibrations were again obtained in Tris buffer (with different potassium concentrations) at a pH of 7.4 (physiological conditions) with and without a constant sodium concentration.

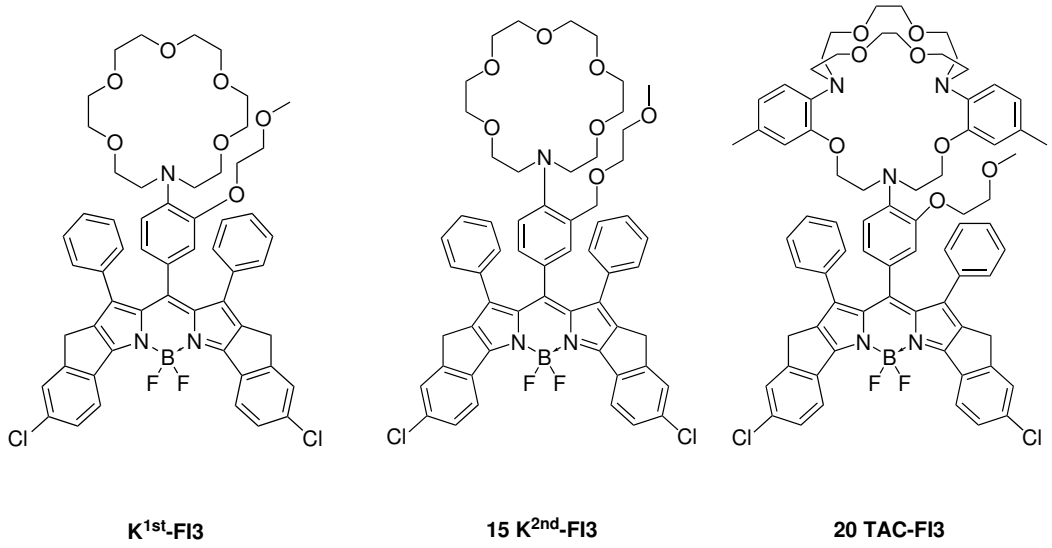

Figure 4.18: Structures of the characterized dyes

4.3.1 Absorption and Emission Spectra

Absorption and emission spectra are recorded in THF. As can be seen in figure 4.19 the absorption and emission spectra of all dyes are similar to each other. Typically for BODIPY dyes the emission and absorption bands are very sharp. All of them have a maximum absorption band at 630 nm whereas the emission maxima is a little bit shifted. Generally, the Stokes shifts of the dyes are rather small and are in the range of 13 to 20 nm. Upon complexation with potassium the fluorescence increases due to the reduction of the PET effect (figure 4.21). Upon protonation of the amine the dye is also in the "on" state and there is also a bathochromic shift.

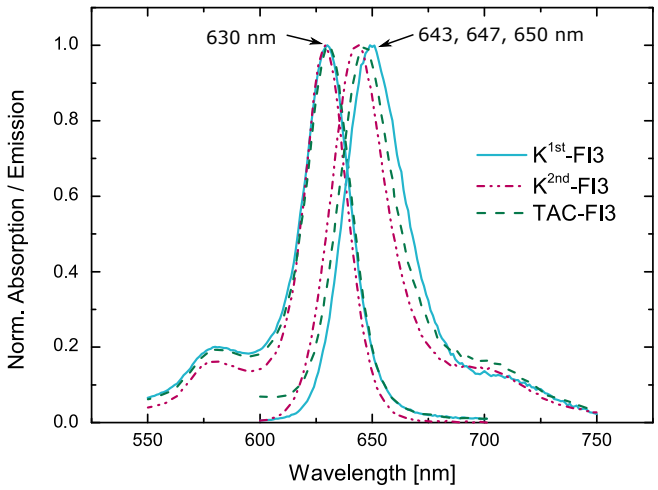

Figure 4.19: Normalized absorption and emission spectra in THF

4.3.2 Calibration in Solution

Calibrations of the fluoroionophores were done in an 1/1 mixture of THF and buffer (0.02 mM Tris buffer with an pH of 7.4).

The potassium-dependent normalized fluorescence intensity is shown on the left side in figure 4.21. The spectra were normalised with regard to the highest intensity of the blank value F_0. At low potassium concentration (0-12.5 mM) the fluorescence enhancement for K^{1st}-FI3 and TAC-FI3 are comparable to each other. An almost linear range of the K^{1st}-FI3 and of TAC-FI3 is from 0 to 12.5 mM whereas it ranges from 0 to 50 mM for K^{2nd}-FI3. In general, the fluorescence enhancement of the new synthesized K^{2nd}-FI3 is worse compared to the others. Both, crown ethers and cryptands changes the conformation upon complexation of the analyte. Therefore, the activation energy of the complexation increases which is disadvantageous for the binding. Maybe, this is the reason for the worse binding properties of potassium for the K^{2nd} fluoroionophore. The sidearm of the K^{2nd}-FI3 is expected to be more flexible and consequently this maybe leads to an additionally increase of the activation energy of the complexation.

Keeping in mind the real sensing applications this dyes were also measured with a continuous Na^+ background of 150 mM with different potassium concentration. The fluorescence enhancement factor decreases drastically for the TAC-FI3 dye although it has nearly no cross sensitivity to sodium (see figure 4.22). A possible explanation could be that Na^+ binds to the crown/cryptand and therefore the fluorescence at 0 mM K^+ is slightly increased (see figure 4.20). Furthermore, Na^+ cannot fill the crown/cryptand completely and therefore the quenching of the PET effect is not as efficient as if K^+ is bound. In the figure can also be seen that the TAC cryptand is not in the "on" state when treated with HCl. The TAC cryptand bears three tertiary amines in its cavity and if not the appropriate amine is protonated which can interrupt the PET effect than there is no fluorescence emission. Therefore, there is only a slight fluorescent enhancement compared to the other dyes when treated with HCl.

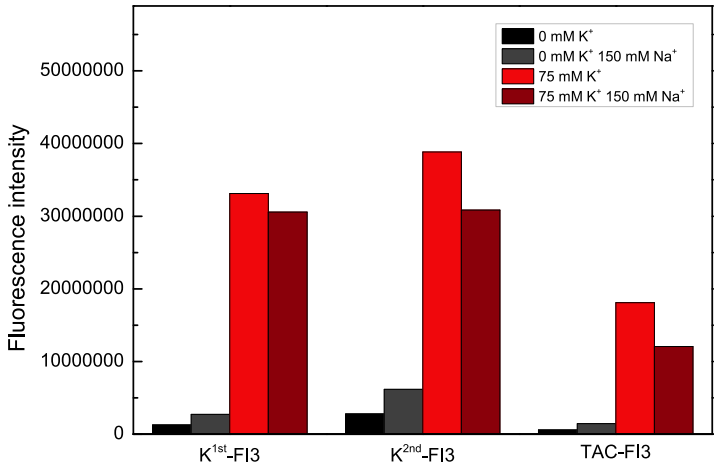

Figure 4.20: Fluorescence intensity for each dye with and without sodium background (150 mM) at 0 mM and 75 mM potassium

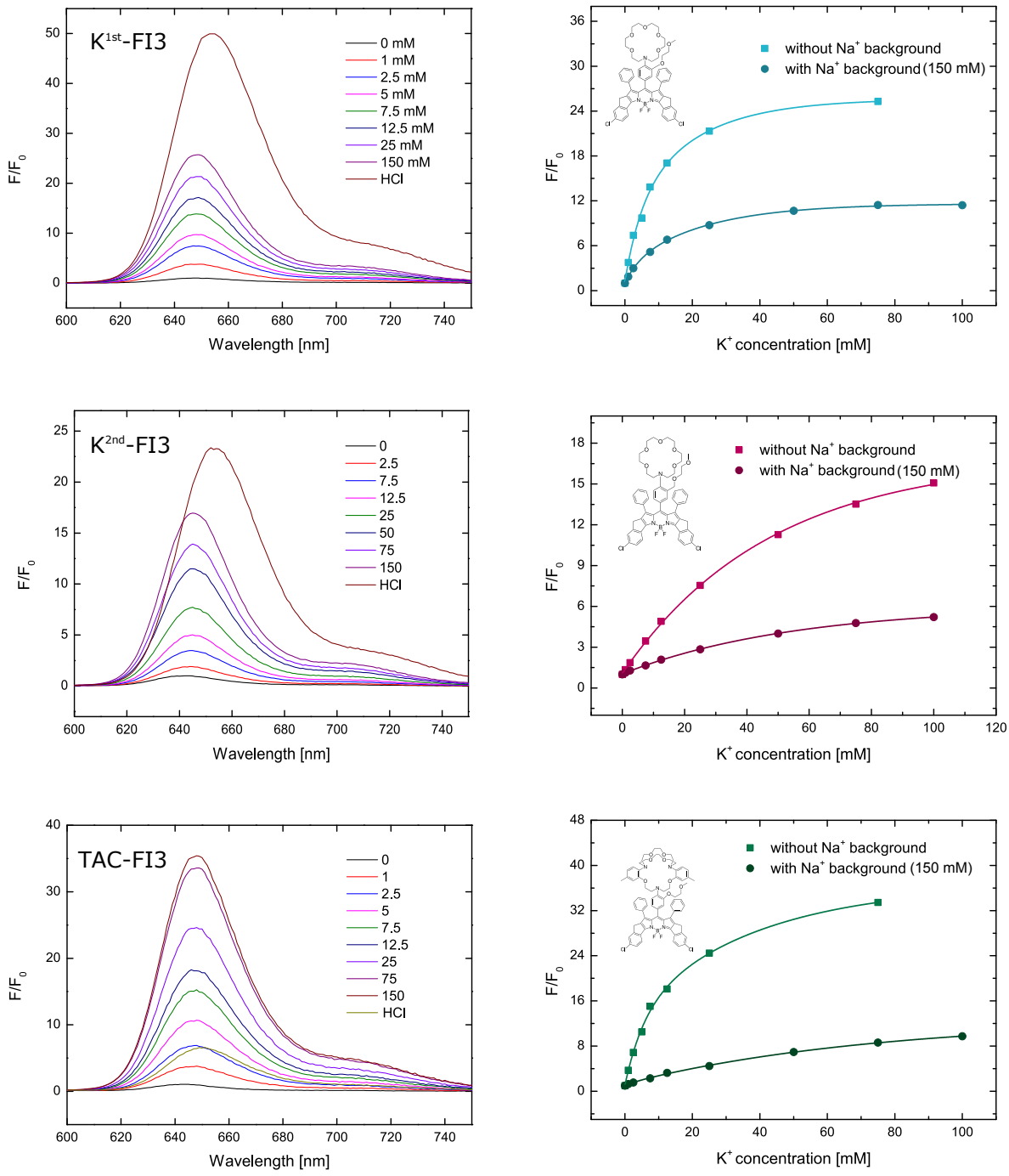

Figure 4.21: Left side: Normalised emission spectra of K^{1st}-FI3, K^{2nd}-FI3 and TAC-FI3 measured in Tris buffer with different K^+ concentration (0.02 mM, pH 7.4) without a constant sodium background. Right side: F/F_0 calibration curve of the fluoroionophores K^{1st}-FI3, K^{2nd}-FI3 and TAC-FI3 measured in Tris buffer solution (0.02 M, pH=7.4) (without and with a constant Na^+ (150 mM) background) using an excitation wavelength at 580 nm

4.3.3 Cross-Sensitivity

For the measurement in whole blood, the fluoroionophores have to be tested against cross sensitvity to other ions (Na^+, NH_4^+ Ca^{2+} and Mg^{2+}). This was performed using Tris puffer (0.02 M, at pH 7.4) at different concentrations of the different ions. Figure 4.22 shows the cross sensitivity of each dye.

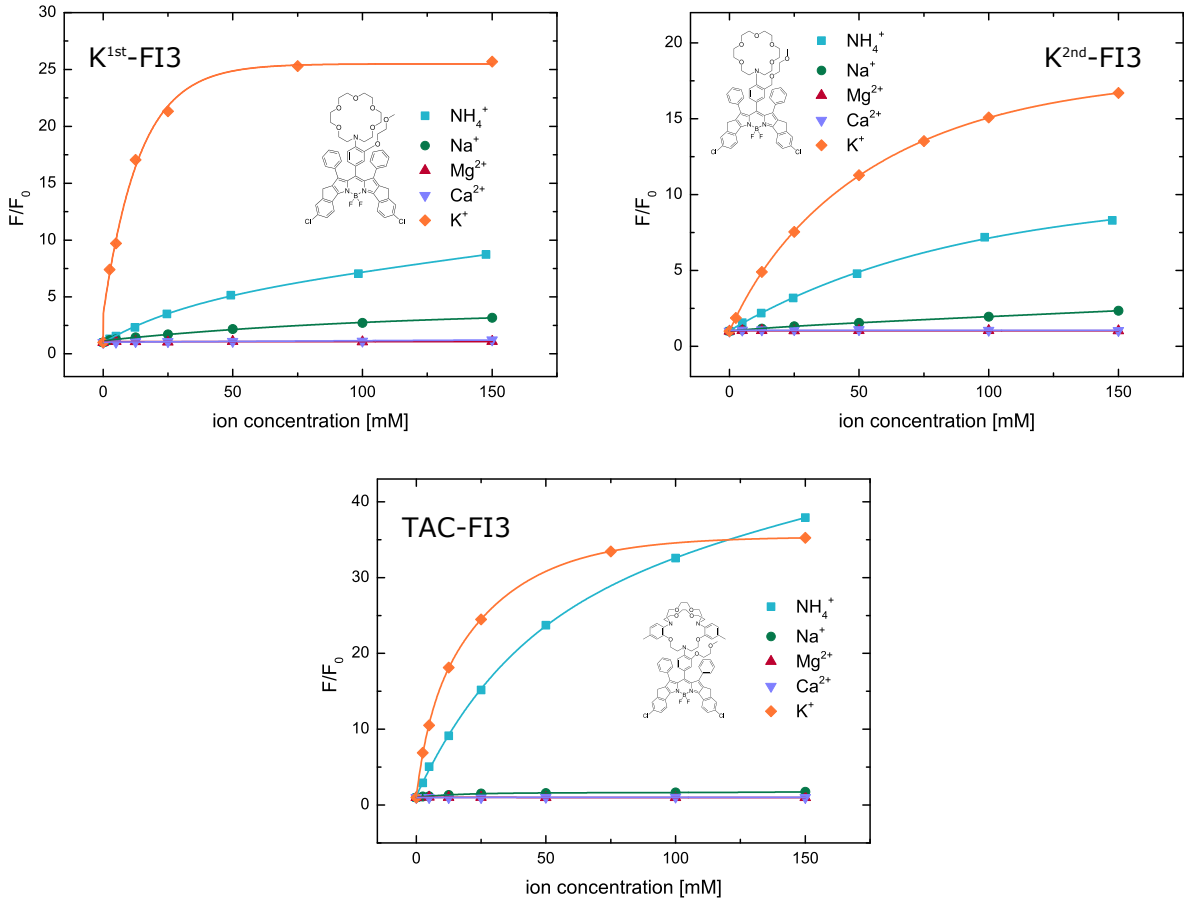

Figure 4.22: Cross sensitivity to common cations at pH 7.4 (20 mM Tris buffer)

A major cross sensitivity for NH_4^+ is visible for every dye due to similar size and charge of this ion compared to K^+ (see figure 4.23). Especially for the TAC-FI3 the fluorescence enhancement to ammonium is more pronounced. This might be no problem for the analysis in blood because the normal blood value for NH_4^+ is in the range of 10–50 μmol/L. However, this could be a problem in cases of severe hyperammonemia where the NH_4^+ concentration is as high as the K^+ concentration. Similarly, there is a publication describing the cross sensitivity of TAC cryptand to NH_4^+ which confirm the results [47].

Also, a minor cross talk to Na^+ at high concentration is visible. However, it should be considered that in most applications the concentration of Na^+ does not differ drastically. It could also be compensated by the use of a second fluoroionophore which measures the accurate sodium concentration. Apparently, even at very high concentration of Ca^{2+} or Mg^{2+} no enhancement of fluorescence is observed.

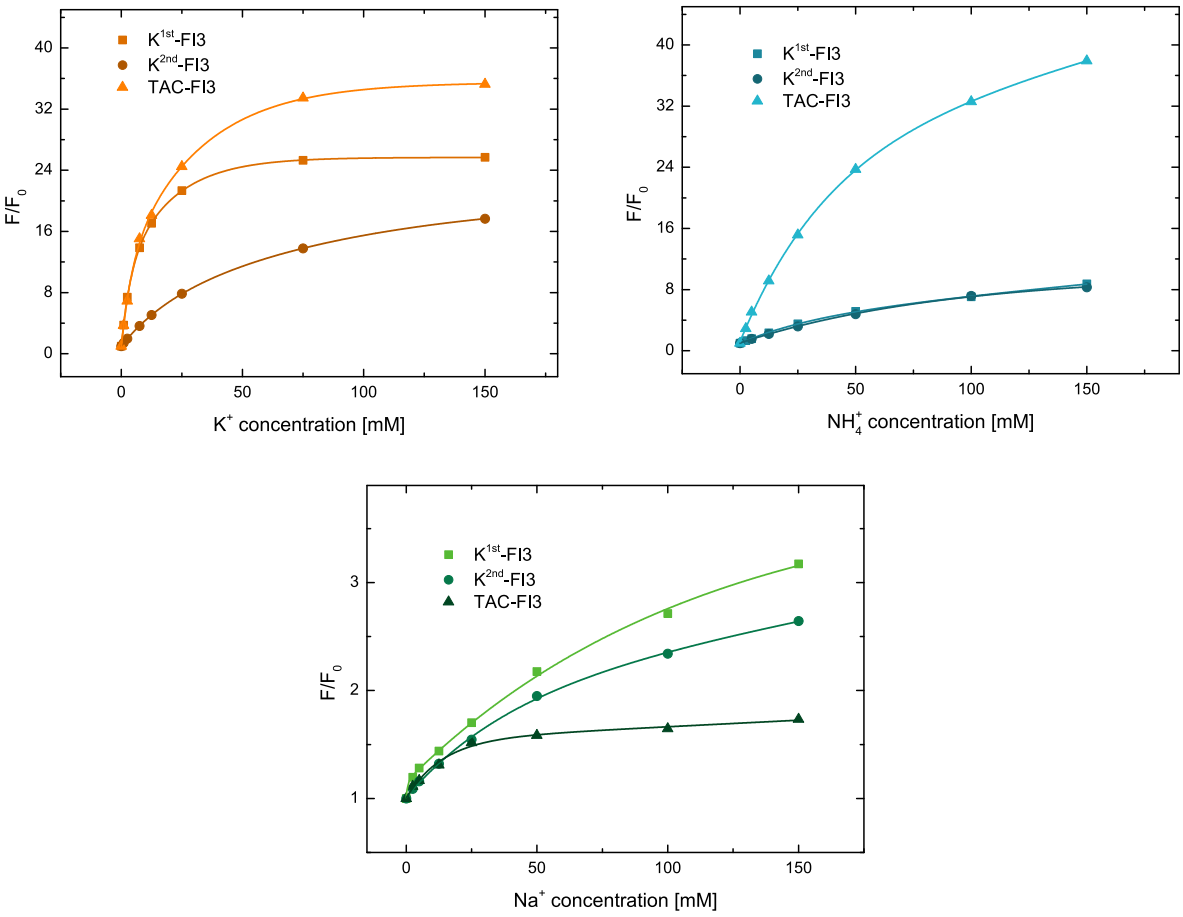

Figure 4.23: Comparison of the cross sensitivities to NH_4^+ and Na^+ for each dye

4.3.4 Calibration in Hydrogel D4

For continuous monitoring the fluoroionophores have to be incorporated into a polymer matrix. For this purpose, stock solutions of the polymer were prepared and the appropriate amount of dye related to the amount of polymer was added. This "cocktail" was then knife coated onto dust-free polyethylene terephthalate foils and were allowed to dry for several hours at RT. The exact preparation of the foils is described in section 3.3.1. As polymer, hydrogel D4 was chosen as it has an water uptake of about 50 %. Furthermore, it is biocompatible, has an good ion permeability and is commercially available. This foils were measured from 0 mM to 100 mM potassium concentration and a second measurement was performed using a constant sodium background of 150 mM (physiological conditions) and varying the potassium concentration from 0 to 100 mM.

As can be seen in figure 4.24 the fluorescence intensity greatly increases at least for the K^{1st} fluoroionophore. For the K^{2nd} - and the TAC-fluoroionophore the fluorescence enhancement is not that pronounced. A possible explanation can be, that the TAC-crown is more hydrophobic than the K^{1st} receptor and therefore it is placed in the hydrophobic part of the polymeric matrix where ions are less located. Perhaps, this is also the explanation for the K^{2nd}-FI3 because the additional CH_2-group would make the dye more hydrophobic. The hydrophobic domain of the polymer could also inhibit the PET effect and therefore already fluorescence can be seen as there is already high fluorescence without K^+ visible compared to K^{1st} fluoroionophore. In general, there is only a small increase in fluorescence observed for this dye in hydrogel D4. A possibility to overcome this issue could be the use of other polymers which do not consist of hydrophobic and hydrophilic domains. PHEMA (poly(2-hydroxyethyl methacrylate)) would be a potential candidate. It could also be that the K^{2nd}- and the TAC-dye are not bright emitting but to make a sure statement one has to measure the quantum yields of the dyes. For real sensing applications this planar foils were measured with an constant Na^+ background of 150 mM with different K^+ concentrations. As explained in section 4.3.2 the fluorescence enhancement is here also lower with a constant Na^+ background. Here, the difference in fluorescence enhancement between the measurement with and without sodium is not that pronounced as it is in solution.

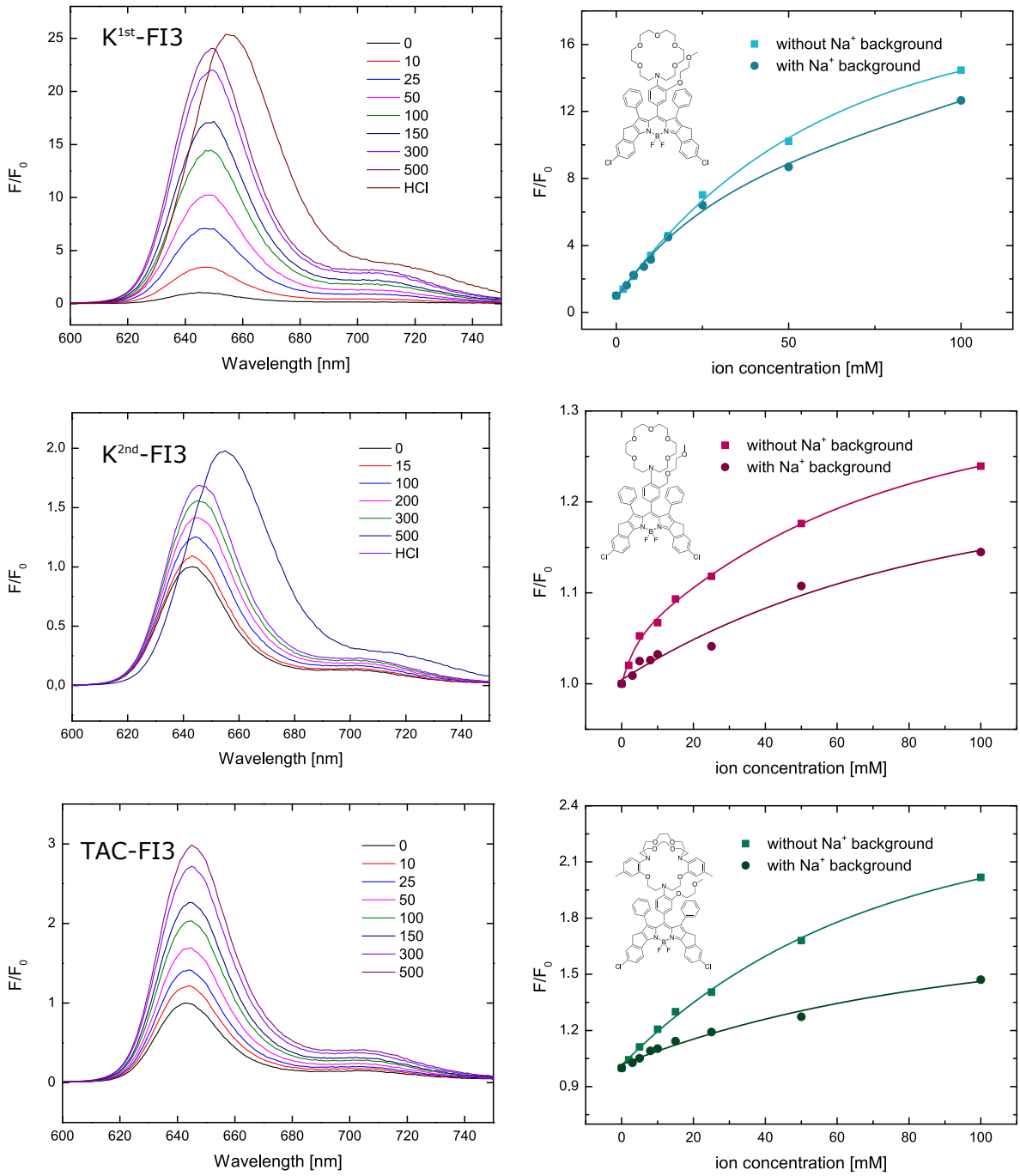

Figure 4.24: Left side: Normalised emission spectra of K^{1st}-FI3, K^{2nd}-FI3 and TAC-FI3 immobilized in hydrogel D4, measured in Tris buffer with different K^+ concentration (0.02 mM, pH 7.4) without a constant sodium background. Right side: F/F_0 calibration curve of the fluoroionophores K^{1st}-FI3, K^{2nd}-FI3 and TAC-FI3 immobilized in hydrogel D4, measured in Tris buffer solution (0.02 M, pH=7.4) using an excitation wavelength at 580 nm

5 Conclusion

In this thesis fluoroionophores for potassium and sodium sensing have been successfully synthesized and characterized. They all consisted of the same bright red-emitting BF_2-chelated dipyrromethene (BODIPY) dye as fluorophore and contained different receptors. For continuous measurement they were incorporated into water-swellable biocompatible polymer matrices (hydrogels). For the sodium sensor several of these hydrogels were tested (D1, D4, D7) whereas for the potassium sensor only the hydrogel D4 was chosen.
Among all hydrogels tested for sodium sensing the hydrogel D1 seemed to be the most suitable because it showed fast and reversible response, the highest dynamic range between the "on" and "off" states, no leaching, no or only minor cross-sensitivity to other ions (Ca^{2+}, Mg^{2+}, K^+) and to pH within the physiologically relevant range. The application of this sensor for determination of the water salinity was shown after the preparation of a referenced sensing material. It was tested in the Baltic Sea where it showed good correlation compared to the conductivity measurements (CTD).
For potassium sensing two new fluoroionophores have been synthesized. The first synthesized dye (K^{2nd}-FI3) consisted of a new receptor, which had a CH_2 spacer at the side arm whereas the second synthesized dye (TAC-FI3) had a commercially available TAC cryptand as receptor. A third dye (K^{1st}-FI3) with the same chromophore which was already available was also compared to the new synthesized ones. All of them showed high fluorescence increase in solution when treated with different K^+ concentrations. Additionally, the new fluoroionophores were tested against cross sensitivity to other ions, where each of them showed no or negligible interferences to Ca^{2+}, Mg^{2+} and Na^+ but a major cross sensitivity to NH_4^+. After the incorporation into the polymer matrices only the K^{1st} fluoroionophore showed a high increase and a good response when treated with potassium solutions. The K^{2nd}- and the TAC-FI3 were not appropriate for the measurement in this hydrogel. In summary, it turned out that the increase of flexibility of the side arm in K^{2nd}-FI3 does not lead to an increase of sensitivity. Notably, even the more complex structure of the TAC cryptand do not increase the binding stability. It seems that the most suitable dye for the determination of K^+ ions in blood is the already existing K^{1st} due to the best behaviour in the polymeric matrix and the best K^+/Na^+ selectivity.

6 References

1. He, H., Mortellaro, M. A., Leiner, M. J. P., Fraatz, R. J. & Tusa, J. K. A Fluorescent Sensor with High Selectivity and Sensitivity for Potassium in Water. *Journal of the American Chemical Society* **125,** 1468–1469. ISSN: 0002-7863, 1520-5126 (Feb. 2003).
2. Müller, B. J., Borisov, S. M. & Klimant, I. Red- to NIR-Emitting, BODIPY-Based, K+-Selective Fluoroionophores and Sensing Materials. *Advanced Functional Materials* **26,** 7697–7707. ISSN: 1616-3028 (Nov. 1, 2016).
3. Krishna, G. G., Miller, E. & Kapoor, S. Increased Blood Pressure during Potassium Depletion in Normotensive Men. *New England Journal of Medicine* **320,** 1177–1182. ISSN: 0028-4793, 1533-4406 (May 4, 1989).
4. Bissell, R. A., de Silva, A. P., Gunaratne, H. Q. N., Lynch, P. L. M., Maguire, G. E. M. & Sandanayake, K. R. A. S. Molecular fluorescent signalling with 'fluor–spacer–receptor' systems: approaches to sensing and switching devices via supramolecular photophysics. *Chem. Soc. Rev.* **21,** 187–195. ISSN: 0306-0012, 1460-4744 (1992).
5. De Silva, A. P., Gunaratne, H. Q. N., Gunnlaugsson, T., Huxley, A. J. M., McCoy, C. P., Rademacher, J. T. & Rice, T. E. Signaling Recognition Events with Fluorescent Sensors and Switches. *Chemical Reviews* **97,** 1515–1566. ISSN: 0009-2665, 1520-6890 (Aug. 1997).
6. Burdette, S. C., Walkup, G. K., Spingler, B., Tsien, R. Y. & Lippard, S. J. Fluorescent Sensors for Zn^{2+} Based on a Fluorescein Platform: Synthesis, Properties and Intracellular Distribution. *Journal of the American Chemical Society* **123,** 7831–7841. ISSN: 0002-7863, 1520-5126 (Aug. 2001).
7. Schultz, R. A., White, B. D., Dishong, D. M., Arnold, K. A. & Gokel, G. W. 12-, 15-, and 18-Membered-ring nitrogen-pivot lariat ethers: syntheses, properties, and sodium and ammonium cation binding properties. *Journal of the American Chemical Society* **107,** 6659–6668. ISSN: 0002-7863 (Nov. 1985).
8. Valeur, B. & John Wiley \& Sons, I. *Molecular Fluorescence* OCLC: 223366416. ISBN: 978-3-527-60024-3. <http://dx.doi.org/10.1002/3527600248> (2017) (Wiley-VCH, Weinheim, 2002).
9. Lakowicz, J. R. *Principles of fluorescence spectroscopy* 3. ed., corr. 4. print. OCLC: 700510097. 954 pp. ISBN: 978-0-387-46312-4 978-0-387-31278-1 (Springer, New York, NY, 2010).

10. Gründler, P. *Chemische Sensoren: eine Einführung für Naturwissenschaftler und Ingenieure ; mit 27 Tabellen* Softcover. OCLC: 820457027. 295 pp. ISBN: 978-3-540-20984-3 978-3-642-32386-7 (Springer, Berlin, 2012).

11. Hulanicki, A., Glab, S. & Ingman, F. Chemical sensors: definitions and classification. *Pure and Applied Chemistry* **63.** ISSN: 1365-3075, 0033-4545. doi:10.1351/pac199163091247. <http://www.degruyter.com/view/j/pac.1991.63.issue-9/pac199163091247/pac199163091247.xml> (2017) (Jan. 1, 1991).

12. Eggins, B. R. *Chemical sensors and biosensors* 273 pp. ISBN: 978-0-471-89913-6 978-0-471-89914-3 (J. Wiley, Chichester ; Hoboken, NJ, 2002).

13. Johnson, R. D. & Bachas, L. G. Ionophore-based ion-selective potentiometric and optical sensors. *Analytical and Bioanalytical Chemistry* **376,** 328–341. ISSN: 1618-2642 (June 2003).

14. Bakker, E., Bühlmann, P. & Pretsch, E. Carrier-Based Ion-Selective Electrodes and Bulk Optodes. 1. General Characteristics. *Chemical Reviews* **97,** 3083–3132. ISSN: 0009-2665, 1520-6890 (Dec. 1997).

15. Valeur, B. Design principles of fluorescent molecular sensors for cation recognition. *Coordination Chemistry Reviews* **205,** 3–40. ISSN: 00108545 (Aug. 1, 2000).

16. Hamilton, G. R. C., Sahoo, S. K., Kamila, S., Singh, N., Kaur, N., Hyland, B. W. & Callan, J. F. Optical probes for the detection of protons, and alkali and alkaline earth metal cations. *Chem. Soc. Rev.* **44,** 4415–4432. ISSN: 0306-0012, 1460-4744 (2015).

17. *Crown ethers and analogous compounds* (ed Hiraoka, M.) *Studies in organic chemistry* **45** (Elsevier, Amsterdam ; New York, 1992). 485 pp. ISBN: 978-0-444-88191-5.

18. Hartley, J. H., James, T. D. & Ward, C. J. Synthetic receptors. *Journal of the Chemical Society, Perkin Transactions 1,* 3155–3184. ISSN: 14704358, 13645463 (2000).

19. Gokel, G. W. Lariat ethers: from simple sidearms to supramolecular systems. *Chemical Society Reviews* **21,** 39. ISSN: 0306-0012, 1460-4744 (1992).

20. Ast, S., Schwarze, T., Müller, H., Sukhanov, A., Michaelis, S., Wegener, J., Wolfbeis, O. S., Körzdörfer, T., Dürkop, A. & Holdt, H.-J. A Highly K^+-Selective Phenylaza-[18]crown-6-Lariat-Ether-Based Fluoroionophore and Its Application in the Sensing of K^+ Ions with an Optical Sensor Film and in Cells. *Chemistry - A European Journal* **19,** 14911–14917. ISSN: 09476539 (Oct. 25, 2013).

21. Jeronimo, P., Araujo, A. & Conceicaobsmmontenegro, M. Optical sensors and biosensors based on sol–gel films. *Talanta* **72,** 13–27. ISSN: 00399140 (Apr. 15, 2007).

22. Janata, J. Introduction: Modern Topics in Chemical Sensing. *Chemical Reviews* **108,** 327–328. ISSN: 0009-2665, 1520-6890 (Feb. 2008).

23. Mistlberger, G., Crespo, G. A. & Bakker, E. Ionophore-Based Optical Sensors. *Annual Review of Analytical Chemistry* **7,** 483–512. ISSN: 1936-1327, 1936-1335 (June 12, 2014).

24. Yeung, M. C.-L. & Yam, V. W.-W. Luminescent cation sensors: from host–guest chemistry, supramolecular chemistry to reaction-based mechanisms. *Chem. Soc. Rev.* **44,** 4192–4202. ISSN: 0306-0012, 1460-4744 (2015).

25. Shin, E. J. Mg $^{2+}$ -Selective Fluorescence Enhancement of Benzo-15-crown-5 Derivative Bearing Vinylanthracene Fluorophore. *Chemistry Letters* **31,** 686–687. ISSN: 0366-7022, 1348-0715 (July 2002).

26. Tsukanov, A. V., Dubonosov, A. D., Bren, V. A. & Minkin, V. I. Organic chemosensors with crown-ether groups (review). *Chemistry of Heterocyclic Compounds* **44,** 899–923. ISSN: 0009-3122, 1573-8353 (Aug. 2008).

27. Minta, A. & Tsien, R. Y. Fluorescent indicators for cytosolic sodium. *The Journal of Biological Chemistry* **264,** 19449–19457. ISSN: 0021-9258 (Nov. 15, 1989).

28. Szmacinski, H. & Lakowicz, J. R. Sodium Green as a Potential Probe for Intracellular Sodium Imaging Based on Fluorescence Lifetime. *Analytical Biochemistry* **250,** 131–138. ISSN: 00032697 (Aug. 1997).

29. He, H., Mortellaro, M. A., Leiner, M. J. P., Young, S. T., Fraatz, R. J. & Tusa, J. K. A Fluorescent Chemosensor for Sodium Based on Photoinduced Electron Transfer. *Analytical Chemistry* **75,** 549–555. ISSN: 0003-2700, 1520-6882 (Feb. 2003).

30. Meuwis, K., Boens, N., De Schryver, F., Gallay, J. & Vincent, M. Photophysics of the fluorescent K+ indicator PBFI. *Biophysical Journal* **68,** 2469–2473. ISSN: 00063495 (June 1995).

31. Malval, J.-P., Leray, I. & Valeur, B. A highly selective fluorescent molecular sensor for potassium based on a calix[4]bisazacrown bearing boron-dipyrromethene fluorophores. *New Journal of Chemistry* **29,** 1089. ISSN: 1144-0546, 1369-9261 (2005).

32. Lakowicz, J. R. *Topics in fluorescence spectroscopy* OCLC: 803642172. ISBN: 978-0-306-47057-8 978-0-306-47058-5 978-0-306-47059-2 978-0-306-47060-8 978-0-306-47070-7 978-0-306-47102-5 978-0-306-47947-2 978-0-306-47387-6. <`http://ebooks.springerlink.com/UrlApi.aspx?action=summary&v=1&bookid=76108`> (2017) (Springer, New York, 2002).

33. Huber, C., Klimant, I., Krause, C. & Wolfbeis, O. S. Dual Lifetime Referencing as Applied to a Chloride Optical Sensor. *Analytical Chemistry* **73,** 2097–2103. ISSN: 0003-2700, 1520-6882 (May 2001).

34. Klimant, I., Huber, C., Liebsch, G., Neurauter, G., Stangelmayer, A. & Wolfbeis, O. S. in *New Trends in Fluorescence Spectroscopy* (eds Valeur, B. & Brochon, J.-C.)red. by Wolfbeis, O. DOI: 10.1007/978-3-642-56853-4_13, 257–274 (Springer Berlin Heidelberg, Berlin, Heidelberg, 2001). ISBN: 978-3-642-63214-3 978-3-642-56853-4. <http://link.springer.com/10.1007/978-3-642-56853-4_13> (2017).

35. Boniello, C., Mayr, T., Bolivar, J. M. & Nidetzky, B. Dual-lifetime referencing (DLR): a powerful method for on-line measurement of internal pH in carrier-bound immobilized biocatalysts. *BMC Biotechnology* **12,** 11. ISSN: 1472-6750 (2012).

36. Boens, N., Leen, V. & Dehaen, W. Fluorescent indicators based on BODIPY. *Chem. Soc. Rev.* **41,** 1130–1172. ISSN: 0306-0012, 1460-4744 (2012).

37. Loudet, A. & Burgess, K. BODIPY Dyes and Their Derivatives: Syntheses and Spectroscopic Properties. *Chemical Reviews* **107,** 4891–4932. ISSN: 0009-2665, 1520-6890 (Nov. 2007).

38. Ulrich, G., Ziessel, R. & Harriman, A. The Chemistry of Fluorescent Bodipy Dyes: Versatility Unsurpassed. *Angewandte Chemie International Edition* **47,** 1184–1201. ISSN: 14337851, 15213773 (Feb. 1, 2008).

39. Huber, C., Klimant, I., Krause, C., Werner, T., Mayr, T. & Wolfbeis, O. S. Optical sensor for seawater salinity. *Fresenius' Journal of Analytical Chemistry* **368,** 196–202. ISSN: 0937-0633, 1432-1130 (Sept. 11, 2000).

40. Chandrappa, S., Vinaya, K., Ramakrishnappa, T. & Rangappa, K. An Efficient Method for Aryl Nitro Reduction and Cleavage of Azo Compounds Using Iron Powder/Calcium Chloride. *Synlett* **2010,** 3019–3022. ISSN: 0936-5214, 1437-2096 (Dec. 2010).

41. Liu, Y., Lu, Y., Prashad, M., Repi?, O. & Blacklock, T. J. A Practical and Chemoselective Reduction of Nitroarenes to Anilines Using Activated Iron. *Advanced Synthesis & Catalysis* **347,** 217–219. ISSN: 1615-4150, 1615-4169 (Feb. 2005).

42. Sui, B., Yue, X., Tichy, M. G., Liu, T. & Belfield, K. D. Improved Synthesis of the Triazacryptand (TAC) and its Application in the Construction of a Fluorescent TAC-BODIPY Conjugate for K^+ Sensing in Live Cells: Fluorescent TAC-BODIPY Conjugate for K^+ Sensing in Live Cells. *European Journal of Organic Chemistry* **2015,** 1189–1192. ISSN: 1434193X (Feb. 2015).

43. Allen, D. W., Cropper, P. E., Smithurst, P. G., Ashton, P. R. & Taylor, B. F. Further studies of the kinetic template effect in the metal ion-catalysed reactions of ortho-donor-substituted aryl halides with tertiary phosphines. Structural requirements of the template. *Journal of the Chemical Society, Perkin Transactions 1,* 1989. ISSN: 0300-922X, 1364-5463 (1986).

44. *HydroMed Products* <http://www.advbiomaterials.com/products/hydrophilic/hydromed.html> (2017).

45. Mller, T. J. in *Methods of Seawater Analysis* (eds Grasshoff, K., Kremling, K. & Ehrhardt, M.) DOI: 10.1002/9783527613984.ch3, 41–73 (Wiley-VCH Verlag GmbH, Weinheim, Germany, Jan. 27, 1999). ISBN: 978-3-527-61398-4 978-3-527-29589-0. <http://doi.wiley.com/10.1002/9783527613984.ch3> (2017).

46. Eilers, J. M., Sullivan, T. J. & Hurley, K. C. The most dilute lake in the world? *Hydrobiologia* **199,** 1–6. ISSN: 0018-8158, 1573-5117 (July 1990).

47. Carayannopoulos, M. O. Equimolar Ammonia Interference in Potassium Measurement on the Osmetech OPTI Critical Care Analyzer. *Clinical Chemistry* **52,** 1603–1604. ISSN: 0009-9147, 1530-8561 (June 22, 2006).

7 List of Figures

8 List of Tables

9 Appendix

9.1 NMR Data

Compound 2

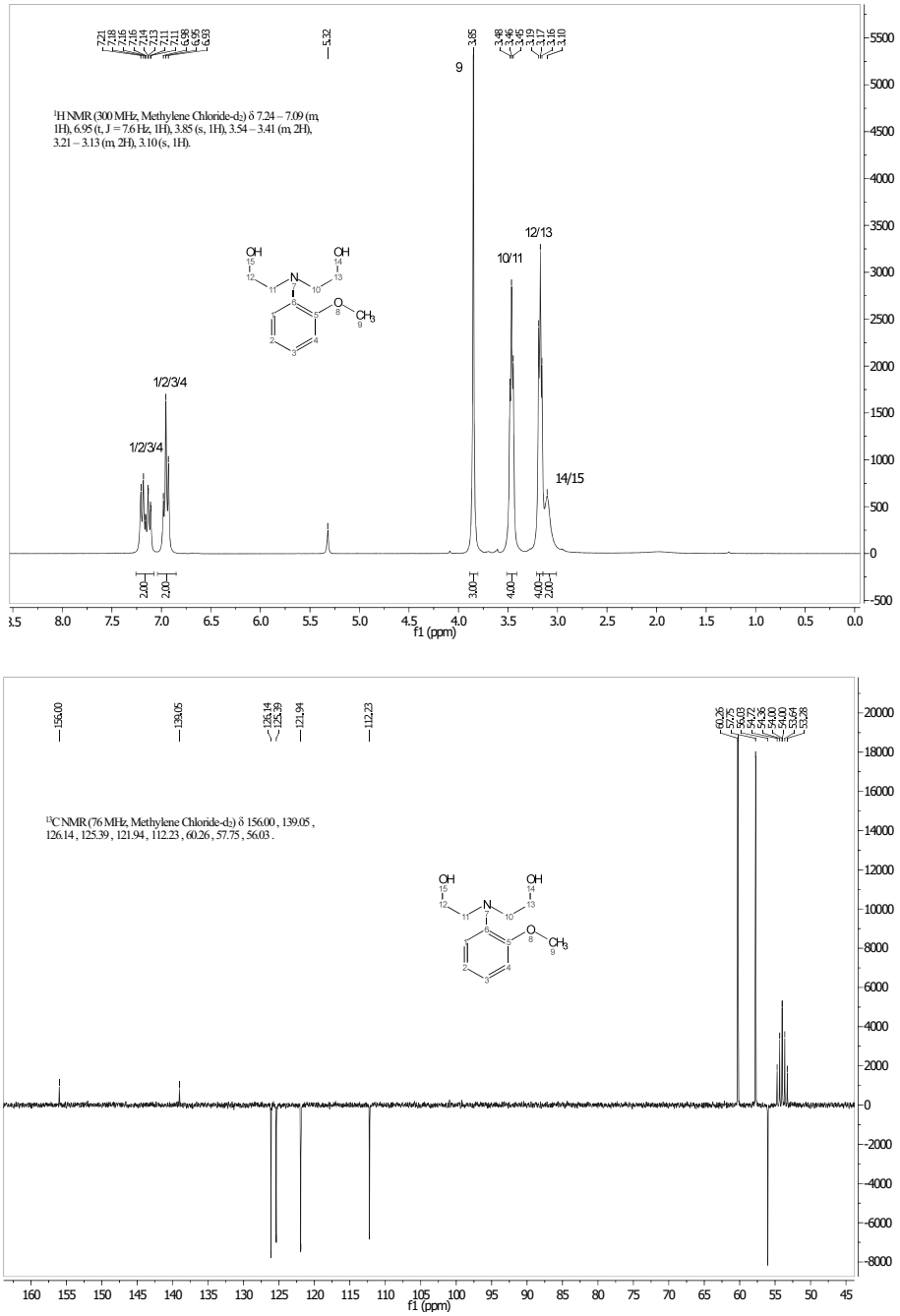

Figure 9.1: ^{1}H-NMR and ^{13}C-NMR spectra of compound **2**

Compound 3

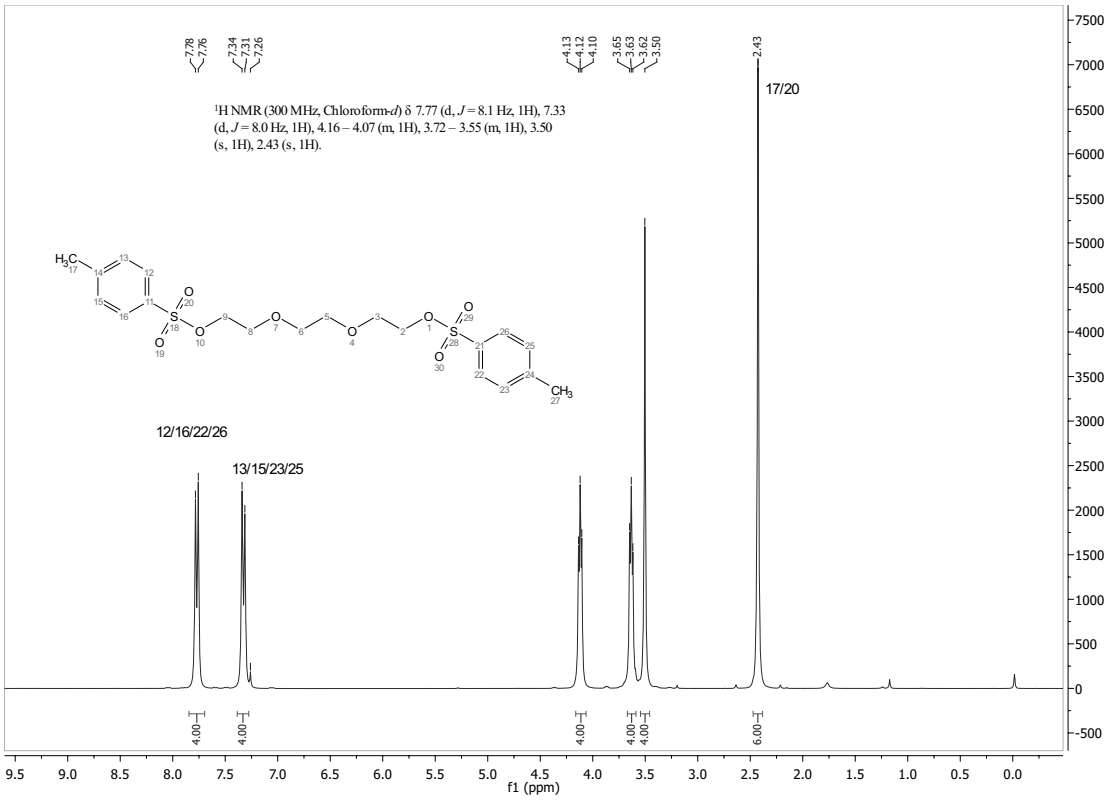

Figure 9.2: ^{1}H-NMR spectrum of compound **3**

Compound 4

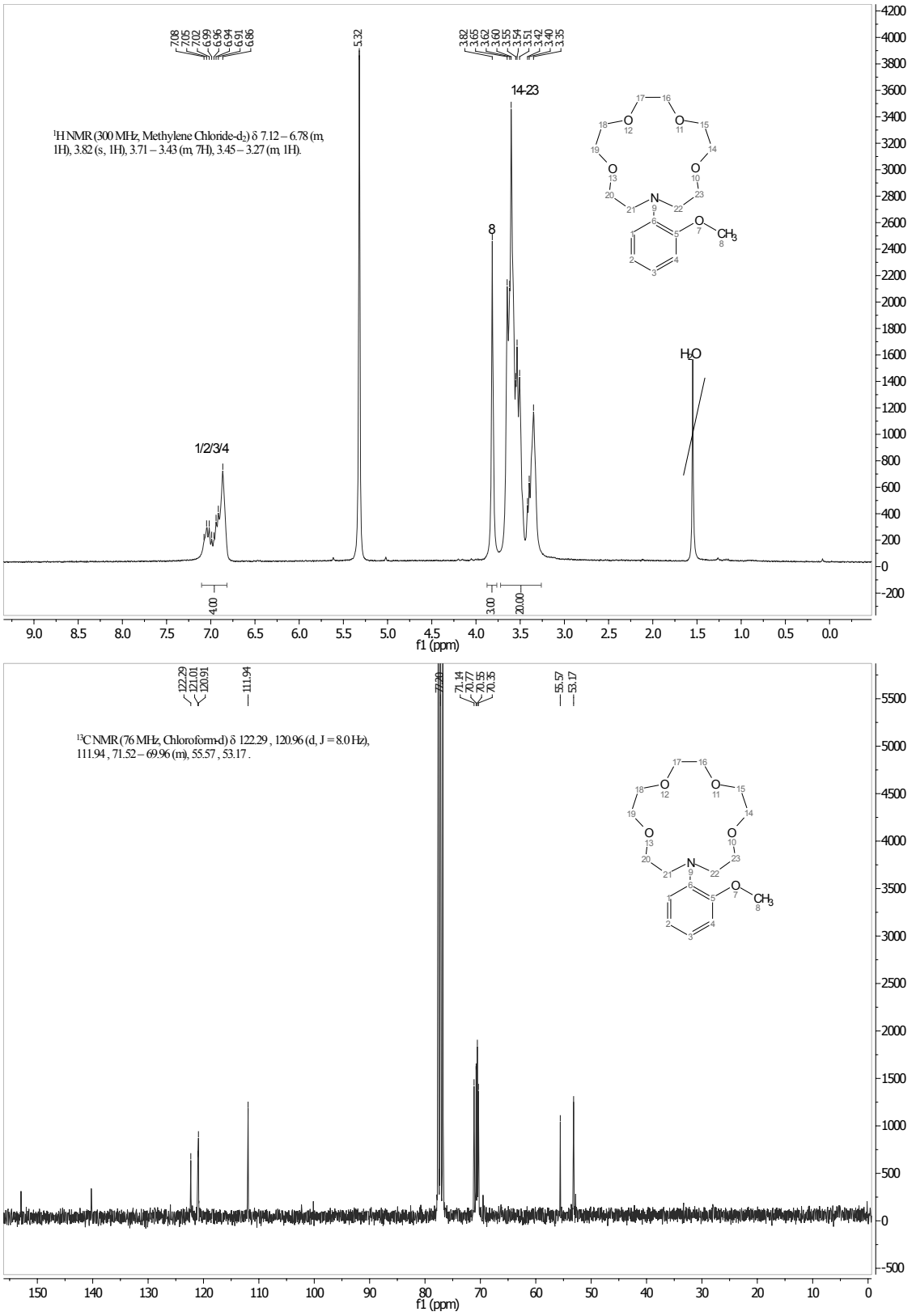

Figure 9.3: ^{1}H-NMR and ^{13}C-NMR spectra of compound **4**

Compound 5

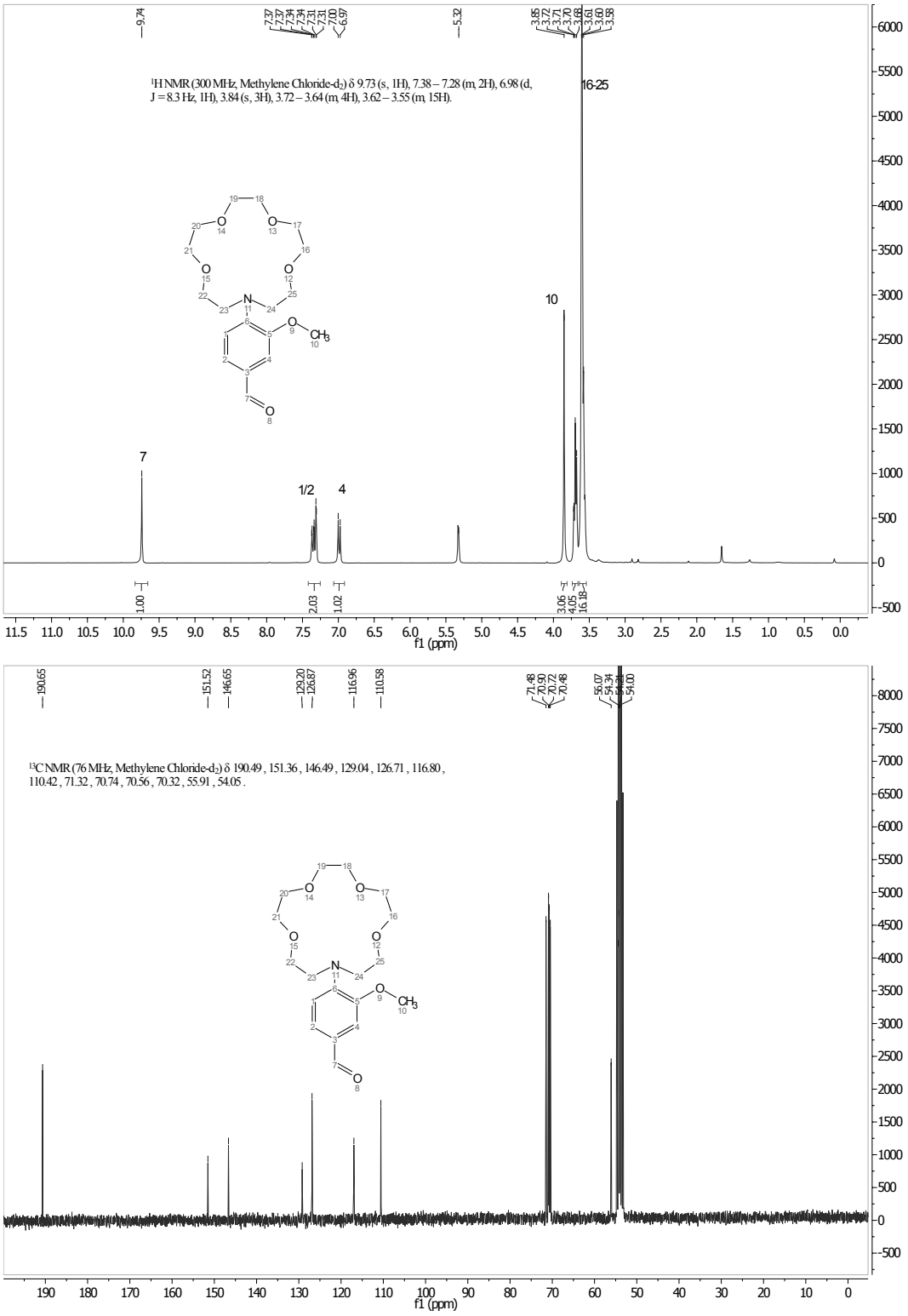

Figure 9.4: ^{1}H-NMR and ^{13}C-NMR spectra of compound **5**

Compound 7

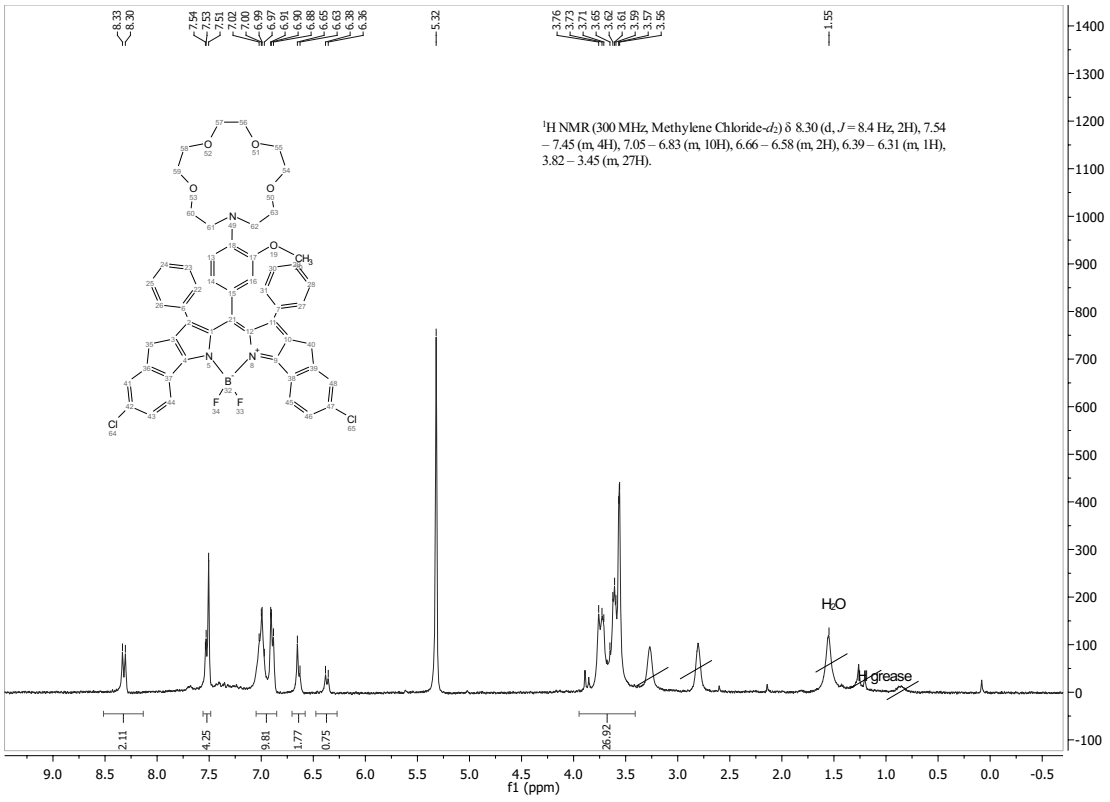

Figure 9.5: ^{1}H-NMR spectrum of compound **7**

Compound 9

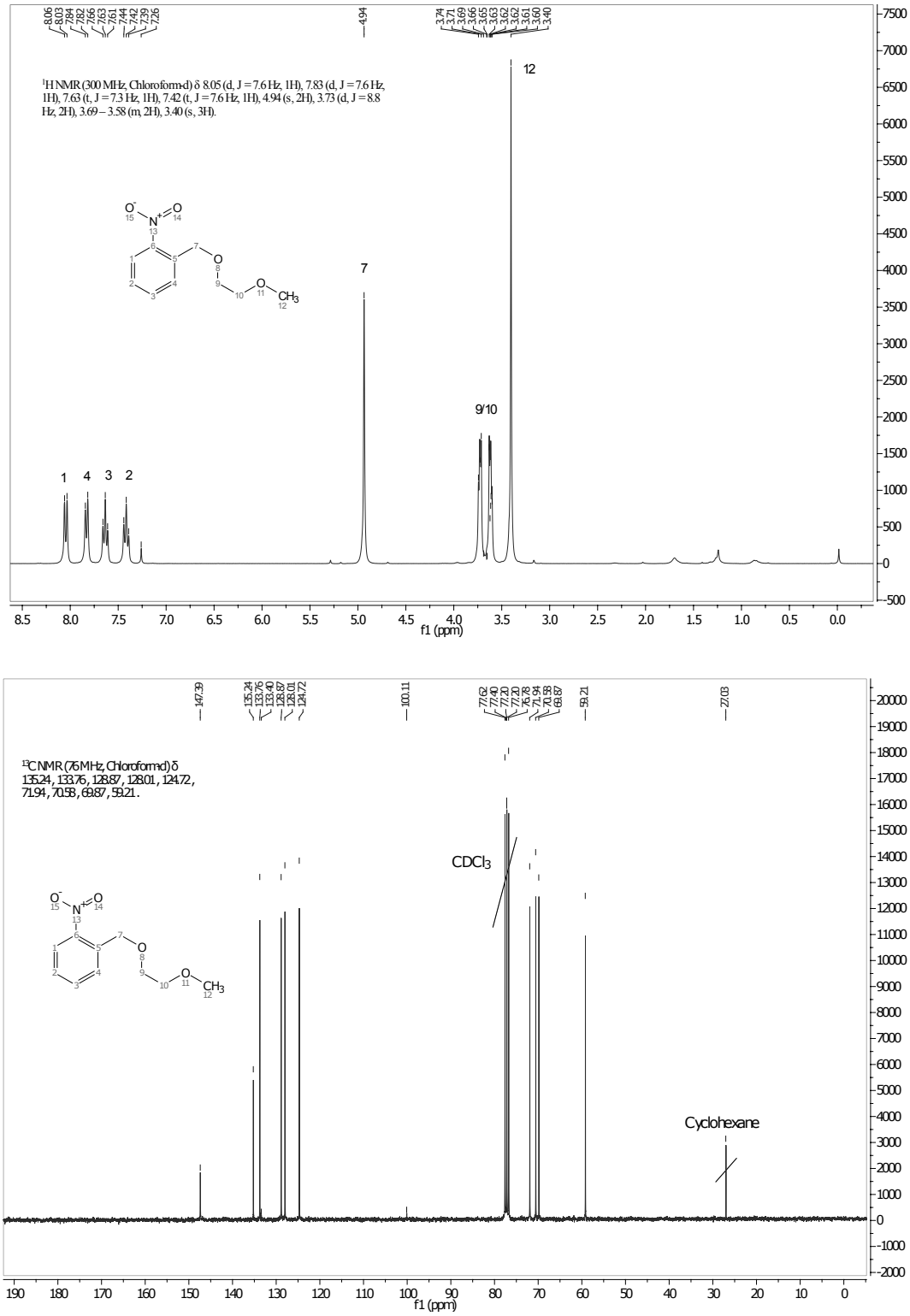

Figure 9.6: ^{1}H-NMR and ^{13}C-NMR spectra of compound **9**

Compound 10

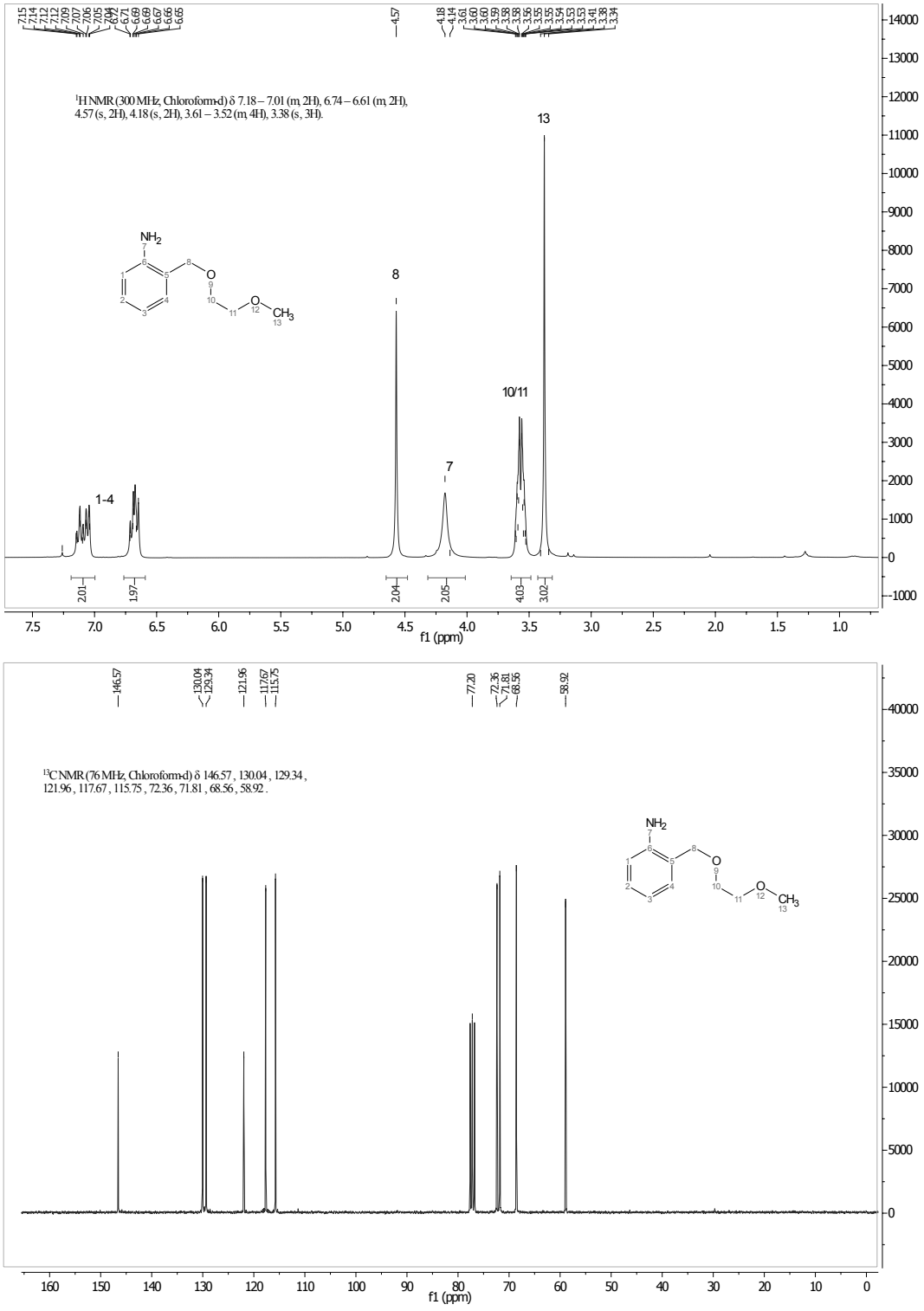

Figure 9.7: ^{1}H-NMR and ^{13}C-NMR spectra of compound **10**

Compound 11

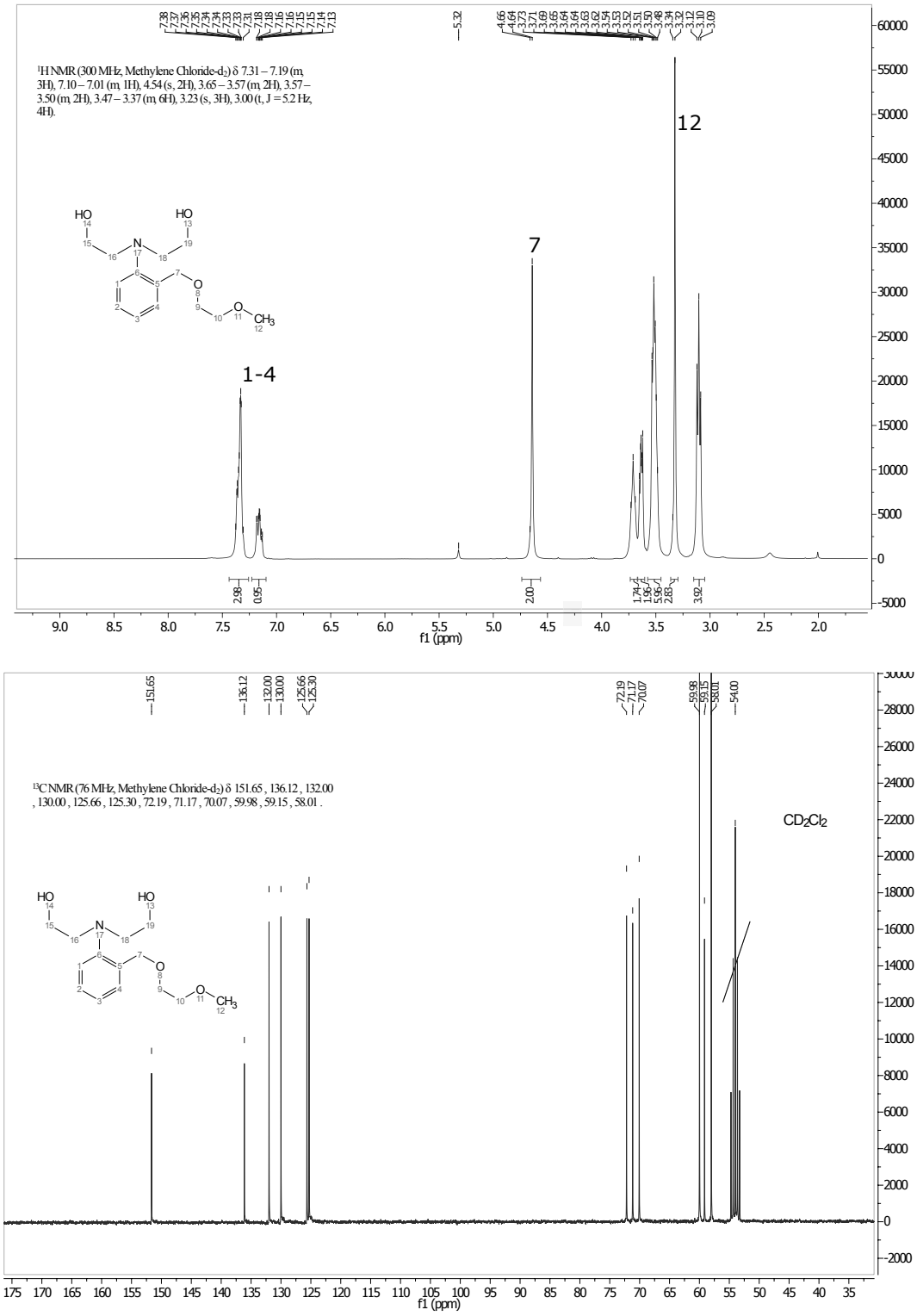

Figure 9.8: ^{1}H-NMR and ^{13}C-NMR spectra of compound **11**

Compound 12

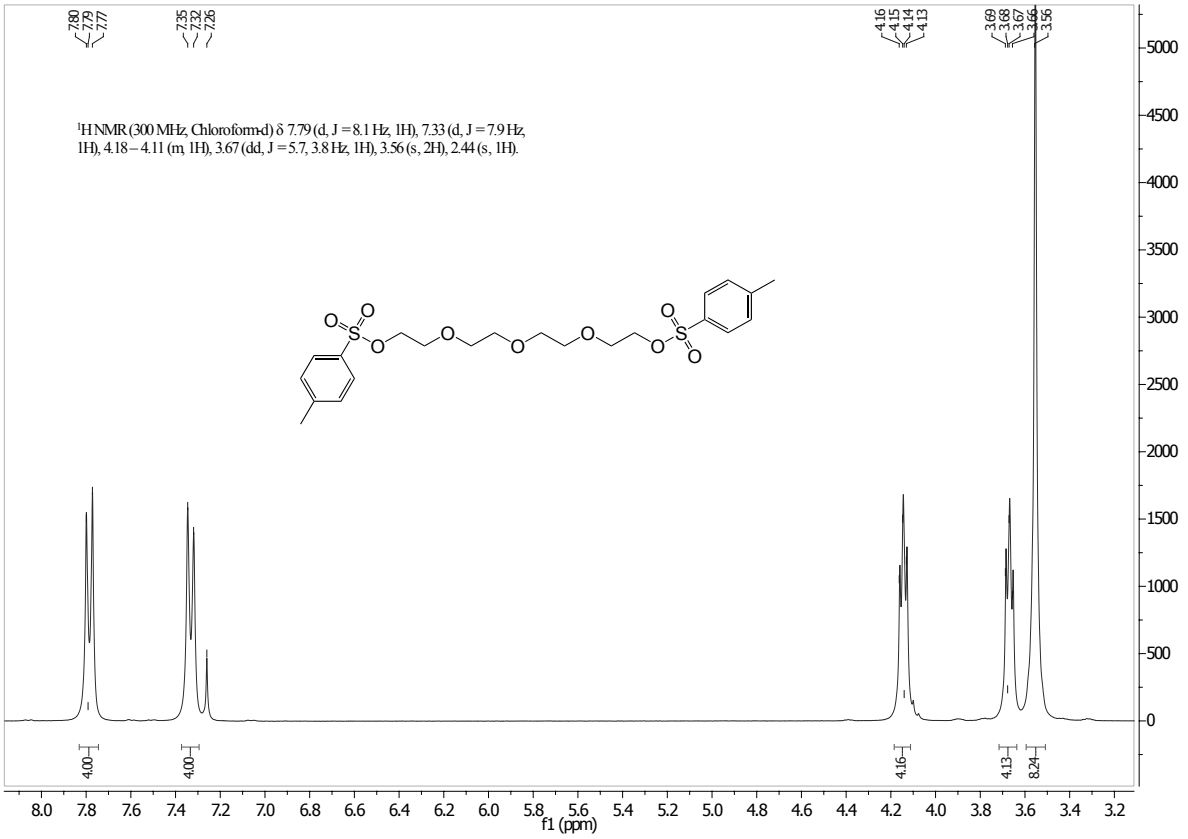

Figure 9.9: ^{1}H-NMR spectrum of compound **12**

Compound 13

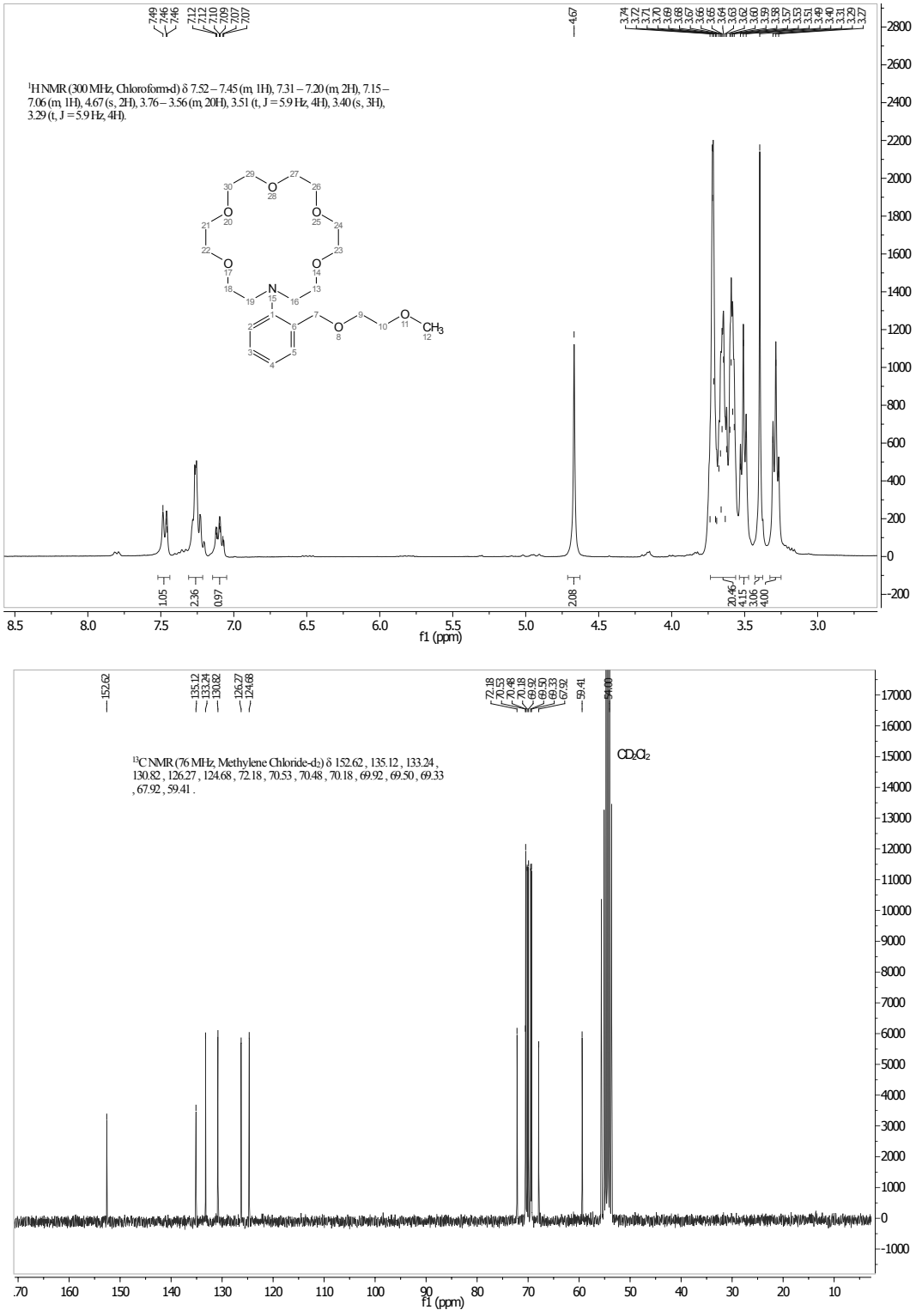

Figure 9.10: ^{1}H-NMR and ^{13}C-NMR spectra of compound **13**

Compound 14

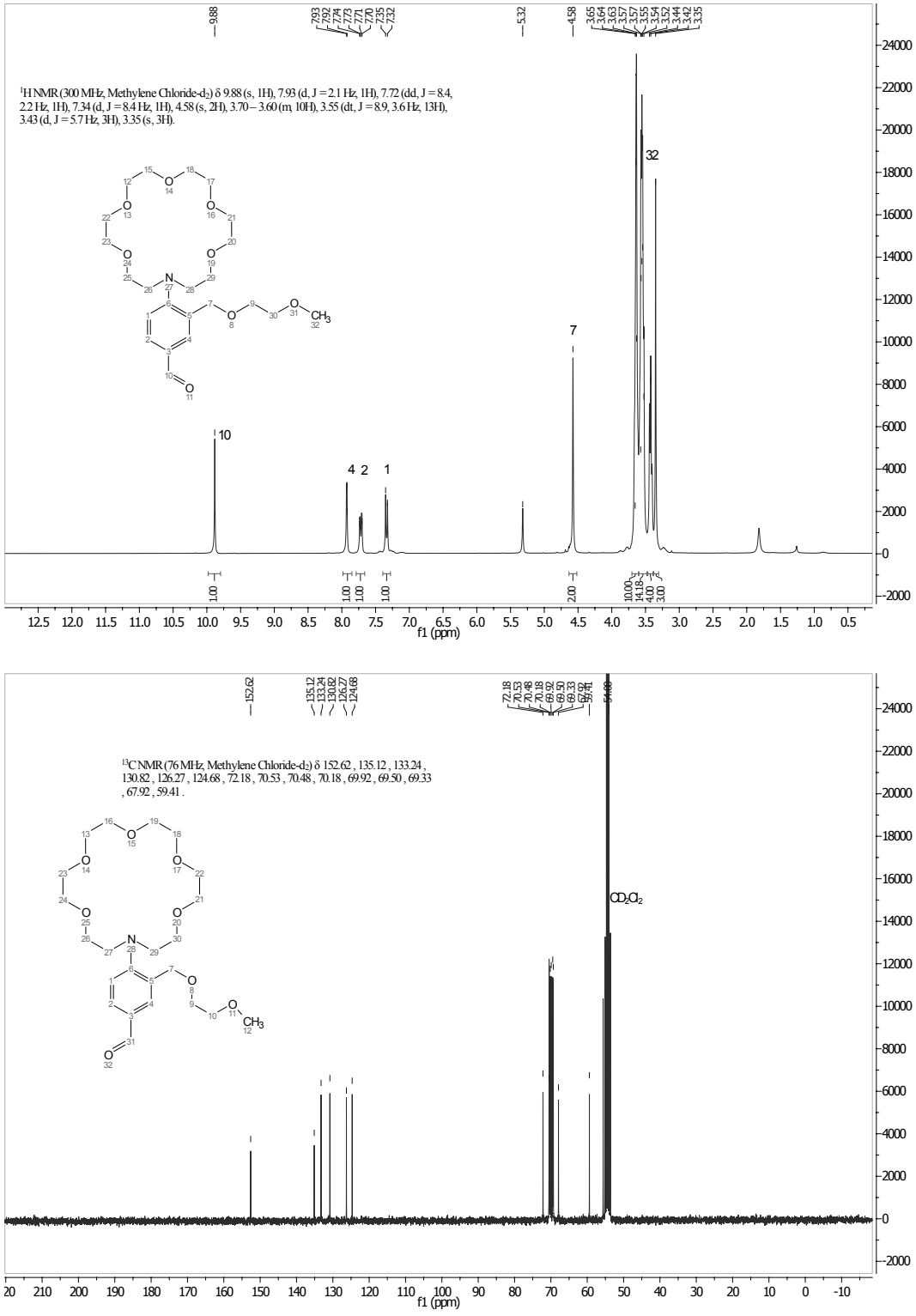

Figure 9.11: ^{1}H-NMR and ^{13}C-NMR spectra of compound **14**

Compound 17

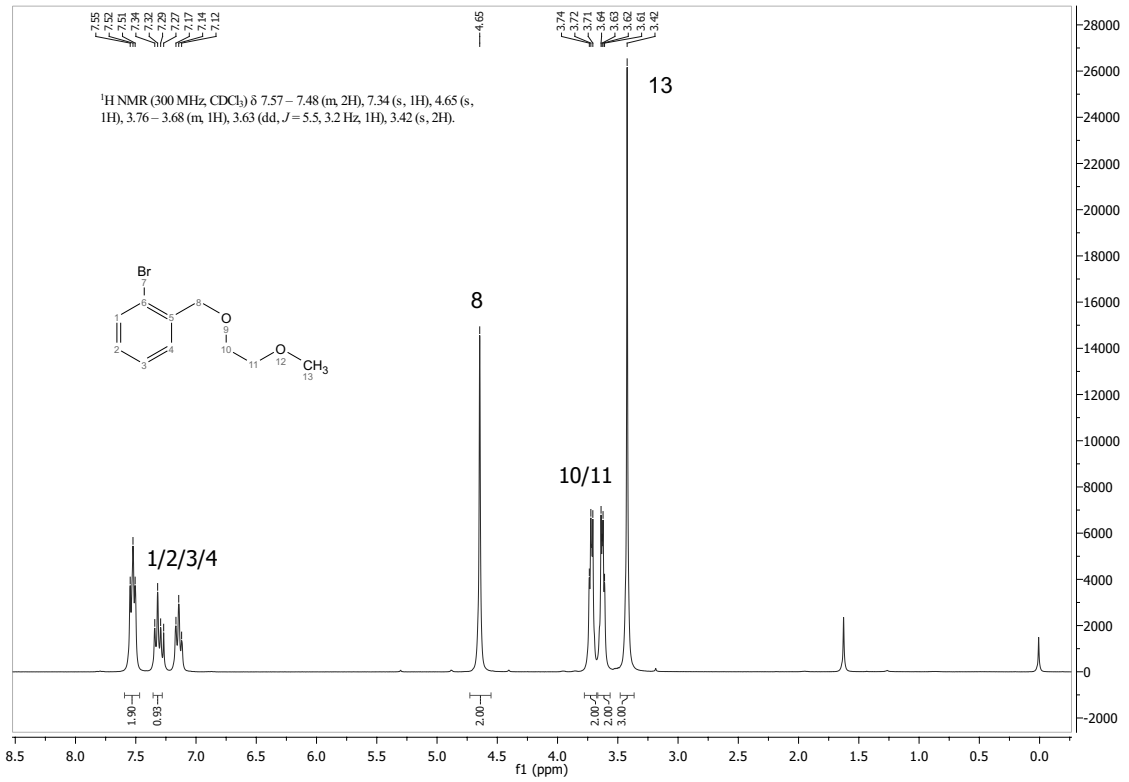

Figure 9.12: ^{1}H-NMR spectrum of compound **17**

Compound 19

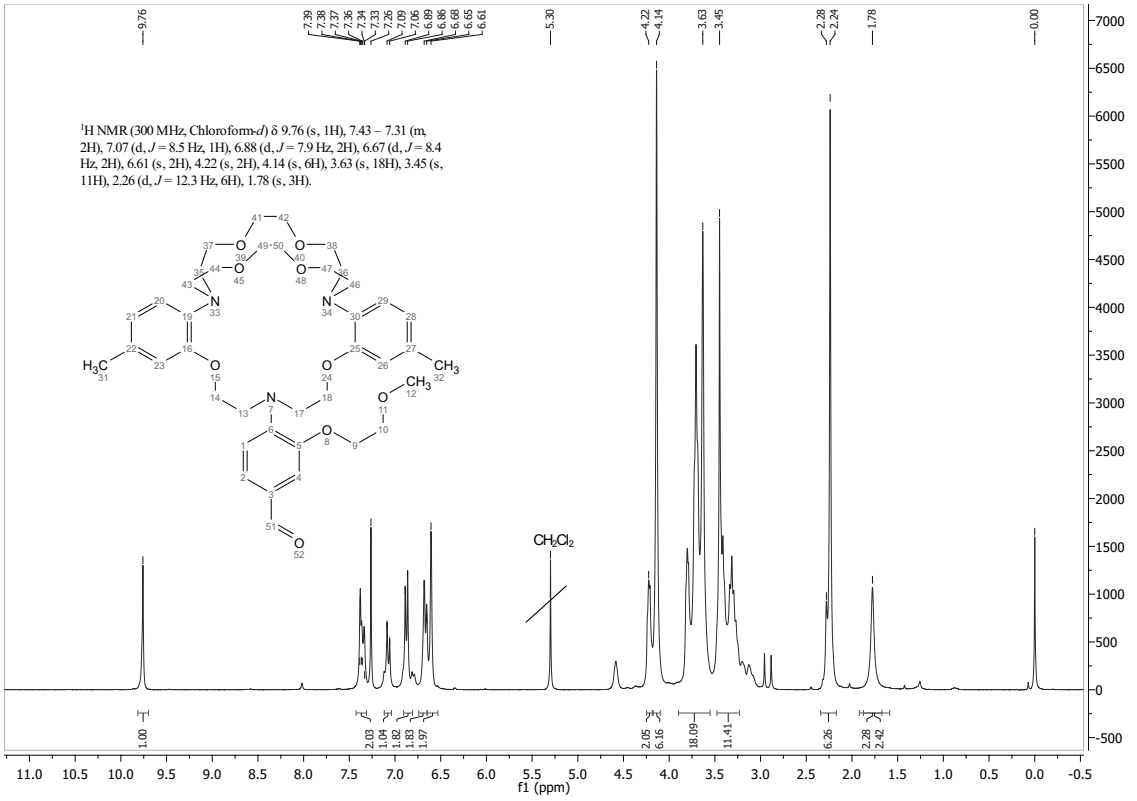

Figure 9.13: ^{1}H-NMR spectrum of compound **19**

9.2 Maldi-TOF Data

Compound 4

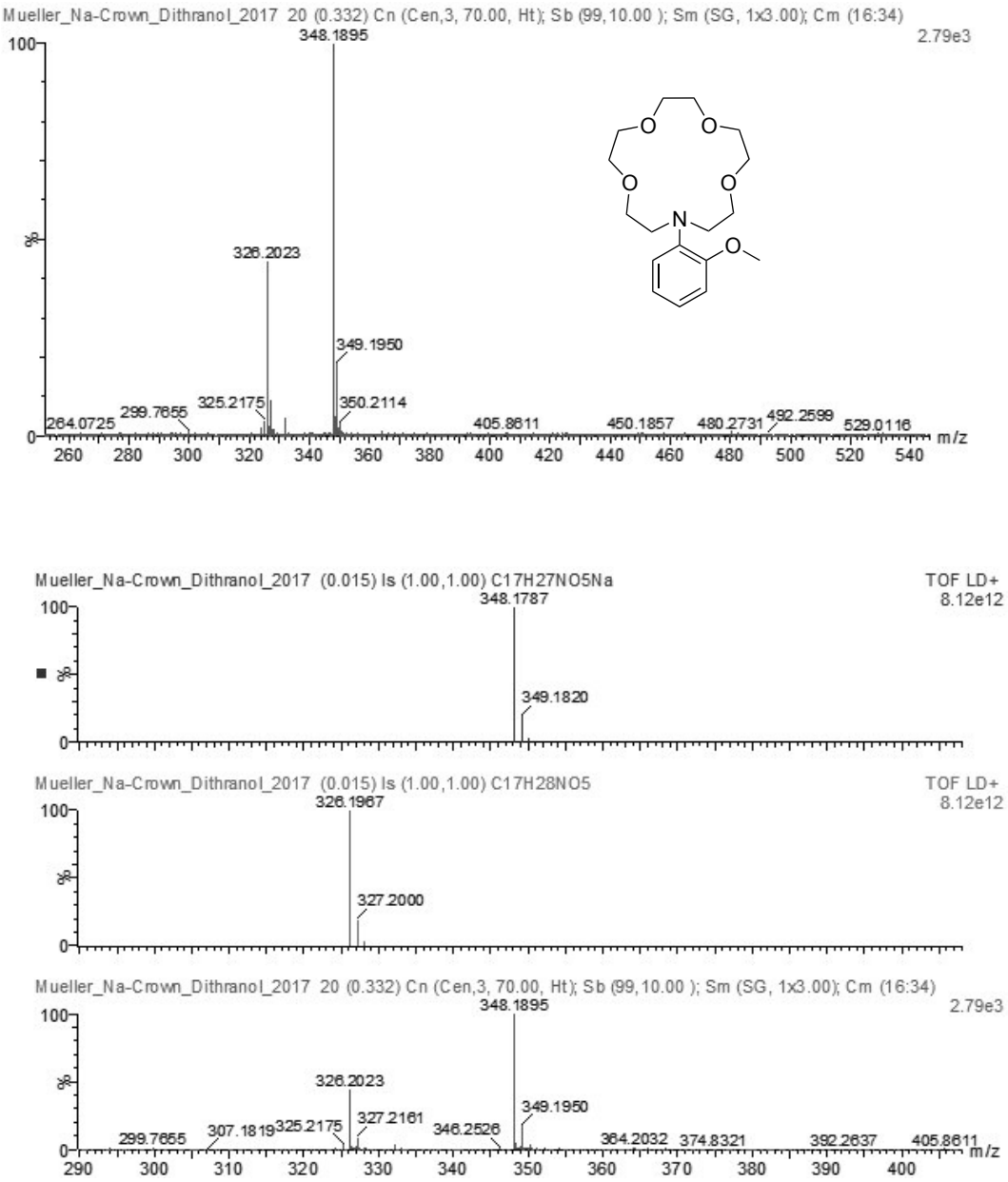

Figure 9.14: MALDI-TOF spectrum of compound **4** in an alpha matrix with the corresponding isotope pattern

Compound 5

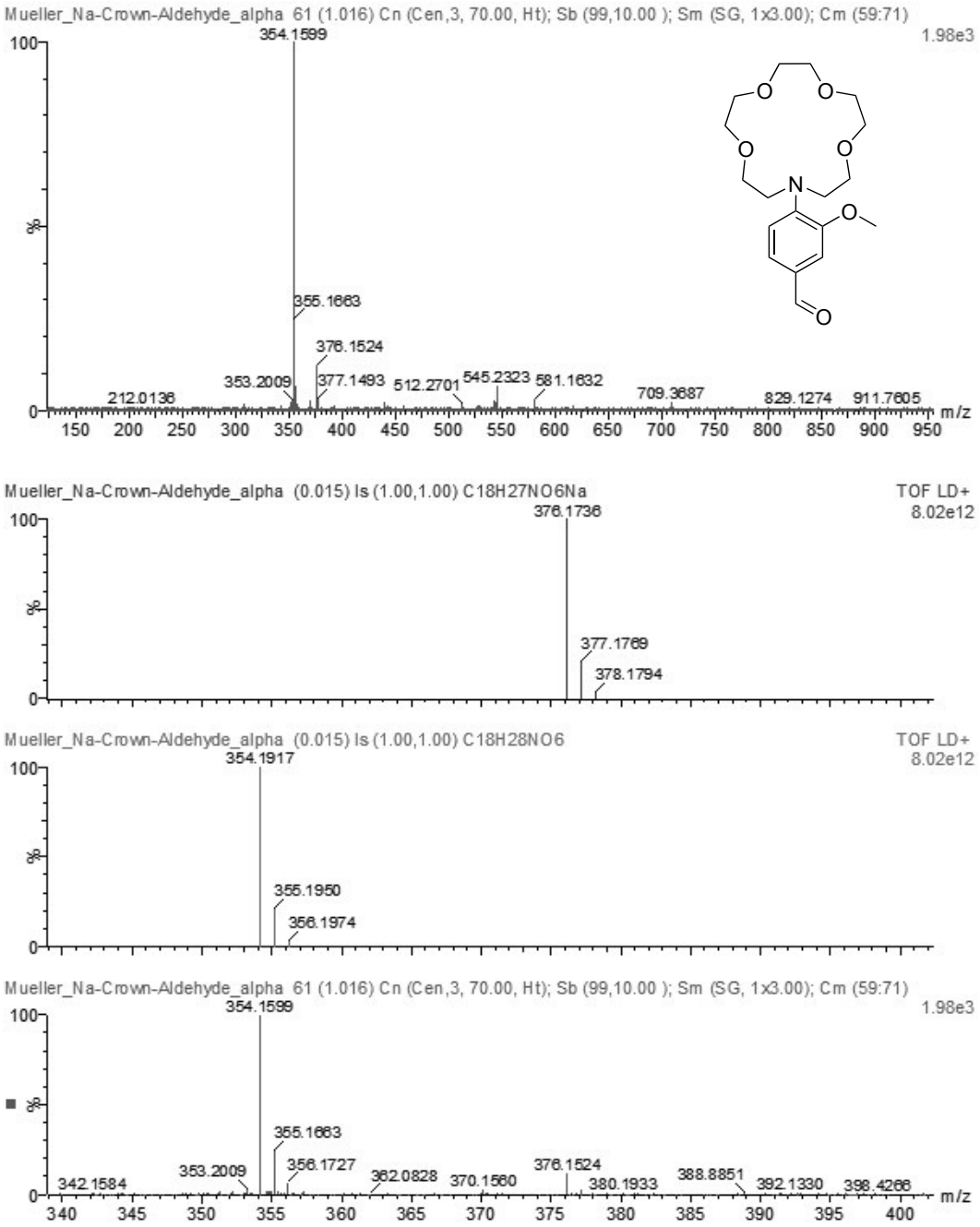

Figure 9.15: MALDI-TOF spectrum of compound **5** in an alpha matrix with the corresponding isotope pattern

Compound 7

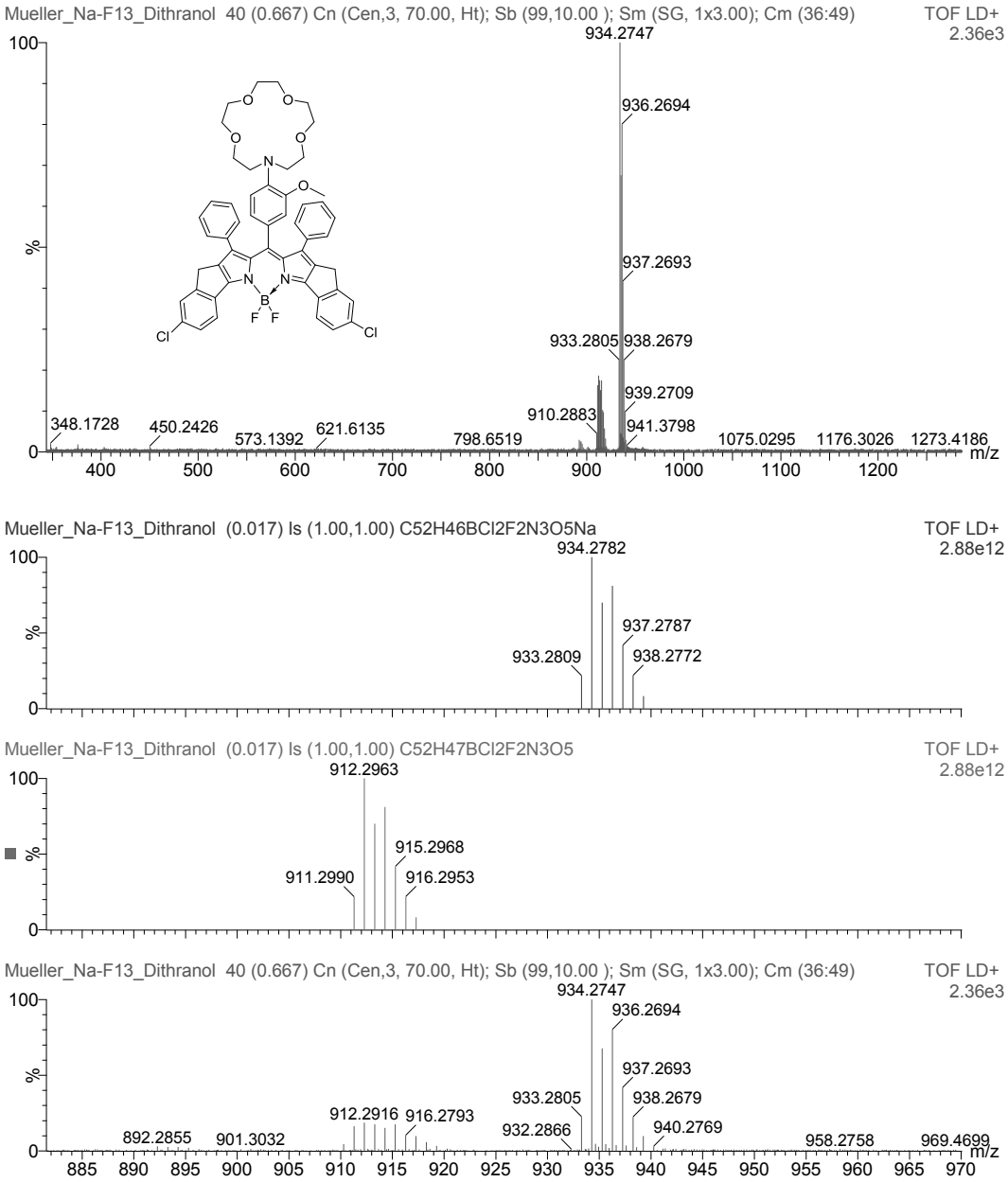

Figure 9.16: MALDI-TOF spectrum of compound **7** in an alpha matrix with the corresponding isotope pattern

Compound 13

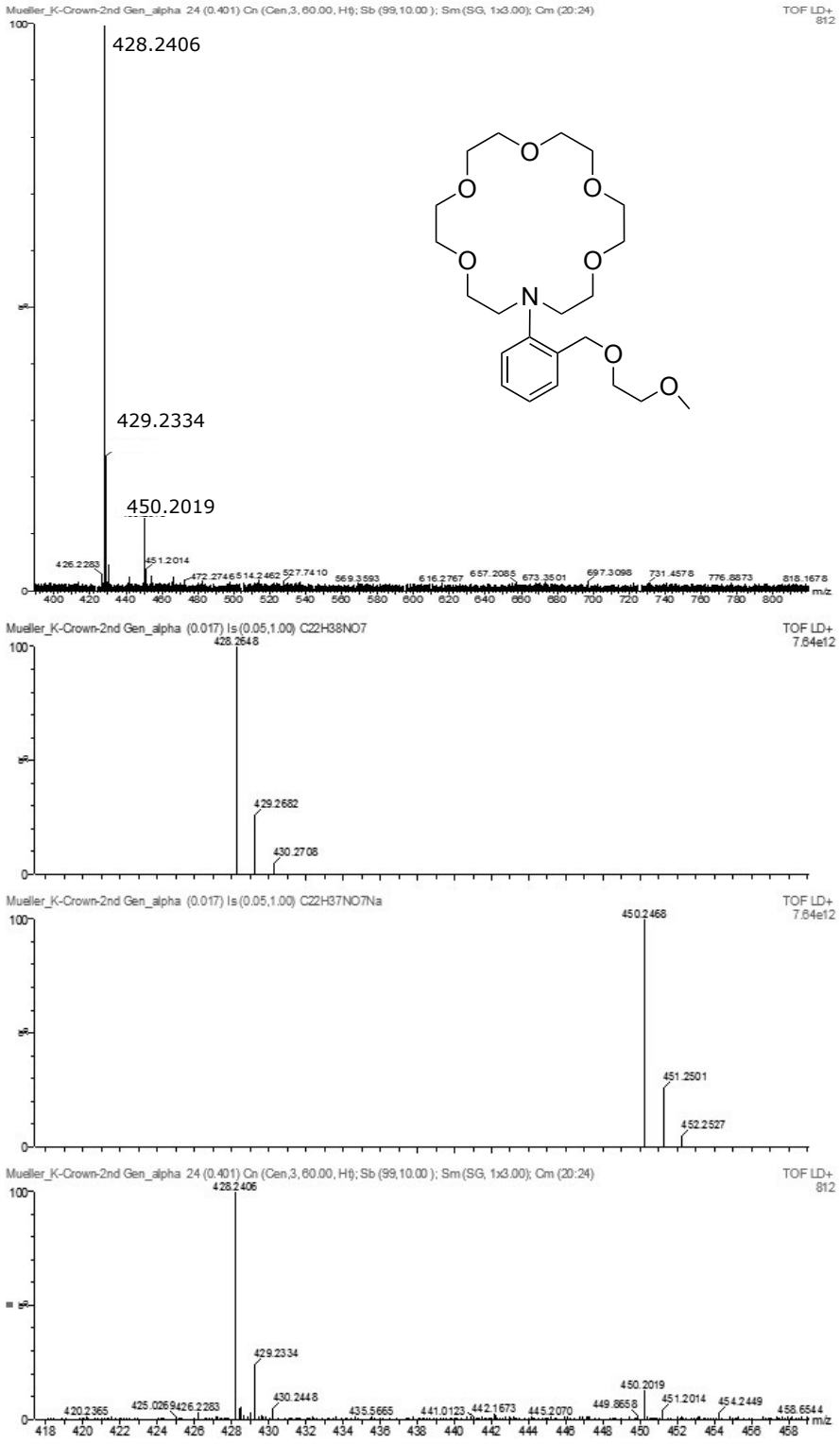

Figure 9.17: MALDI-TOF spectrum of compound **13** in an alpha matrix with the corresponding isotope pattern

Compound 14

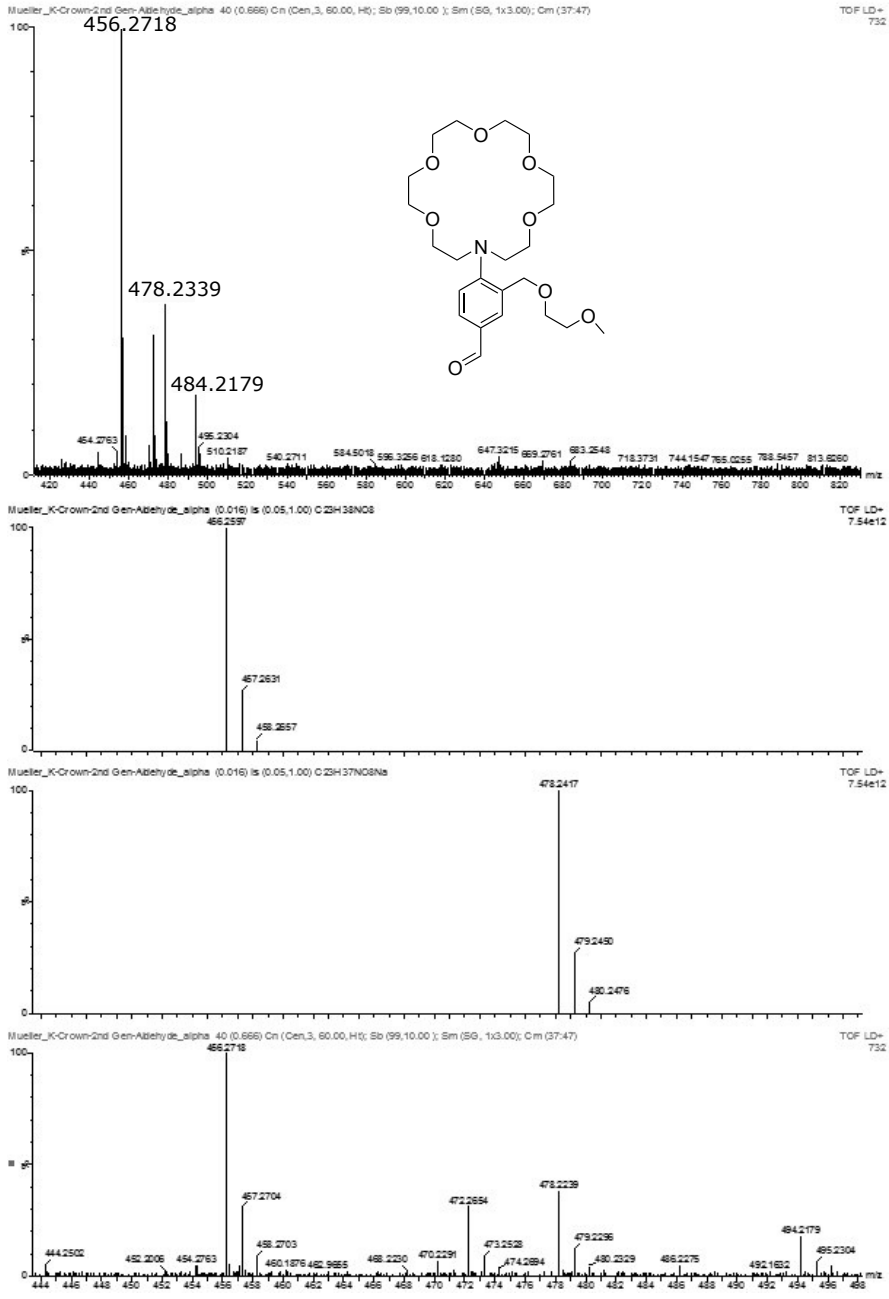

Figure 9.18: MALDI-TOF spectrum of compound **14** in an alpha matrix with the corresponding isotope pattern

Compound 15

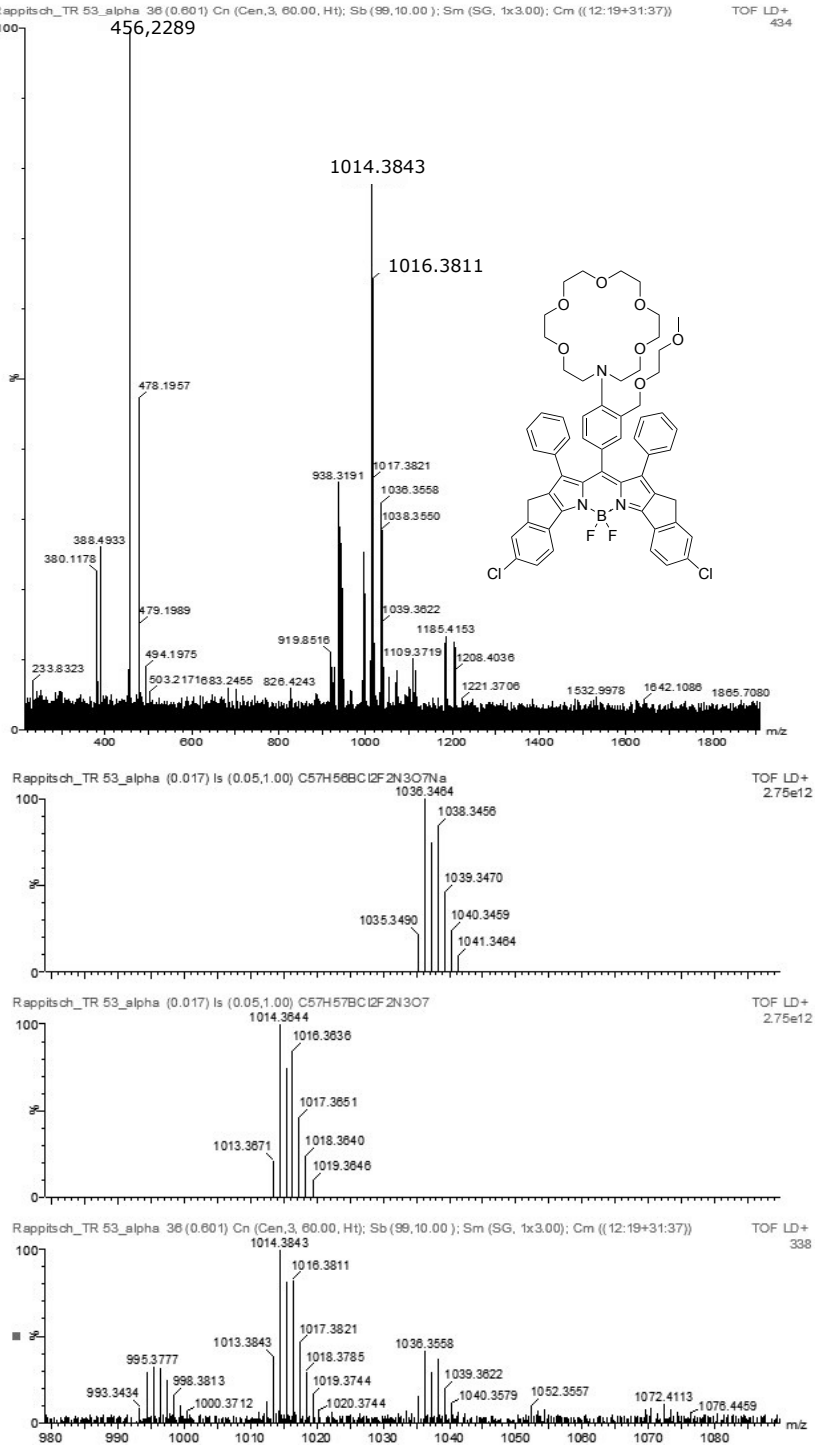

Figure 9.19: MALDI-TOF spectrum of compound **15** in an alpha matrix with the corresponding isotope pattern

Compound 21

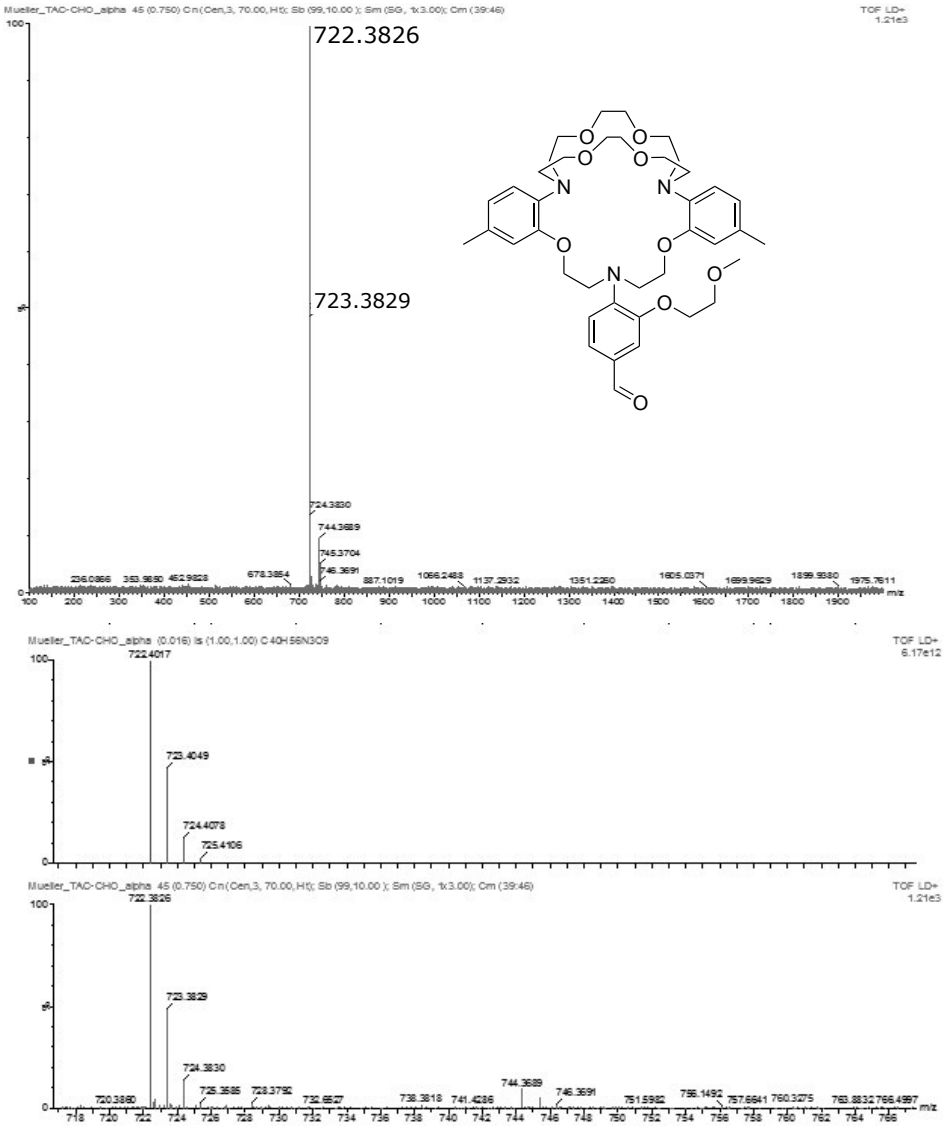

Figure 9.20: MALDI-TOF spectrum of compound **21** in an alpha matrix with the corresponding isotope pattern

Compound 20

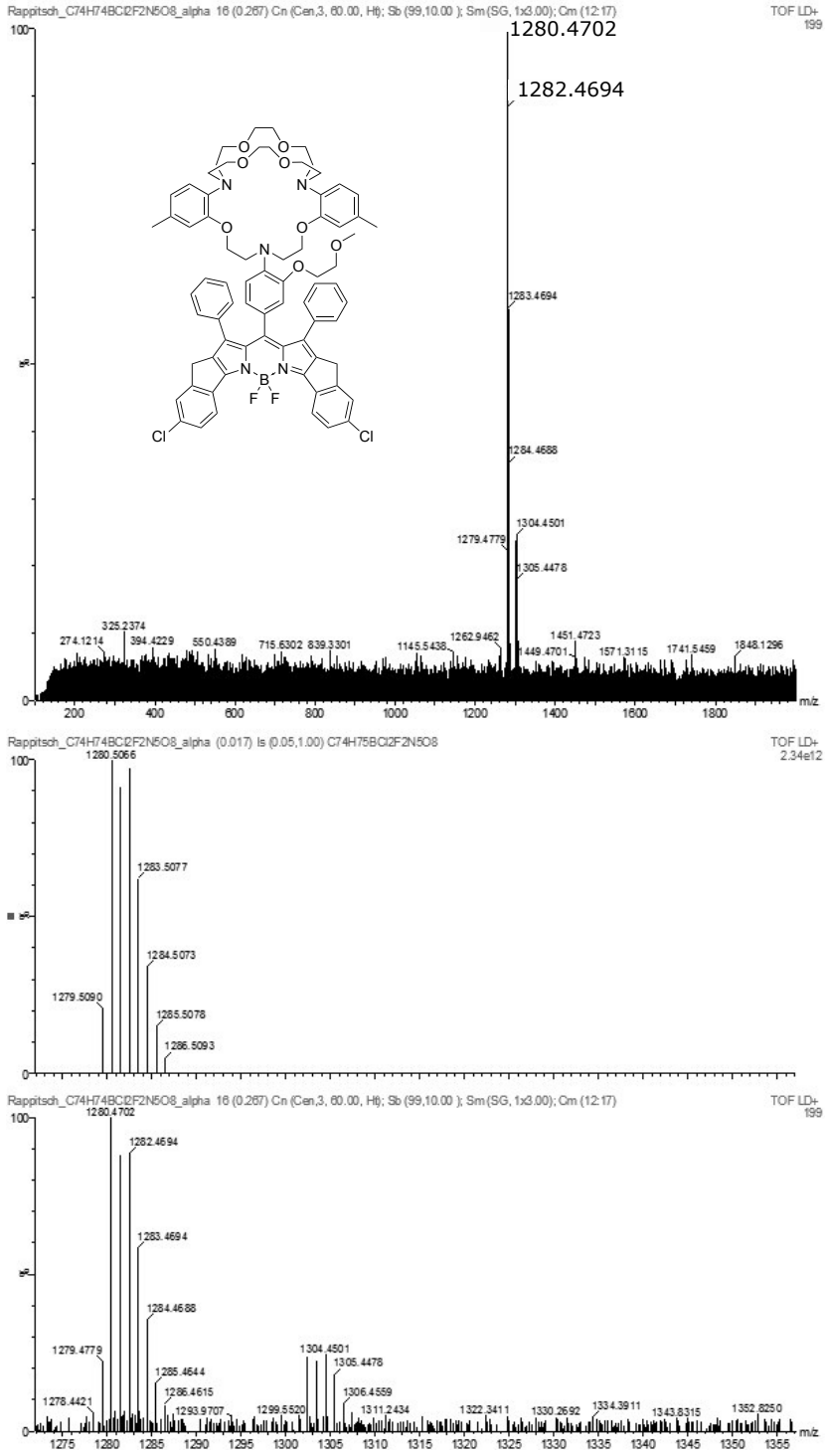

Figure 9.21: MALDI-TOF spectrum of compound **20** in an alpha matrix with the corresponding isotope pattern

9.3 Chemicals

Table 9.1: List of used chemicals

Chemicals	CAS	Supplier
Triethylene glycol	112-27-6	TCI
4-toluenesulfonyl chloride	98-59-9	TCI
5-chloro-1-indanone	42348-86-7	ABCR
Lithium diisopropylamide	4111-54-0	Aldrich
Tetraethylene glycol	112-60-7	Aldrich
2-anisidine	900-04-0	TCI
2-chloroethanol	107-07-3	Aldrich
NaH	7646-69-7	TCI
$POCl_3$	10025-87-3	Aldrich
N,N-diisopropylethylamine	7078-68-5	Aldrich
Boron trifluoride diethyl etherate	09-63-7	Aldrich
Trifluoroacetic acid	76-05-1	Fluka
2-nitrobenzylbromide	3958-60-9	TCI
2-methoxyehanol	109-86-4	TCI
Iron powder	7439-89-6	Fluka
2-bromoethanol	540-51-2	TCI
Silica Gel	112926-00-8	Acros
Aluminium oxide	1344-28-1	Acros
$CaCO_3$	471-34-1	Merck
KI	7681-11-0	Roth
Na_2SO_4	7757-82-6	Roth
Acetone	67-64-1	Brenntag
Cyclohexane	110-82-7	VWR
Dichlormethane	75-09-2	Fisher Scintific
Ethylacetate	141-78-6	VWR
Methanol	67-56-1	Roth
Tetrahydrofuran	109-99-9	Merck
Tetrahydrofuran	109-99-10	VWR
Dimethylformamid	68-12-2	Merck

9.4 Abbreviations

Table 9.2: Abbreviations

Abbreviation	Explanation
DCM	Dichloromethane
EA	Ethyl acetate
CH	Cyclohexane
THF	Tetrahydrofuran
MeOH	Methanol
DMF	Dimethylformamide
$POCl_3$	Phosphorusoxy chloride
DIPEA	N,N-diisopropylethylamine
DDQ	2,3-dichloro-5,6-dicyano-1,4-benzoquinone
HCl	Hydrochloric acid
H_2O	water
KOH	potassium hydroxide
PET	Photoinduced electron transfer
PMMA	Poly(methyl methacrylate)
$CaCO_3$	Calcium carbonate
KI	Potassium iodide
Na_2SO_4	Sodium sulfate
RT	Room Temperature
FI	fluoroionophore